ANNUAL REPORT
2000

2000

IBR

IN-SITU
SURFACE
CHEMISTRY

(211)
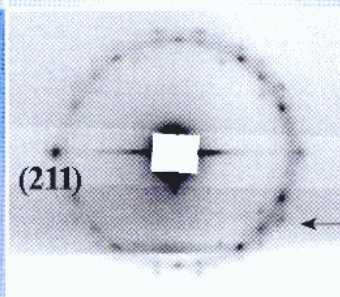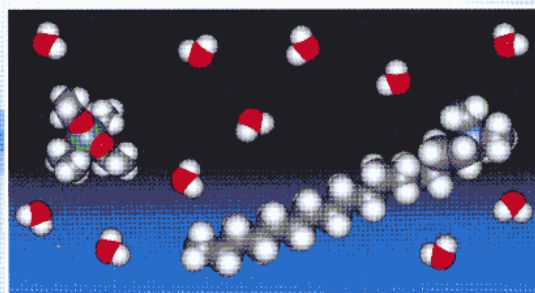
Final Structure: Pm3n – cubic

CTAB/TEOS = 0.12

39 Å *(211)*

cps

41 Å
43 Å

74 Å

30s

$(Å^{-1})$

Deposition
T_0

AUSTRIAN SAX BEAMLINE AT

elettra

Austrian Small Angle X-ray Scattering (SAXS) Beamline at ELETTRA

Annual Report 2000

Compiled by the SAXS-Group:

- for IBR: M. Rappolt & H. Amenitsch
- for ELETTRA: S. Bernstorff

Table of Contents

Preface

Peter Laggner
Director
Institute of Biophysics and X-Ray Structure Research
Austrian Academy of Sciences

I am very glad to welcome this new edition of the Annual Report of the Austrian Small Angle X-Ray Scattering (SAXS) beamline, reporting the continuing activity at and around the beamline.

The popularity of the beamline among potential users from all over the world is witnessed by a number of requested shifts which exceeds the number of available ones by a factor of nearly 2. Although this high ratio translates into a lot of frustration for some users, it is a guarantee of a scientific program of consistently high quality.

The scientific community served by the beamline is quite diverse, ranging from Materials Science to Structural Biology. Some recent developments in the instrumentation, such as the Differential Scanning Calorimetry set up, the upgrade of the high pressure apparatus and the detector developments have further broadened the scope of possible experiments.
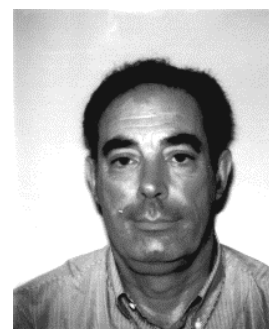
An extension of the agreement between Sincrotrone Trieste and the Austrian Academy of Sciences was signed in March 2001 and is the basis for a continuing collaboration between the two institutions. I am therefore optimistic that more good science can be expected in the years to come.

Massimo Altarelli
Director
Elettra Synchrotron Light Laboratory

The SAXS-Group

HEAD OF PROJECT: Peter Laggner[1]

                              e-mail: Peter.Laggner@oeaw.ac.at

SCIENTISTS: Heinz Amenitsch[1,3]

                              e-mail: Heinz.Amenitsch@elettra.trieste.it

                        Sigrid Bernstorff [2]

                              e-mail: Sigrid.Bernstorff@elettra.trieste.it

POSTDOCS: Pavo Dubcek[2]

                              e-mail: Pavo.Dubcek@elettra.trieste.it

                        Michael Rappolt[1,3]

                              e-mail: Michael.Rappolt@elettra.trieste.it

PhD-STUDENT: Georg Pabst[1,4]

                              e-mail: Georg.Pabst@elettra.trieste.it

CHEMICAL ASSISTANT: Marlene Strobl[1,3]

                              e-mail: Marlene.Strobl@elettra.trieste.it

TECHNICIAN: Christian Morello[2]

                              e-mail: Christian.Morello@elettra.trieste.it

1) Institute for Biophysics and X-ray Structure Research, Austrian Academy of Sciences, Schmiedlstraße 6, 8042 Graz, Austria.
Tel 0043-316-4120 302
Fax 0043-316-4120 390

2) Sincrotrone Trieste, Strada Statale 14, km 163.5, 34012 Basovizza (TS), Italy.
Tel 0039-040-375 81
Fax 0039-040-938 0902

3) Institute for Biophysics and X-ray Structure Research, Austrian Academy of Sciences c/o Sincrotrone Trieste

4.) Neutron Program for Materials Research, National Research Council of Canada, Chalk River Laboratories, Chalk River, Ontario (present address)

The SAXS-Beamline in General

Small Angle X-ray Scattering has become a well known standard method to study the structure of various objects in the spatial range from 1 to 1000 nm, and therefore instruments capable to perform such experiments are installed at most of the synchrotron research centers. The high-flux SAXS beamline at ELETTRA is mainly intended for time-resolved studies on fast structural transitions in the sub-millisecond time region in solutions and partly ordered systems with a SAXS-resolution of 1 to 140 nm in real-space.

The photon source is the 57-pole wiggler whose beam is shared and used simultaneously with a Macromolecular Crystallography beamline. The wiggler delivers a very intense radiation between 4 and 25 keV of which the SAXS-Beamline accepts 3 discrete energies, namely 5.4, 8 and 16 keV. The beamline optics consists of a flat double crystal monochromator and a double focusing toroidal mirror.

A versatile SAXS experimental station has been set-up, and an additional wide-angle X-ray scattering (WAXS) detector monitors simultaneously diffraction patterns in the range from 0.1 to 0.9 nm. The sample station is mounted move-able onto an optical table for optimising the sample detector distance with respect to SAXS resolution and sample size.

Besides the foreseen sample surrounding the users have the possibility to install their own specialised sample equipment. In the design phase, besides technical boundary conditions, user friendliness and reliability have been considered as important criteria.

The optimisation of the beamline with respect to high-flux and consequently high flux density, allows to perform the following experiments:

- Low Contrast Solution Scattering
- Grazing Incidence Surface Diffraction
- Micro-Spot Scanning
- X-ray Fluorescence Analysis
- Time-Resolved Studies ≥ 11 µs
- Simultaneously Performed Small- and Wide-Angle Measurements (SWAXS) on:
  - Gels
  - Liquid Crystals
  - (Bio) Polymers
  - Amorphous Materials
  - Muscles

Furthermore, using 5.4 and 16 keV energies, the beamline is widely applicable also to very thin, e.g. single muscle fibers, and optically thick (high Z) specimen, as often used in e.g., material science and solid state physics.

THE INSERTION DEVICE

The wiggler for the SAXS beamline consists of three 1.5 m long segments, each having 19 poles. The device can work with a minimum gap of 20 mm, which corresponds to K=20 at 2 GeV. The main parameters of the wiggler are:

- Critical Energy 4.1 keV
- Radiation Power 8.6 kW
- Flux 3.5×10^{14} ph/s/mrad/0.1%BW (at 400 mA)

The wiggler radiation cone has a horizontal width of 9 mrad. From this the SAXS-beamline accepts vertically 0.3 mrad, and horizontally +/-0.5 mrad at a 1.25 mrad off-axis position. The resulting source size for 8 keV photons is 3.9 x 0.26 mm^2 (horiz. x vert.).

THE OPTICS

The optics common with the diffraction beamline consists of:
- C-Filter and Beryllium window assembly to reduce the power load on the first optical elements by a factor of 2 and to separate the beamline vacuum from the storage ring.
- Beam defining slit chamber which allows to define the SAXS beam on three sides before the monochromator in order to reduce the straylight in the downstream beamline sections.

The SAXS beamline optics consists of:
- A double-crystal monochromator consisting of four individual chambers, in which three interchangeable asymmetric Si(111) crystal pairs are used to select one of three fixed energies. Each of the crystal pairs is optimised for the corresponding energy to accomplish a grazing angle of 2°. The energy resolution $\Delta E/E$ of the monochromator is in the range of 0.7 - 2.5 10^{-3}.
- A baffle chamber after the monochromator is used as an adjustable straylight fenditure.
- A segmented toroidal mirror focuses the light in horizontal and vertical direction with a 1/2.5 magnification onto the SAXS-detector.
- An aperture slit reduces the straylight after the monochromator and the toroidal mirror.
- A guard slit defines the illuminated region around the focal spot. The spot size on the detector is 1.6 mm horizontally and 0.6 mm vertically. The calculated flux at the sample is in the order of 10^{13} ph/s at 400 mA. For a maximum sample size of 5.4 x 1.8 mm^2 correspondingly a flux density of 10^{12} ph/s/mm^2 has been calculated.

SAMPLE STAGE

The multipurpose sample stage allows to perform fast time-resolved relaxation studies based on temperature- or pressure-jumps as well as stopped flow experiments. Shear jump relaxation experiments are planned. Specifically, T-jumps can be induced by an infra-red light pulse (2 ms) from an Erbium-Glass laser, raising the temperature about 20 °C in an aqueous sample volume of 10 μl. A hydrostatic pressure cell with a maximal accessible angular range of 30° for simultaneous SAXS and WAXS measurements is available. P-jumps are realised by switching fast valves between a low and a high pressure reservoir, increasing or decreasing the hydrostatic pressure in the range from 1 bar to 2.5 kbar within a few ms. A newly installed Differential Scanning Calorimeter (DSC) allows for DSC-scans simultaneously to SWAXS measurements. Also a 1.5 T magnet is available. In an overview, the following sample manipulations are possible (further details, see page 25-34):

- Temperature Manipulations: Ramps, Jumps and Gradient Scans
- Pressure Manipulation: Scan and Jumps
- Stopped Flow Experiments
- SWAXS Measurements Applying Mechanical Stress
- SWAXS Measurements Applying Magnetic Fields
- Calorimetric measurements

Scientific applications	Low Contrast Solution Scattering, Grazing Incidence Surface Diffraction, Micro-Spot Scanning, X-ray Fluorescence Analysis, Time-Resolved Studies $\geq$ 11 μs and Simultaneously Performed Small- and Wide-Angle Measurements (SWAXS) on:
	        Gels
	        Liquid Crystals
	        (Bio) Polymers
	        Amorphous Materials
	        Muscles

Source characteristics	<u>Wiggler (NdFeB Hybrid):</u> Period 140 mm No. full poles 57 Gap 20 mm B_{max} 1.607 T Critical Energy ε_c 4.27 keV Power (9 mrad) 8.6 kW Effective source size FWHM 3.9 x 0.26 mm^2(HxV)
Optics	<u>Optical elements:</u> Double crystal monochromator: Si (111) asym. cut, water cooled. Mirror: two–segment,toroidal, Pt coated. <u>Distance from source:</u> 18.4 m 26.5 m Acceptance 1 mrad/0.3 mrad (HxV) Energy (3 selectable) 5.4, 8, 16 keV (0.077, 0.154, 0.23 nm) Energy resolution $\Delta E/E$ 0.7-2.5 x 10^{-3} Focal spot size FWHM 1.2 x 0.6 mm^2 (HxV) Spot at Sample FWHM 5.4 x 1.8 mm^2(HxV) Flux at sample 5 x 10^{12} ph s^{-1}(2 GeV, 200 mA, 8 keV)
Experimental apparatus	<u>Resolution in real space:</u> 1-140 nm (small-angle), 0.1- 0.9 nm (wide-angle) <u>Sample stage:</u> temperature manipulations: ramps, jumps and gradient scans, pressure manipulation: scan and jumps, stop flow experiments, SWAXS measurements applying mechanical stress, SWAXS measurements applying magnetic fields. In-line calorimetric measurements simultaneously with SWAXS. <u>Detectors:</u> 1D gas-filled detectors for simultaneous small- and wide-angle (Gabriel type), 2D CCD-detector for small-angle.
Experiment control	<u>Beamline control:</u> Program-units written in LabView for Windows <u>1 D detector control</u>: PC-card and software from Hecus & Braun, Graz. <u>2 D detector control</u>: Software from Photonic Science, Oxford.

CURRENT STATUS

The beamline has been built by the Institute for Biophysics and X-ray structure Research (IBR), Austrian Academy of Science in collaboration with staff members from Sincrotrone Trieste, and is in user operation since September 1996. The set-up of the beamline started at the beginning of January 1995 with the installation of the support structure. Until the end of 1995, the 8 keV single energy system had been realised. The upgrade to the full three energy system was finished in spring 1998. Time resolved experiments require fast X-ray detectors and data acquisition hard- and software. Depending on the desired resolution in time and in reciprocal space, on isotropic or anisotropic scattering of the sample, one-dimensional position sensitive (delay-line type) or two-dimensional CCD detectors are employed. In 2000 two more devices have been added to the instrumental beamline pool: a chemical exhaust system for gases in order to study in-situ chemical reactions including toxic reactants, and a Differential Scanning Calorimeter, which can be used in-line simultaneous to SWAXS measurements.

In conclusion, due to wide versatility of the beamline and the highly flexible sample stage, there are nearly no limits for the realisation of an experiment, and you are welcome by our team to propose any interesting and highlighting investigation for the benefit of material and life sciences.

Application for Beamtime at ELETTRA

1. Beamtime Policy at SAXS beamline

A new agreement regarding the collaborating research group, and the co-operation between the Austrian Academy of Sciences and Sincrotrone Trieste concerning the SAXS beamline, has been signed in March 2001. It defines also the beamtime distribution between the partners and the beamtime policy.
The following points are of interest for users:

The available beamtime of about 5000 hours/year is distributed as follows:

- 35% for Austrian Users, type: "CRG" (Collaborating Research Group)
- 35% for Users of Sincrotrone Trieste (General Users (GU))
- 30% is reserved for beamline maintenance and in-house research

In both user beamtime contingents also any industrial, proprietary and confidential research can be performed according to the "General User Policy" of Sincrotrone Trieste.

To apply for CRG and GU user beamtime proposals must be submitted according to the rules of Sincrotrone Trieste. The international review committee at ELETTRA will rank the proposals according to their scientific merit assessment. Based on this decision beamtime will be allocated according to the specific quotes for the beamtimes (CRG/GU) either for the following semester ("normal application") or for the next two years ("long term application"). However, at the moment no more than a maximum of 10% of the beamtime will be assigned to "long term" projects.

2. How to apply for beamtime

There are two deadlines each year for proposals, namely August 31st and February 28th. Accepted proposals will receive beamtime either in the then following first or second half year period, respectively. The Application Form must be completed on-line according to the following instructions. In addition, one printed form is also required and must be send to:

ELETTRA USERS OFFICE
Strada Statale 14 - km 163.5
34012 Basovizza (Trieste), ITALY
Tel: +39 040 3758628 - fax: + 39 040 3758565
e-mail: useroffice@elettra.trieste.it

INSTRUCTIONS GIVEN BY THE USERS OFFICE
(see also: www.elettra.trieste.it/guides/users/how.html)

1. Read carefully the following Guidelines.

2. Connect to the Virtual Users' Office: http://users.elettra.trieste.it using your favorite browser (Netscape 3.0 or above, Internet Explorer 4.0 or above, etc.) with JavaScript enabled.

3. Select the Virtual Users Office link.

4. When prompted, insert your ID and password. If you are a new user fill in the registration form with your data and choose your institution with the search button; in case your institution does not appear in the list, please contact useroffice@elettra.trieste.it giving all the details about it. When registered, you will receive an acknowledgment with your ID and password. You can change your password, if you wish. In case you forget your password, please don't register again but contact useroffice@elettra.trieste.it. At any moment you can select the help button and view more detailed instructions. By inserting your ID and password you will be able to continue.

5. Select the proposals button in the User functions group.

6. Select add and fill in on-line the proposal form. Please, type your proposal in English. Repeat this procedure for each proposal you intend to submit.

7. In case of continuation proposal: a) attach the experimental report of previous measurements; b) give your previous proposal number.

8. When finished, submit the proposal electronically, selecting the save button.

9. Print the proposal form together with each related safety form.

10. Sign the safety form(s).

11. Mail one complete printed copy to the Users Office.

NOTE

For further information, e.g., financial support for travel expenses, please have a look into the web-pages http://www.elettra.trieste.it/guides/users/EU-Support.html or contact the USERS OFFICE.

List of Institutes Participating in Experiments

Austria

Austrian Academy of Science, Erich Schmid Institut für Materialwissenschaft, Leoben, and Institut für Metallphysik, Montanuniversität, Leoben

Fratzl Peter
Hebesberger Thomas
Keckes Josef
Pippan R.
Puxkandl R.
Paris Oskar

Austrian Academy of Science, Institute for Biophysics and X-ray Structure Research, Graz

Amenitsch Heinz
Kriechbaum Manfred
Laggner Peter
Rappolt Michael
Strobl Marlene
Vidal Monika

Hecus Braun, Graz

Leingartner Werner

Ludwig Boltzmann-Institut for Osteology, 4th Medical Department, Hanusch-Hospital, Vienna

Roschger Paul
Tesch Walter

Technische Universität Graz, Technische Versuchs- und Forschungsanstalt (TVFA)

Tritthart J.

Universität Wien, Institut für Materialphysik, Wien

Kopacz Ireneusz
Schafler Erhard
Zehetbauer Michael

Canada

Neutron Program for Materials Research, National Research Council of Canada, Chalk River Laboratories, Chalk River, Ontario *(formerly Austrian Academy of Sciences, Graz)*

Pabst Georg

Croatia
"Ruder Boskovic" Institute, Zagreb
Desnica-Frankovic I. Dunja
Desnica Uros V.
Pivac Branko
Salomon Kresimir
Turkovic Aleksandra

University of Split, Faculty of Faculty of Electrical and Mechanical
Engineering, and Naval Architecture, Split
Zulim I.

University of Zagreb, Institute for Physics, Zagreb
Milat Ognjen

Czech Republic
Academy of Sciences of the Czech Republic, Institute of Macromolecular Chemistry,
Prague
Baldrian Josef
Sikora A.
Steinhart Milos

Czech Technical University, Faculty of Nuclear Science and Physical Engineering,
Prague
Horky Martin

Finland
Åbo Akademi University, Dept. of Physical Chemistry, Materials Research Group,
Turku
Andersson Jenny
Lindén Mika

France
CNRS UMR 8612, University Paris-Sud, Paris
Artzner Franck
Kalnin Daniel
Lopez Christelle
Ollivon Michel

INSERM Unite 321, Paris
M.J.Chapman

Lure, Orsay / Paris
Pierre Lesieur

University Paris 6, Chimie de la Matiere Condensee, Paris
Alonso Bruno
Babonneau Florence
Grosso David
Sanchez C.
Soler-Illia Galo

University Paris-Sud, Solid State Physics, Orsay/Paris
Albouy Pierre-Antoine

Germany

Bauhaus-Universität Weimar, F.A. Finger-Institut für Baustoffkunde, Weimar
Eckart A.

Hahn-Meitner-Institut, Berlin
Triolo Alessandro
Zizak Ivo

Max-Planck-Institut für Kohlenforschung, Mülheim / Ruhr
Ågren Patrik
Bussian Patrik

Techn. Universität Bergakademie Freiberg, Inst. für Werkstofftechnik, Freiberg
Biermann Horst

Universität Erlangen-Nürnberg, Inst. für Werkstoffwissenschaften, Lehrstuhl I, Erlangen
Pyczak Florian

Universität Leipzig, Institut für Massivbau und Baustofftechnologie, Leipzig
Häußler F.
Palzer S.

Universität Siegen, Walter Flex Strasse, 57068 Siegen
Besch Hans-Juergen
Orthen Andre'
Wagner Hendrik
Walenta Albert Heinrich

Hungary

Eötvös Lorand University, Institute for General Physics, Budapest
Hanak Peter
Simon Kornel
Ungár Tamas

India

Bhabha Atomic Research Centre, Solid State Physics Division, Trombay, Mumbai
Mazumder Subhasish

Indian Institute of Technology, Department of Chemistry, Madras
Bokare Alok D.
Palnaih Archita

Inter University Consortium for DAE Facilities, Univ. Campus, Khandwa Road, Indore
Amitesh Paul
Dasannacharya B.A.
Gupta Ajay
Gupta Ratnesh
Paul Neelima

Italy

CNR, Centro di Studio sui Meccanismi di Reazione, c/o Dept of Chemistry, Univ. La Sapienza, Rome
Mancini Giovanna

Sincrotrone Trieste, Trieste
Bernstorff Sigrid
Dubcek Pavo
Menk Ralf
Morello Christian

Università del Piemonte Orientale, Dip. Scienze e Tecnologie
Avanzate (DISTA), Alessandria
Croce Gianluca
Frache Alberto
Milannesio Marco

Università di Ancona, Istituto di Scienze Fisiche,Facolta' di Scienze Matematiche
Fisiche e Naturali, Ancona
Corsi Federica
Mariani Paolo
Pisani Michaela
Spinozzi Francesco
Teixeira Cilaine Veronica

Università di Firenze, Dip. Scienze Fisiologiche, Firenze
Bagni Maria Angela
Cecchi Giovanni
Colombini Barbara
Linari Marco
Lombardi Vincenzo
Lucii Leonardo
Piazzesi Gabriella

Reconditi Massimo

Università di Padova, Dep. of Mechanical Engineering, Padova
Maddalena Amadeo
Principi Giovanni

Università di Palermo, dipartimento di Chimica Fisica, Palermo
Crapanzano Laura
Di Giovanni Caterina
Geppi Marco
Lo Celso Fabrizio
Triolo Roberto

Università di Palermo, dipartimento d'Ingeneria, Palermo
Piccarolo Stefano
La Carruba Vincenzo

Università di Parma, dipartimento di Fisica
Favilla, Roberto

Università di Perugia, Dipartimento di Fisica and INFM, Perugia
Cinelli S.
Onori G.

University of Trieste, Dep. of Biochemistry, Biophysics and Macromolecular Chemistry, Trieste
Cesàro Attilio
Sussich Fabiana
Tiziani Stefano

University of Trieste, Dep. of Earth Sciences, Trieste
Princivalle Francesco

Poland

Institute of Coal Chemistry, Polish Academy of Sciences, Gliwice
Wolinska-Grabczyk A.

Institute of Nuclear Chemistry and Technology, Warsaw
Chmielewski A.G.
Griegoriew Helena

Polish Academy of Sciences, Institute of Physics, Warsaw
Domagala Jaroslaw

Polish Academy of Sciences, Institute of Metallurgy and Materials Science, Krakow
Bonarski Jan T.
Swiatek Zbigniew

Slovenia
National Institute of Chemistry, Ljubljana
Crnjak-Orel Z.

Spain
IIQAB-CSIC, Dep. Tecnologia de Tensioactius, Barcelona
Caelles Jaime
Cocera Merce
Carrera I.
Lopez Olga
de la Maza A.
Pons Ramon

Sweden
Department of Molecular Biology, Biomedical Center, SLU Uppsala
Forstner Michael
Friemann Rosemarie

Switzerland
University of Fribourg, Department of Physics, Fribourg
Schurtenberger Peter
Stradner Anna

The Netherlands
Laboratory of Macromolecular and Organic Chemistry, Technical University
Eindhoven
Kleppinger Ralf
Meijer E.W.

Philips Research Laboratories (Philips Natuurkundig Laboratorium), Eindhoven
Balkenende A. Ruud

United Kingdom
Heriot Watt University, Department of Chemistry, Edinburgh
Arrighi V.
Mc Ewen I.J.
Holmes Paul

University Laboratory of Physiology, Oxford
Ashley Christopher C
Griffiths Peter J.

University of Edinburgh, Dept. Preclinical Veterinary Sciences, R.(D.)S.V.S., Summerhall, Edinburgh
> *Ashley Richard H.*
> *Bradshaw Jeremy P.*
> *Darkes Malcolm J.*
> *Harroun Thad*
> *Pratt Nicola*

The University of Edinburgh, Dept. of Physics and Astronomy, R.(D.)S.V.S., Summerhall, Edinburgh
> *Stefan Egelhaaf*

USA

Mount Sinai School of Medicine, New York, NY
> *Triolo Fabio G.*

Oak Ridge National Laboratory, Oak Ridge TN
> *Sonder E.*
> *White C.W.*
> *Zuhr R.A.*

List of Performed Experiments

2000 (first half year)

Proposal	Proposer	Institution	Country	Title	Research Area
1999070	Piccarolo Stefano	Università di Palermo - Dipartimento di Ingegneria Chimica dei Processi e dei Materiali	Italy	SAXS/WAXS study of the structural and morphological rearrangements of the mesophases in quenched iPB-1 and sPP	Chemistry
1999103	Schurten-berger Peter	ETH-Zürich - Institut für Polymere	Switzerland	Transient Structures in the Micelle-to-Vesicle Transition of Bile Salt/Lecithin Systems	Life Sciences
1999199	Kriechbaum Manfred	Austrian Academy of Sciences (A.A.S.)-Inst. of Biophysics and X-Ray Structure Re-search (IBR), Graz	Austria	Time-resolved SAXS-experiments of the unfolding and folding process of the enzyme creatine kinase	Life Sciences
1999202	Bradshaw Jeremy P.	University of Edinburgh, Dept. Preclinical Veterinary Sciences, Edinburgh	United Kingdom	Mechanism of membrane disruption by human islet amyloid polypeptide	Life Sciences
1999214	Triolo Alessandro	Hahn Meitner Institut, Berlin	Germany	Phase Diagram Characterization of solid state Polymer Electrolytes: PEO-NaSCN and PEO-LiTriflate	Chemistry
1999218	Triolo Alessandro	Hahn Meitner Institut, Berlin	Germany	iPP-limonene and iPP-a-pinene blends: phase diagram characterization by combined SAXS-WAXS	Chemistry
1999219	Triolo Alessandro	Hahn Meitner Institut, Berlin	Germany	Critical Micellar Density for block copolymers in SC-CO_2	Chemistry
1999231	Biermann Horst	Universität Erlangen-Nürnberg - Inst. für Werkstoffwissen-schaften	Germany	Microbeam X-ray diffraction investigation of materials with heterogeneous microstructure: Influence of the local chemical composition on the internal stresses	Materials Sciences
1999233	Forstner Michael	University of Uppsala - Dept. of Cell and Structural Molecular Biology	Sweden	Thermal denaturation of proteins from a thermophilic organism	Life Sciences
1999234	Babonneau Florence	Universite' Paris 6 - Chimie de la Matiere Condensee	France	Time resolved in-situ X-ray diffraction study of the formation of mesoporous silica films	Chemistry
1999240	Baldrian Josef	Czech Academy of Sciences - Inst. of Macromolecular Chemistry, Prague	Czech Republic	Time-resolved SAXS/WAXS Studies on Macromolecular Materials: Structure Development in PEO/PEO-PPO Blends	Physics
1999261	Lombardi Vincenzo	Universita' di Firenze - Dip. di Scienze Fisiologiche	Italy	Combined mechanical and X-ray diffraction study on the molecular aspect of muscle contraction	Life Sciences

1999264	Paris Oskar	A.A.S. - University of Leoben - Erich Schmid Inst. für Material-wissenschaft	Austria	Correlation of degree of mineralization with mineral crystal size in human trabecular and osteonal bone in normal and pathological cases	Physics
1999270	Haeussler Frank	Universität Leipzig - Wirtschafts-wissenschaftliche Fakultät Institut für Massivbau und Baustoff-technologie	Germany	Time dependent structural studies on hydrating cement clinker phases and Portland cement by SAXS and WAXS	Materials Sciences
1999274	Grigoriew Helena	Institute of Nuclear Chemistry and Technology, Warsaw	Poland	Temperature time-resolved SAXS study of polyurethane - penetrant systems	Physics
1999281	Mancini Giovanna	C.N.R. - C.S. Meccanismi di Reazione	Italy	Stereochemical Recognition in Selfassemblies	Chemistry
1999283	Rappolt Michael	A.A.S. - IBR, Graz	Austria	Structural investigation of the sub-main transition in highly aligned lecithin bilayers	Life Sciences
1999299	Grigoriew Helena	Institute of Nuclear Chemistry and Technology, Warsaw	Poland	Depth-sensitive SAXS study of permeation in dense polymer membrane	Physics
1999320	Rappolt Michael	A.A.S. - IBR, Graz	Austria	Simultaneous Time-Resolved X-ray Diffraction and Differential Scanning Calorimetry for New Standards in Phase Diagramming	Life Sciences
1999341	Pavel Nikolaus	Universität GHS Siegen - Dept. of Physics	Germany	Detector tests on novel 1-d and 2-d gaseous x-ray detectors	Instrumen-tation
1999342	Cesáro Attilio	Universita' di Trieste - Dip. Biochim., Biofisica, Chim. Macromol.	Italy	In-situ dynamics of phase transitions of trehalose polymorphic forms involved in cryptobiosys	Life Science
1999351	Neubauer Angela	TSP Nano-engineering, Vienna	Austria	In-situ Assembly of S-layers on Silicon-Surfaces Studied by GISAXS	Life Sciences
1999358	Amenitsch Heinz	A.A.S. - IBR, Graz	Austria	Time-Resolved-Study on Phospholipids Langmuir-Blodgett-Films and their Interaction with Delta-Lysin	Life Sciences
1999361	Kleppinger Ralf	FOM - Inst. for Atomic and Molecular Physics (AMOLF), Amsterdam	Netherlands	The Role of Structural Defects and their Creation in Highly Ordered Triblock Copolymer Networks	Physics
1999366	Mazumder Subhasish	Bhabha Atomic Research Centre, Solid State Physics Division, Mumbay	India	Kinetics of spinodal decomposition in Cu-9Ni6Sn at different temperatures	Materials Science
1999374	Zehetbauer Michael	Universität Wien - Inst. für Materialphysik	Austria	In-Situ Synchrotron Bragg Peak Profile Analysis of Microstructural Parameters During Discontinuous Plastic Deformation of fcc Metals	Materials Science

| 1999375 | Zehetbauer Michael | Universität Wien - Inst. für Materialphysik | Austria | Structure Disturbances of Near-Surface Areas in Implanted Silicon Platelets for Solar Cells | Materials Science |
| **Test** | SAXS-Group & Ollivon, Michel | A.A.S. - IBR, Graz & Sincrotrone Trieste & CNRS UMR, University Paris-Sud | Austria & Italy & France | Calorimetry Tests & Crystallization in milk fat globules after quenching | Instrumen-tation & Life Sciences |

2000 (second half year)

Proposal	Proposer	Institution	Country	Title	Research Area
2000003	Mariani Paolo	Università di Ancona - Ist. di Scienze Fisiche	Italy	Time-resolved structural study of alpha-B crystallin in solution	Life Sciences
2000040	Triolo Alessandro	Hahn Meitner Institut, Berlin	Germany	Local Order in amorphous polymers: effect of side-chains	Chemistry
2000091 Long Term	Mariani Paolo	Università di Ancona - Ist. di Scienze Fisiche	Italy	Phase behaviour, molecular conformation and compressibility of inverse lipid systems	Biophysics
2000093	Principi Giovanni	Università di Padova - Dip. Ingegneria Meccanica (Settore Materiali)	Italy	Small angle x-ray scattering study of amorphous to nanocrystalline transformation in Fe-Cu-Nb-Si-B and Fe-Cu-Zr-B alloys	Physics
2000098	Teixeira Cilaine Veronica	Università di Ancona - Ist. di Scienze Fisiche	Italy	The kinetics of conformational changes and denaturation of tissue Transglutaminase induced by ligands and temperature through time-resolved technique	Life Sciences
2000102	Kriechbaum Manfred	A.A.S. - IBR, Graz	Austria	Protein folding mechanisms and kinetics	Life Sciences
2000103 Long Term	Besch Hans-Jürgen	Universität GHS Siegen - Dept. of Physics	Germany	Test measurements on advanced gaseous detectors for time resolved SAXS experiments	Technology/Instrumen-tation
2000107	Triolo Alessandro	Hahn Meitner Institut, Berlin	Germany	iPP blends: crystallization kinetics via combined SAXS-WAXS techniques	Materials Science
2000110 Long Term	Triolo Alessandro	Hahn Meitner Institut, Berlin	Germany	Critical Micellisation Density (CMD): a Synchrotron SAXS Structural Study of the Unimer-Aggregate Transition of block-copolymers in near- and super-critical fluids	Chemistry
2000126	Desnica Uros	Ruder Boskovic Institute, Zagreb	Croatia	CdS nanocrystals formed in SiO_2 substrate by ion implantation	Physics
2000134	Babonneau Florence	Université Paris 6 - Chimie de la Matiere Condensee	France	Time resolved in-situ X-ray diffraction study of the formation of mesoporous films	Chemistry
2000144	Pons Ramon	Consejo Superior de Investigaciones Cientìficas - Inst. de Investigaciones Quimicas y Ambientales de Barcelona	Spain	Dynamics of non-equilibrium processes in surfactant systems	Physical Chemistry

2000158	Gamini Amelia	Università di Trieste - Dip. Biochim., Biofisica, Chim. Macromol.	Italy	Structural investigation of polysaccharide mesophases	Physical Chemistry / Biophysics
2000164	Pivac Branko	Ruder Boskovic Institute, Zagreb	Croatia	Oxygen precipitation in crystalline silicon	Physics
2000168	Cecchi Giovanni	Università di Firenze - Dip. di Scienze Fisiologiche	Italy	Time resolved mechanical and X-ray diffraction studies on single frog muscle cells	Life Sciences
2000171 Long Term	Paris Oskar	A.A.S. - University of Leoben - Erich Schmid Inst. für Material-wissenschaft	Austria	Correlation between Degree of Mineralization and Mineral Crystal Size in differently mineralized Connective Tissue	Materials Science
2000182 Long Term	Laggner Peter	A.A.S. - IBR, Graz	Austria	MemPeptide: Self-Assembly and Structural Dynamics of Membrane-Mimetic Systems: 1. Anomalous swelling in phospholipid bilayers 2. Salt-induced phase separation in the liquid crystalline phase of phosphatidylcholines 3. Non-linear concentration effects of cholesterol on lipid bilayers studied by pressure scanning 4. High pressure X-ray surface diffraction on highly aligned lipid systems under excess water conditions	Life Sciences
2000201	Forstner Michael	Univ. of Uppsala - Dept. of Cell and Molecular Biology (ICM) -Structural Molecular Biology	Sweden	Thermal denaturation of proteins from a thermophilic organism	Life Sciences
2000202	Amenitsch Heinz	A.A.S. - IBR, Graz	Austria	Nucleation and Growth of ZnS Particles in the Early Stages	Chemistry
2000204	Forstner Michael	Univ. of Uppsala - Dept. of Cell and Molecular Biology (ICM) -Structural Molecular Biology	Sweden	Control of actin turnover by the actin depolymerizing factor from Toxoplasma gondii	Life Sciences
2000209 Long Term	Zehetbauer Michael	Universität Wien - Inst. für Materialphysik	Austria	Spatial Distribution of Deformation Induced Lattice Defects in Ultrafine-Grained and Nanostructured Metallic Materials	Materials Science
In-house research	Dubcek Pavo	Sincrotrone Trieste S.C.p.A.	Italy	Grazing incidence small angle X-ray scattering investigation of structural changes in annealed H implanted monocrystalline silicon	Physics
Test	Patnaik Archita	Dep. of Chemistry, Indian Institute of Technology, Madras	India	Phase Transitions in a Schiff's base liquid crystal probed by small angle x-ray scattering	Chemistry

User Statistics

1. Number of submitted proposals and assigned shifts from 1995 until December 2001

The Austrian SAXS-beamline at ELETTRA opened to users in September 1996. Since then many experiments have been performed related to the fields of life science, material science, physics, biophysics, chemistry, medical science, technology and instrumentation.

From September 96 on users gained access to the SAXS-beamline on the basis of the proposals received for the periods shown in Fig. 1. The assignment of beamtime at this beamline is done separately for the group of "General Users" (GU) and the "Collaborating Research Group" (CRG), i.e., the Austrian users. Beamtime was assigned to the proposals of each group in the order of the rating received by the Scientific Committee, and up to the maximum number of shifts available to each group according to the contract between "The Austrian Academy of Sciences" and the "Sincrotrone Trieste". Until December 1997 up to 55 % of the beamtime was given to CRG, up to 30 % to GU, and 15% was reserved for maintenance purposes. From January 98 to June 2001 the quota for beamtime was up to 35 % for CRG, up to 50 % for GU, and again 15% reserved for maintenance purposes. From July 2001 on the two contingents for user proposals from CRG and GU will receive up to 35% of the beamtime each. The remaining 30 % of beamtime will be used for inhouse research projects as well as for maintenance purposes.

Fig. 1 gives an overview of the numbers of received proposals, the numbers of requested and assigned shifts, as well as the percentage between assigned and requested shifts. Included in Fig.1 are also the same data for the period End 1995 - August 1996, during which some beamtime had been given already to users in order to perform first pilot- and test-experiments together with the beamline staff. These first experiments during the commissioning phase were not yet based on proposals, since the goal was mostly to evaluate and improve the performance of the beamline and the equipment of its experimental station. As can be seen in Fig.1, the request for beamtime at the SAXS-beamline increased continuously and strongly until the first half year of 1999 (also during the period Sept.-Dec. 1997, if one takes into account that this period was only 4 instead 6 month long, and that for this reason less proposals were submitted). Then, probably due to the high rejection rates, the number of submitted proposals decreased somewhat, and - since the last three semesters - remains now about constant.

In 2000, in total 73 proposals (13 from CRG, and 60 from GU) were submitted. From these 21 proposals (3 from CRG, 18 from GU, corresponding to a total of 29 % (or 23 % CRG and 30 % GU, respectively) were submitted by "new" usergroups, i.e. groups which so far had never beamtime at the SAXS beamline. From these 10 proposals (3 CRG, 7 GU) were accepted, corresponding to 21 % (23 %, 20 %, respectively) of all accepted proposals.

Fig. 1 (Next page): The statistical information about the beamtime periods since end of 1995 are given for the groups "CRG", and "GU" separately, as well as for both together ("Total"). Shown are, for all beamtime periods:
 (a) Number of received proposals
 (b) Number of requested shifts
 (c) Number of assigned shifts
 (d) Relation between assigned and requested shifts
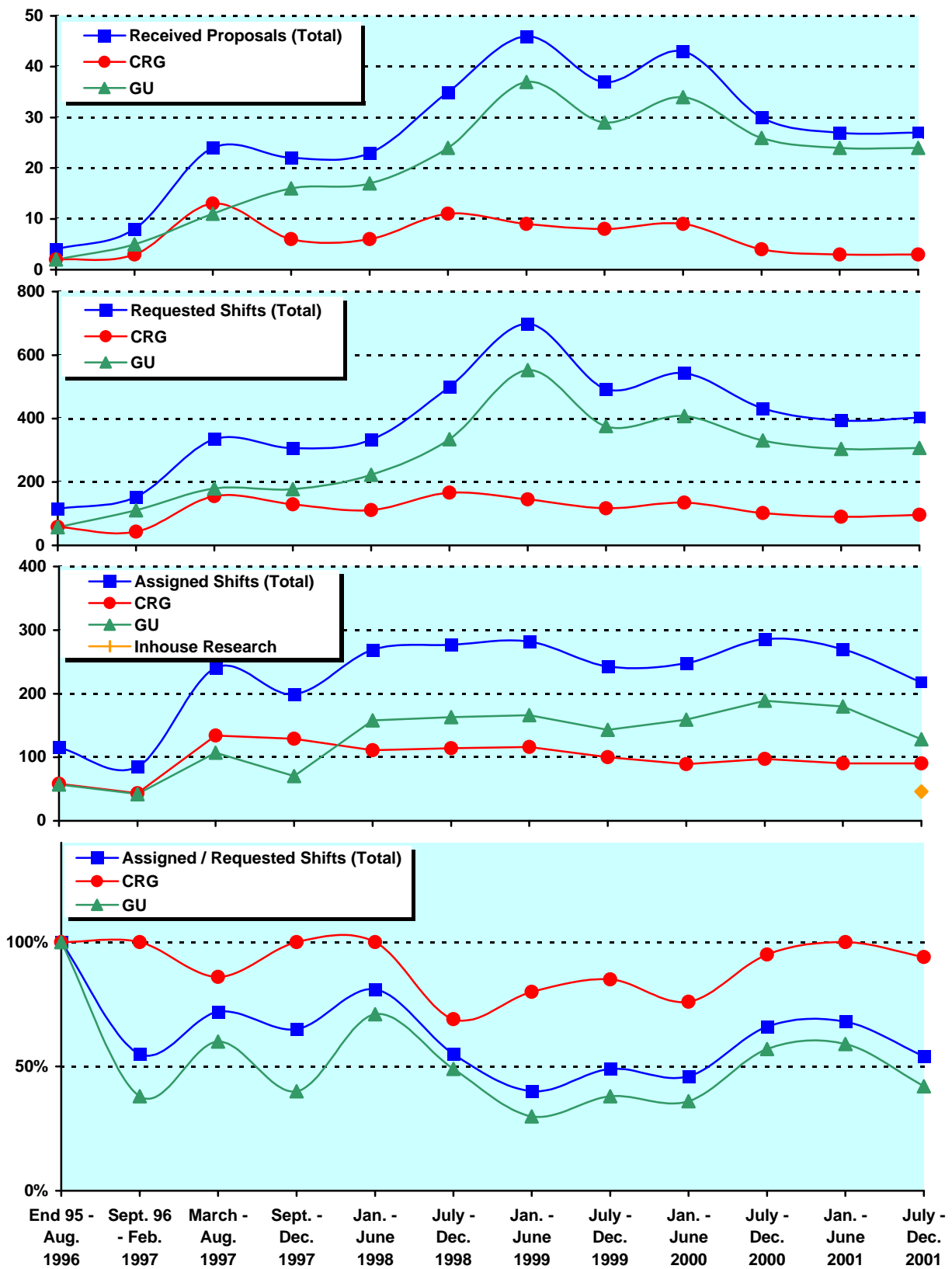
2. Provenience of Users

During 2000, 140 users from 56 institutes in 18 countries have performed experiments at the SAXS beamline. In Fig. 2 are shown both the provenience of these users, and of their respective institutes. Each user or institute was counted only once, even though many users performed experiments in both beamtime periods of 2000.
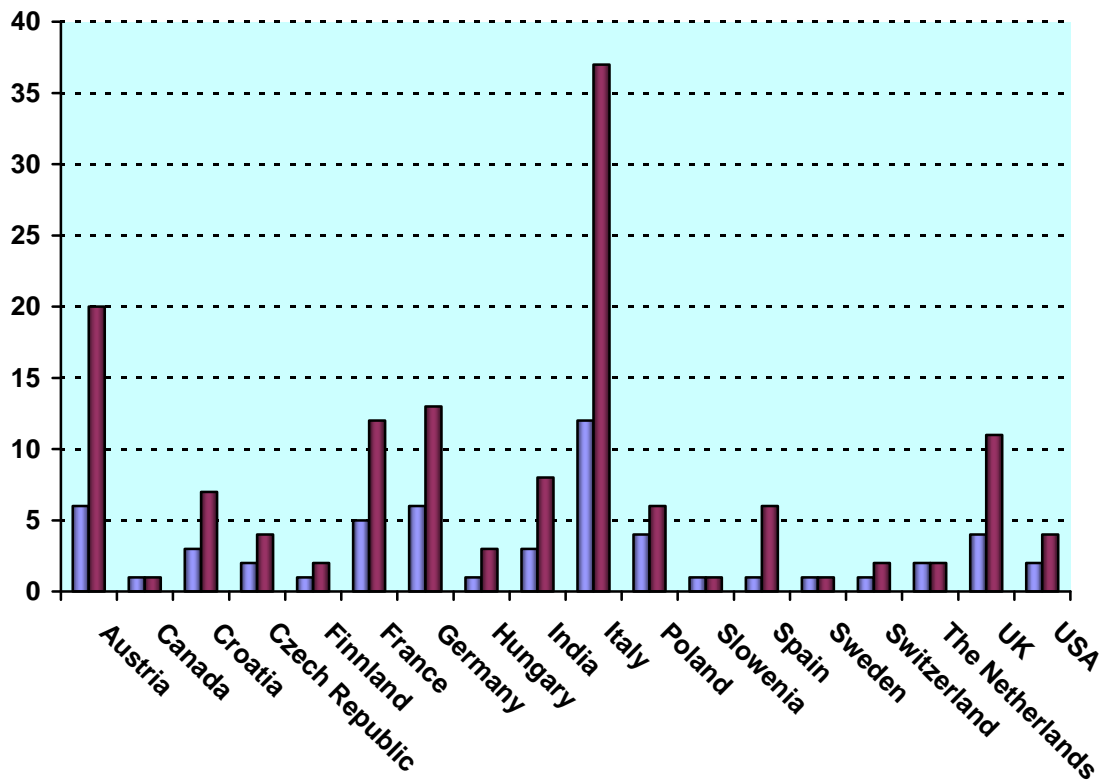

Fig. 2: Provenience of users (dark grey) and of their corresponding institutes (light grey).

3. Documentation of experimental results

As could be expected, with the start of user-operation at the SAXS-beamline the number of contributions to conferences started to increase strongly. With a delay of one year - the average time needed for paper publications - also the number of publications increased accordingly, as can be seen in Fig. 3 .
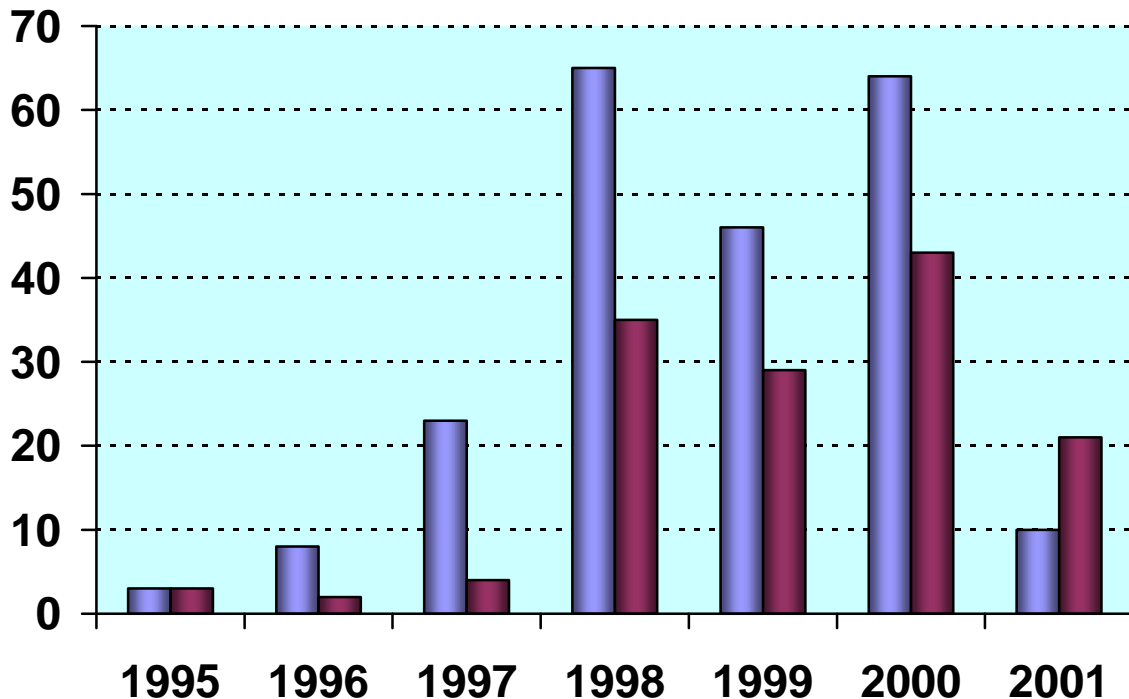

Fig. 3: Number of conference contributions (light grey) and of refereed paper publications (dark grey) for the years 1995-2000. Also refereed papers, which have been published in 2001, or were in press until 30.4.01, are included.

In addition, from 1995 until March 2001, the following documentations based on instrumentation of the SAXS-beamline, or on data taken with it, have been produced.

Unrefereed publications:
      Technical Reports on Instrumentation: 5
      Contributions to Elettra Newsletters: 13
      Contributions to Elettra Highlights: 9
PhD Thesis: 12
Diploma Thesis :   11

Experimental Possibilities at the SAXS-beamline

1. Installation of an in-line Differential Scanning Calorimeter (DSC)

As a new instrument in the SAXS sample-stage pool an in-line micro-calorimeter built by the group of Michel Ollivon (CNRS, Paris, France) has been installed and tested at the beamline. With this instrument, simultaneous time-resolved synchrotron X-ray Diffraction as a function of the Temperature (XRDT) and high sensitivity DSC can be taken from the same sample.

The microcalorimetry and XRDT scans can be performed at any heating rate comprised between 0.1 and 10 °C/min with a 0.01 °C temperature resolution in the range -30/+130 °C. However, maximum cooling rates are T dependent and 10°C/min rates cannot be sustained below 30°C since cooling efficiency is a temperature dependent process. Microcalorimetry scans can be recorded independently, and also simultaniously, of X-ray patterns. The microcalorimeter head can also be used as a temperature controlled sample-holder for X-ray measurements while not recording a microcalorimetry signal. Isothermal microcalorimetry is also possible when a time dependent thermal event such as meta-stable state relaxation or self-evolving reaction, is expected. The sample capillaries have a diameter of 1.5 mm and are filled over a length of 10 mm.

MICROCALIX WORKING PRINCIPLE

The working principle of the microcalorimeter MICROCALIX is based on the comparison of the thermal fluxes exchanged between a sample and a reference, and their respective environments. Figure 1 shows schematically the respective positions of the components in the measuring head in which the sample and the reference are placed to be compared for thermal properties.
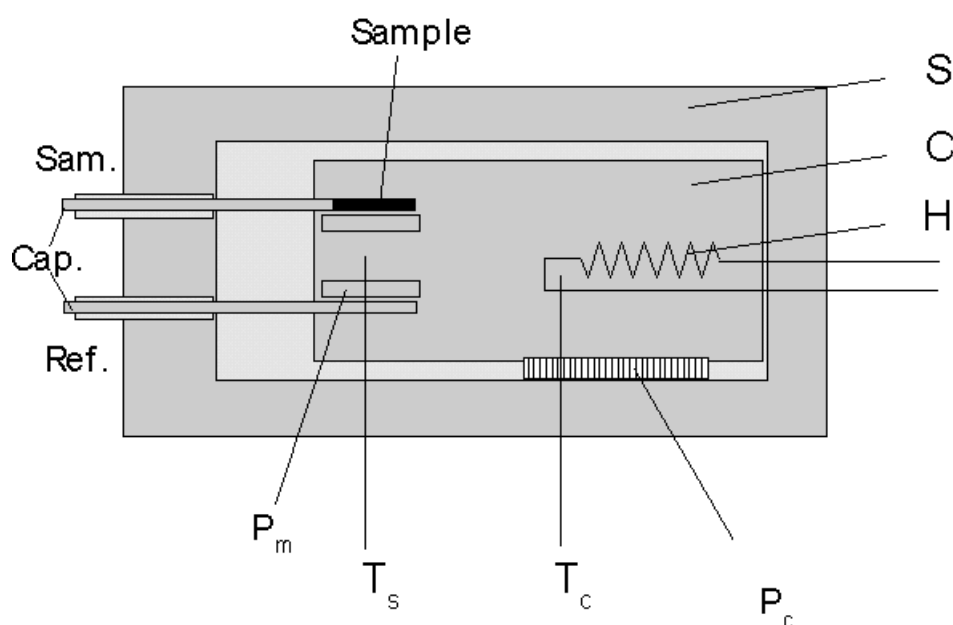

Fig. 1: Schematic horizontal cut of the MICROCALIX head block diagram showing the component locations in the microcalorimeter head. Sample (Sam.) and reference (Ref.) located in capillaries (Cap.) are placed near measurement Peltier modules (Pm). The measuring cell (C) temperature (Tc) is controlled through a heating resistor (H) and a Control Peltier module (Pc). The temperature of screen (S) is externally controlled by a cryostat and

circulating fluid. Both the sample (Ts) and the cell (Tc) temperatures are measured by thermocouples T_s and T_c, respectively. The MICROCALIX head is shown in Fig 2.

The respective sample and reference thermal fluxes are measured by Peltier modules and compared. The difference signal which is proportional to the flux difference is applied to a microvoltmeter and recorded. The variations as a function of temperature of this signal represent the DSC recording. The absolute value of this signal is proportional to the difference of specific heat between the sample and the reference (Δc_p), weighted by their respective masses. As thermal variations of specific heat in the absence of transitions are continuous and monotonic (soft), the signal variation in the absence of first or second order thermal event can be fitted by a straight line or a second order equation (this is also the usual way to express specific heat variations as a function of temperature, $c_p = a + bT + cT^2$). The signal variation recorded in this condition is termed baseline. Then, any deviation of the DSC signal from the baseline corresponds to thermal events (first or second order transitions).

Generally, deviations from the baseline resembling to a peak are first order transitions while others (e.g. baseline jumps and breakpoints) are second order. The calorimetric signal is in fact recorded as a function of time, $S = f(t)$. However, in a scanning calorimeter, the temperature variation is linearly related to the time $\Delta T \propto \Delta t$. The energy exchanged by the sample during a transition is proportional to the area of the peak above the baseline. This energy corresponds to a melting enthalpy (noted ΔH and expressed in mcal/sec). The ratio (melting enthalpy/melting temperature) ($\Delta H/T_m$) provides the entropy measurement associated to the transition.
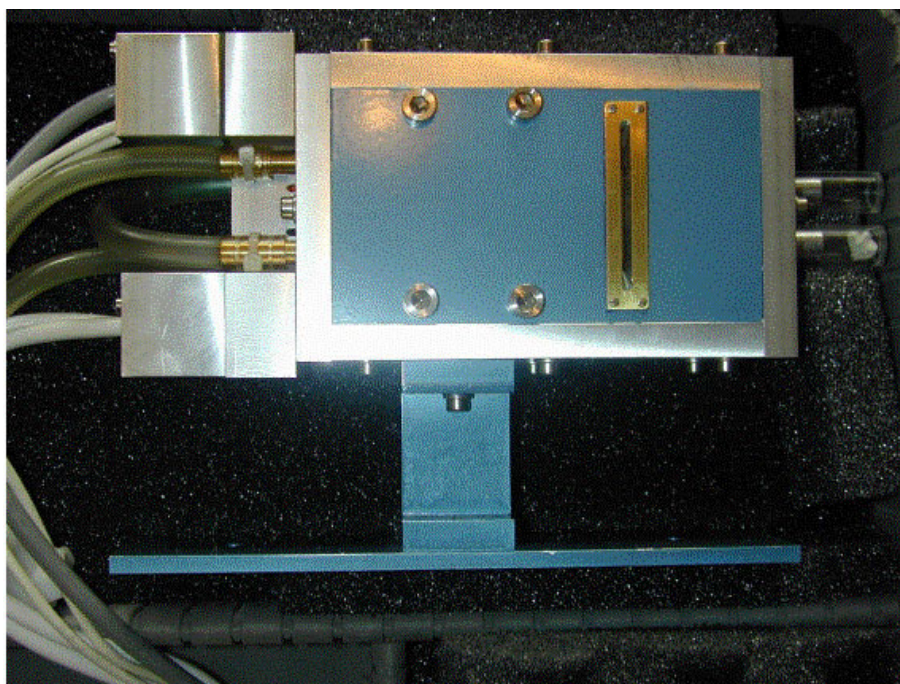

Fig. 2: Photo of the MICROCALIX cell (the vertical X-ray window is seen at right)

2. Improvements in High Pressure Cell System

High-pressure measurements have been among the first special sample environment techniques available at the SAXS (see previous Annual SAXS-Reports, and [1, 2]). SWAXS measurements of samples under pressure can be performed from 1 to 2500 bar, from 0 to 80 °C in the scattering angle region up to 30 degrees, both in the static or time-resolved mode, e.g. p-jump or p-scan, with a time-resolution down to the ms range.

In the year 2000 these measurements have accomplished their fourth season of a relatively successful performance. During that period several considerable improvements in the hardware, its control and integration with the data acquisition system and other sample-parameters controls have been achieved.

Recently, in most applications diamond windows of 0.75 mm thickness (each) are used. The transmission of one pair (entrance and exit window) is 0.1 at 8 keV, i.e. lower than 0.3, the value for the originally used 1.5 mm thick Be-windows. However the loss in intensity is more than compensated for by the considerably lower background scattering of diamond thus leading to higher q-resolution in the experiments.

The sample thickness can be 0.6-4.0 mm, with a volume of approximately 0.5-3 mm^3 completely irradiated by pin-hole collimated (< 1.0 mm diameter) X-rays.

Positioning of the high-pressure cell on the sample stage and in the beam-path is now reliable, fast and stable. The cell needs not to be realigned for typically a whole series of measurements. The system is flexible and can be built according to the needs of the particular experiment. Fig. 3 shows as an example the large set-up used for kinetic measurements.

Fig. 3: Scheme of the high pressure cell system layout. T: temperature sensor; P: p-sensor; M: motor; G: pressure generator; hp-cell: high pressure cell; FC: frequency converter, ADC: analog to digital converter.

The difficult problem of separation of samples from the pressurising media has been addressed several ways. For some experiments Teflon pistons in the cell are sufficient. More delicate measurements (were samples must not get in contact with the pressurising medium)

were performed using a small Al or brass capsule sealed with Kapton or Mylar foils fitted inside into the high-pressure cell. These foils, however, show a pressure dependent parasitic SAXS-scattering. A further improvement should be a membrane separator build directly in the pressure cell, or a piston separator placed right next to it in the hydraulic system. A newly designed piston-separator is currently in the testing phase. It will mainly simplify the use of various other liquids as solvents for the sample, besides of water being the main pressurising media. So far, when other liquids were used (ethanol or octanol) the system had to be re-filled entirely with them.

In principle, gaseous media can be employed as well. N_2 has been successfully tested and measurements in supercritical CO_2 became frequent.

An AC-frequency controller has been used to drive the three-phase motor of the pressure generator. It speeds up the necessary service-runs but mainly gives a possibility of precise pressure scans of any speed within a broad range (e.g. ca. 1.0 bar/s - 50 bar/s in the case of water as pressurising medium, and a typical sample volume). Slower pressure changes allow more accurate control. The reasons are that the limited sampling rate of the control hardware becomes more appropriate and the pressurised system has more time to equilibrate. Alternatively, dynamic processes can be studied in pressure-jump relaxation experiments with jump amplitudes up to 2.5 kbar/10ms in both directions (pressurising and depressurising jumps).

Beside bulk samples also grazing incidence experiments using silicon wafer with highly aligned samples on its surface inserted in the high-pressure cell have been carried out successfully.

Last but not least should be mentioned, that now a user friendly software is used for running the experiments. The Fig. 4 shows some of the recently at the SAXS-beamline performed experiments.
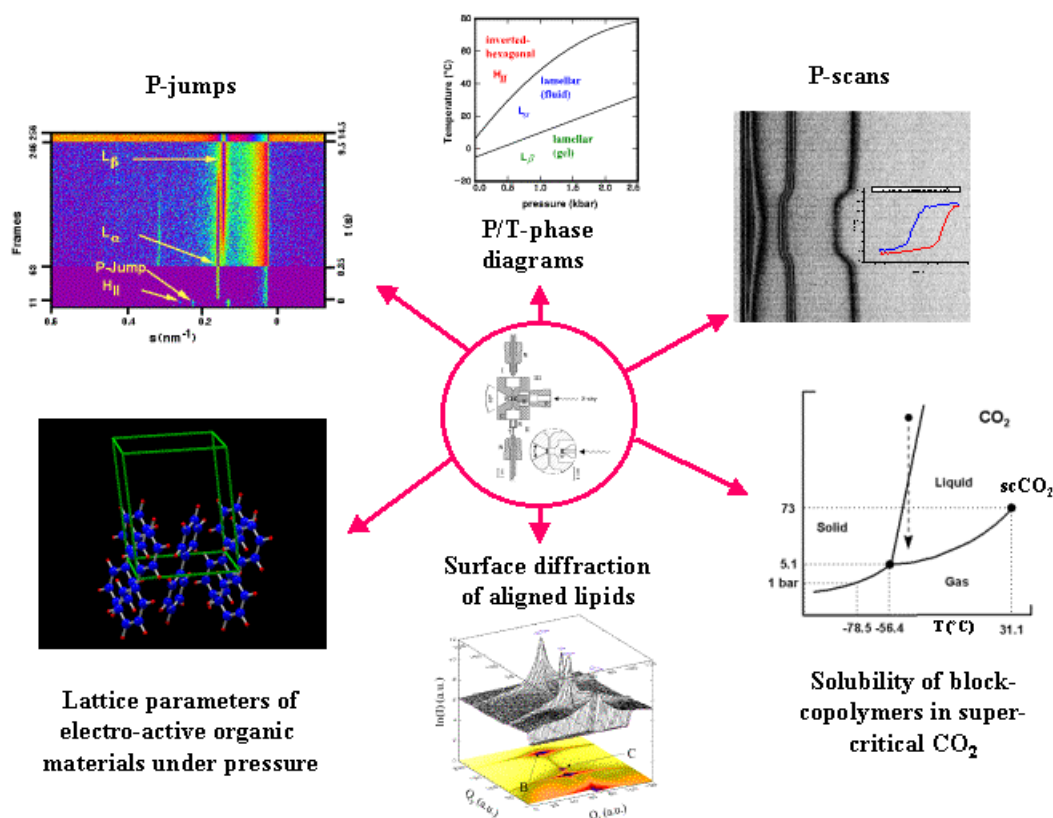

Fig. 4: Collection of some typical examples of high pressure experiments, demonstrating the versatility of the high-pressure cell system. Shown are, from higher left corner, clockwise:

1. + 2. SAXS-pattern and phase diagram of lipids, 3. for details see contribution of Vidal et al., page 69, 4. for details see contribution of Triolo et al., page 110, 5. for details see contribution of Amenitsch et al., page 51 and 6. electro-active material under pressure.

[1] K. Pressl, M. Kriechbaum , M. Steinhart and P. Laggner, "High Pressure Cell for Small- and Wide-Angle X-Ray Scattering",Rev. Sci. Instrum. 68 (1997) 4588-4592

[2] M. Steinhart, M. Kriechbaum, K. Pressl, H. Amenitsch, P. Laggner, S. Bernstorff, "High-Pressure Instrument for Small- and Wide-Angle X-Ray Scattering. II. Time-Resolved Experiments", Rev. Sci. Instrum. 72/2, 1540-1545 (1999)

3. Implementation of an exhaust system

For the experimental station a fume cover and a chemical exhaust system for toxic gases has been developed and installed (e.g., page 91 & 97). Thus now it is possible to e.g. also study in-situ chemical reactions, during which toxic gases might develop.

4. Accessible SAXS and WAXS ranges

Simultaneous SAXS- and WAXS-measurements can be performed using a linear sensitive gas detector (Gabriel type, windows size 8 x 100 mm, active length 86.1 mm with a resolution of 0.135 mm/channel) for the WAXS-range, and either a second linear Gabriel type detector (windows size 10 x 150 mm, active length 134 mm with a resolution of 0.159 mm/channel), or the 2D CCD-system for the SAXS-range. A specially designed vacuum chamber (SWAXS-nose, see Annual Report of 1996/97, p. 32) allows to use both scattering areas below (for SAXS) and above (for WAXS) the direct beam, respectively.

Depending on the photon energy maximum SAXS resolutions of 2000 Å (5.4 keV) or 630 Å (16 keV) are available. The available possible WAXS-ranges are summarised in Table 1. The overall length of the SWAXS-nose in the horizontal direction, measured from the sample position, is 512 mm and the fixed sample to WAXS-detector distance is 324 mm. At the shortest SAXS camera-length an overlap in the d-spacings covered by the SAXS- and WAXS-detectors, respectively, is possible: then, the common regime lies around 9 Å.

Range	2θ [deg]	d-spacing (Å)		
		8 keV	5.4 keV	16 keV
1	9.4	*9.40*	14.03	4.27
	27.6	*3.23*	4.82	1.47
2	27.4	3.25	4.86	1.48
	45.6	1.99	2.97	0.90
3	45.4	2.00	2.98	0.91
	63.6	1.46	2.18	0.66
4	63.4	1.47	2.19	0.67
	81.6	1.18	1.76	0.54

Table 1: Possible d-spacing ranges in the WAXS-regime at the SAXS-beamline at ELETTRA. Since the WAXS-detector can be mounted at four different fixed positions on the SWAXS-nose (range 1-4), with the three possible energy choices (5.4, 8 and 16 keV) this results in 12 different d-spacing regimes. In italic the most common choice (8 keV, range 1) is highlighted. This range is suited for experiments, e.g., on lipid-systems and (bio)polymers.

5. Available sample manipulations stages

1. General

Usually the sample is mounted onto the sample alignment stage which allows the user to place the sample into the beam with a precision of 5 µm (resolution: 1 µm). In fig. 5 the ranges for vertical and horizontal alignment as well as the maximum dimensions of the sample holders are given. The maximum weight on the sample stage is limited to 10 kg. In case the envelope dimensions of a sophisticated sample station provided by the users are slightly larger than those given in fig. 5, the user can ask the beamline responsible for a check up of his space requirements. If it does not fit at all to these specifications, user equipment can also be mounted directly onto the optical table, which allows much larger spatial dimensions.
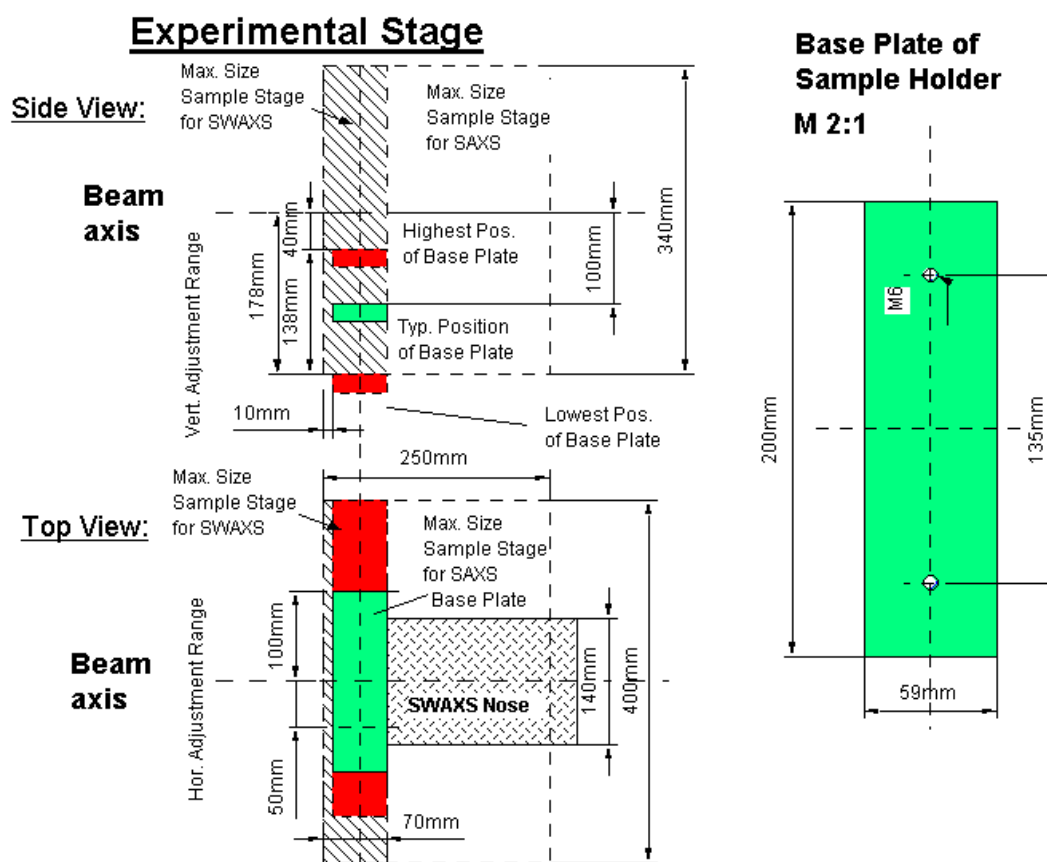
Fig. 5: Maximum dimensions and alignment range of the sample holder to be mounted via a base-plate onto the standard alignment stage (left), and dimensions of the base-plate (right).

2. Sample holders

As standard equipment for liquid samples Paar capillaries (diameter: 1 and 2 mm) are used thermostated with the KHR (electrical heating) or KPR (Peltier heating/cooling) sample holders (Anton Paar, Graz, Austria). For use in these sample holders flow through capillaries and Gel holders are standard equipment. Temperature scans can be performed with KHR and/or KPR in the range from 0 to 150 °C, typically the precision and the stability of this systems is < 0.1 °C. Additionally thermostats for temperature control or cooling proposes can

be used at the beamline (0-95 °C, at present). Helium and Nitrogen gas bottles are available at the beamline, for other gases please contact the beamline responsible.

Multiple-sample holders can be mounted onto the standard sample manipulator. At present holders are available for measuring in automatic mode up to 30 solid samples at ambient temperature or up to 4 liquid or gel samples in the temperature range 0 – 95 °C.

3. Magnet System

For studying magnetic effects in samples, capillaries or sample holders with suitable dimensions can be mounted inside an electromagnet. Up to now a sample holder for standard Paar capillaries (Anton Paar, Graz, Austria) is available for ambient temperature only. The alignment of the magnetic field is horizontal or vertical (transversal to the photon beam). For short times the maximum magnetic field can be up to 1.5 T, and 1.0 T for continues operation, respectively, assuming a pole gab of 10 mm for both.

4. Stopped Flow Apparatus

A commercial stopped flow apparatus (manufactured by Bio-Logic, Paris, France), especially designed for Synchrotron Radiation SAXS investigations of conformation changes of proteins, nucleic acids and macromolecules, is available. The instrument consists of a 4 syringe cell with 3 mixer modules manufactured by Bio-Logic. Each syringe is driven independently from the others by an individual stepping-motor, which allows a high versatility of the mixing sequence (flow-rate, flow duration, sequential mixing). For example, injection sequences using one or up to 4 syringes, unequal filling of syringes, variable mixing ratio, reaction intermediate ageing in three- or four-syringe mode etc.. The solution flow can be entirely software-controlled via stepping motors, and can stop in a fraction of a millisecond.
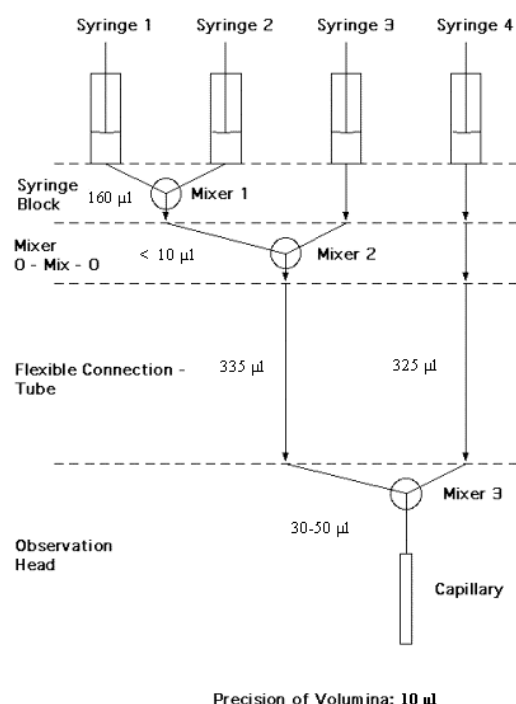
The software allows the set-up of the shot volumes of each of the 4 syringes in a certain time interval. Up to 20 mixing protocols can be programmed. Additionally macros for the repeated execution of individual frames can be defined. Furthermore, the input and output trigger accessible for user operation can be programmed. In the usual operation modus the start of rapid mixing sequence is triggered from our X-ray data-acquisition system (input trigger).

After the liquids have been rapidly mixed, they are filled within few ms into a 1 mm quartz capillary - situated in the X-ray beam- , which is thermostated with a water bath. Depending on the diffraction power of the sample time resolutions of up to 10 ms can be obtained.

Fig. 6: Sketch of the stop flow system.

The main parameter of the system are:

- Thermostated quartz capillary (1 mm)
- Temperature stability 0.1 °C
- Total sample used per mixing cycle (shot volume): 100 µl
- Maximum 2θ angle of 45°
- Total Volume 8 ml
- Dead volume 550 µl
- Speed: 0.045 – 6 ml/s
- Duration of flow 1 ms to 9999 ms/Phase
- Dead time: 1 ms
- Reservoir volume: 10 ml each

Further information can be found in the homepage: http://www.bio-logic.fr/

5. Grazing Incidence Small Angle X-ray Scattering

Grazing incidence studies on solid samples, thin film samples or Langmuir-Blodget-films can be performed using a specially designed sample holder, which can be rotated around 2 axes transversal to the beam. Furthermore the sample can be aligned by translating it in both directions transversal to the beam. The precisions are 0.001 deg for the rotations and 5 µm for the translations. Usually the system is set to reflect the beam in the vertical direction. According to the required protocol and the actual assembly of the rotation stages ω, θ, 2θ and φ scans can be performed.

6. Temperature Gradient Cell

A temperature gradient cell for X-ray scattering investigations on the thermal behaviour of soft matter manybody-systems, such as in gels, dispersions and solutions, has been developed. Depending on the adjustment of the temperature gradient in the sample, on the focus size of the X-ray beam and on the translational scanning precision an averaged thermal resolution of a few thousands of a degree can be achieved.

7. IR-Laser T-Jump System for Time-Resolved X-ray Scattering on Aqueous Solutions and Dispersions.

The Erbium-Glass Laser available at the SAXS-beamline (Dr. Rapp Optoelektronik, Hamburg, Germany) delivers a maximum of 4 J per 2ms pulse with a wavelength of 1.54 µm onto the sample. The laser-beam is guided by one prism onto the sample, which is filled in a glass capillary (1 or 2 mm in diameter) and Peltier or electronically thermostated in a metal sample holder (A. Paar, Graz, Austria). With a laser spotsize of maximal 7 mm in diameter a sample-volume of maximal 5.5 µl or 22 µl, respectively, is exposed to the laser-radiation. In a water-solutions/dispersions with an absorption coefficient of $A = 6.5$ cm^{-1} T-jumps up to 20 °C are possible.
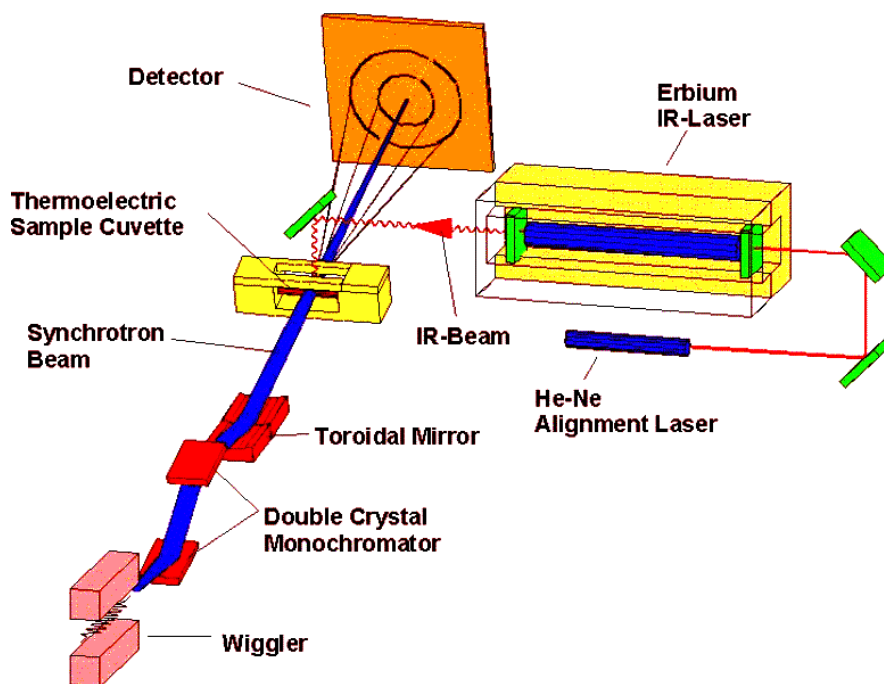
Fig. 7: Sketch of the T-jump set-up.

8. Oxford Cryostrem Cooler

The Cryostream cooler creates a cold environment only a few millimeters from the nozzle position. The temperature and the flow of the nitrogen gas stream is controlled and regulated by a Programmable Temperatur Controller based on an 'in stream' heater and a thermo-sensor before it passes out over the sample.

The system has been especially developed for X-ray crystallography to perform diffraction experiments on e.g. shock frozen bio-crystals. However, the programmable temperature controller allows further implication for SAXS-experiments, e.g., rapid temperature drops in solvents. The design of the Cryostream Cooler facilitates:

- nitrogen stream temperatures from -190 to 100 °C,
- a stability of 0.1 °C,
- a system that can be refilled without creating any disturbance of the temperature at the sample,
- temperature ramps can easily be carried out remotely controlled with scan rates up 6 °C/min
- individual temperature protocols can be cycled
- T-jumps in both directions can be performed by rapid transfer of the sample in a pre-cooled or -heated capillary using an fast syringe driver reaching a minimum temperature of -80 °C. Here, typical scan rates are about 15 °C/sec with a total process time in the order of 10 sec.

9. The 2D CCD-camera system

The CCD has a 115 mm diameter input phosphor screen made of a gadolinium oxysulphide polycrystalline layer. The screen is coupled by means of a fiber optic to the image intensifier. The image intensifier is coupled again with an additional taper to the CCD itself. The achieved spatial resolution of a pixel is 79 μm for the whole set-up.

The number of pixels is 1024 x 1024 and they can be pinned down to 2 x 2 and 4 x 4. The dynamic range of the CCD is 12 bit. The dark current of the CCD is in the order of 100 ADU (off-set) and the readout noise (read out speed: 10 MHz) is in the order of 6 ADU. (The CCD is cooled by multistage Peltier element for reducing the dark noise.) The intensifier gain is adjustable between 200 and 20000 photons full dynamic range. Typical readout times and exposure times are 150 ms and 100 ms, respectively. The readout times can be reduced down to 100 ms by using the pinning mode of the CCD. Between the frames additional wait times can be programmed e.g. for reducing the radiation damage in the sample or to extend the time for measuring long time processes.

For the external control a TTL trigger signal is provided (active low, when the CCD is accumulating an image), which is used to control the electromagnetic fast shutter of the beamline on one hand. On the other hand this signal can be used also to trigger processes as requested by the user.

The CCD is controlled by Image Pro+, which also includes non too sophisticated data treatment capabilities. The program is featuring a comprehensive set of functions, including:

- flat fielding/background corrections
- enhanced filters and FFT
- calibration utilities (spatial and intensity)
- segmentation and thresholding
- arithmetic logic operations
- various measurements, like surface, intensity, counts, profiles
- advanced macro management

The data are stored in 12 bit – TIFF format. At the present state up to 300 full images (1024 x 1024) can be recorded by the system, but a strict conservation of the timing sequence is maintained only for the first 15 - 17 frames until the RAM memory is full. Afterwards the images are stored in the virtual memory on the hard disk. At present a software development for the CCD readout system is under way to improve the stability of the readout cycles.

For the complete treatment of the 2D data Fit2D available from the ESRF is used, which is able to perform both interactive and "batch" data processing (homepage: http://www.esrf.fr/computing/expg/subgroups/data_analysis/FIT2D/index.html, programmed by Dr. Andy Hammersley) , which supports a complete spatial correction, flat field correction and background correction. Furthermore more elevated data-treatment can be performed within this software package, like circular integration, segment integration and similar.

User Contributions

1. Materials Science

INVESTIGATION OF LATTICE PARAMETER CHANGES IN NICKEL-BASE SUPERALLOYS DUE TO VARIATIONS IN THE LOCAL CHEMICAL COMPOSITION

H. Biermann[1], F. Pyczak[2], E. Schafler[3], S. Bernstorff[4] and H. Amenitsch[5]

1.) Institut für Werkstofftechnik, Technische Universität Bergakademie Freiberg, Gustav-Zeuner-Strasse 5, D-09596 Freiberg/Sachsen, Germany
2.) Institut für Werkstoffwissenschaften, Lehrstuhl I, Universität Erlangen-Nürnberg, Martensstrasse 5, D-91058 Erlangen, Germany
3.) Institut für Materialphysik, Universität Wien, Strudlhofgasse 4, 1090 Vienna, Austria
4.) Small Angle X-Ray Scattering Beamline (SAXS), Elettra Synchrotron, 34012 Basovizza, Trieste, Italy
5.) Institute of Biophysics and X-ray Structure Research, Austrian Academy of Sciences, Schmieldstr. 6, A8042, Graz, Austria

In modern nickel-base superalloys the content of so called refractory elements like rhenium, tungsten or tantalum is increased to improve the mechanical properties of the alloys. These elements are known for their tendency to segregate between dendritic cores and interdendritic regions of the alloys during the solidification of the material after the casting process. Hence the local chemical composition of the alloys vary and these variations of the local chemical composition affect also the local lattice parameters of the material.

Until now, these effects were only investigated by the use of Convergent beam electron diffraction (CBED) or utilizing sophisticated specimen preparation methods in conventional X-ray diffractometers [1,2]. Taking advantage of the high beam intensity accessible in the synchrotron it was possible to generate beam diameters of sufficient size on the specimen surface to measure these lattice parameter variations, which should occur on a length scale of some hundred microns, directly. With the help of a slit diaphragm the beam size was reduced to less than 100 µm (the actual beam diameter was checked with the help of an image plate and was smaller than the resolution limit of the plate).

Using this setup, a series of measurements in a nickel-base superalloy was performed scanning perpendicular to the dendritic structure of the material and recording X-ray profiles of the {002}-reflections. The distance between two subsequent X-ray measurements was chosen to be 100 µm. Many of the X-ray profiles show a distinct asymmetry because nickel-base superalloys are two phase materials with a so called γ'-precipitate phase embedded coherently in a γ-matrix. The lattice parameters of the two phases are slightly different and hence the recorded profiles are a superposition of the peaks of the precipitate and the matrix phase. The investigated experimental alloy contains rhenium as a refractory element, which is known to concentrate in the γ-matrix and to enrich in the dendritic cores. Rhenium increases the lattice constant of the γ-matrix and hence the X-ray profiles recorded in the dendritic cores should exhibit a more pronounced asymmetry. The measurement situation is shown in the upper left corner of figure 1. The specimen was etched and the dendritic structure is clearly visible. The series of measurements was performed along the line where the zero position is in the dendrite core. Figure 1 also shows the corresponding X-ray profiles. Due to the effect of the rhenium segregation the lattice constants of the matrix phase are modified near the dendritic core and hence the profiles at 0 and –100 µm show a asymmetric shape. All other profiles show a weaker asymmetry of the X-ray peaks, which is also in good agreement with the lower rhenium contents and hence smaller matrix lattice constant, which should be present in interdendritic regions. The result, that the most pronounced asymmetry is observed at –100 µm instead of 0 µm, could occur due to a miscalibration of the optical microscope, which was used to observe the X-ray spot position on the specimen surface. For the profiles at -200 and -300 µm the symmetric shape is not so pronounced as for the corresponding measurement

positions at 0 and 100 μm (assuming the dendritic core is located at the measurement position of -100 μm). Deviations of this kind can be explained with the occurrence of secondary dendrite arms clearly visible in figure 1. The rhenium concentration in those secondary dendrite arms is also higher than the rhenium concentration in the interdendritic regions and hence the asymmetry is more pronounced here. Unfortunately, it was not possible to control the beam position on the specimen with sufficient precision to decide, whether a single measurement position hits a secondary dendrite arm or an interdendritic region. The presented results are in good agreement with measurements of rhenium containing alloys known from literature [1,2].
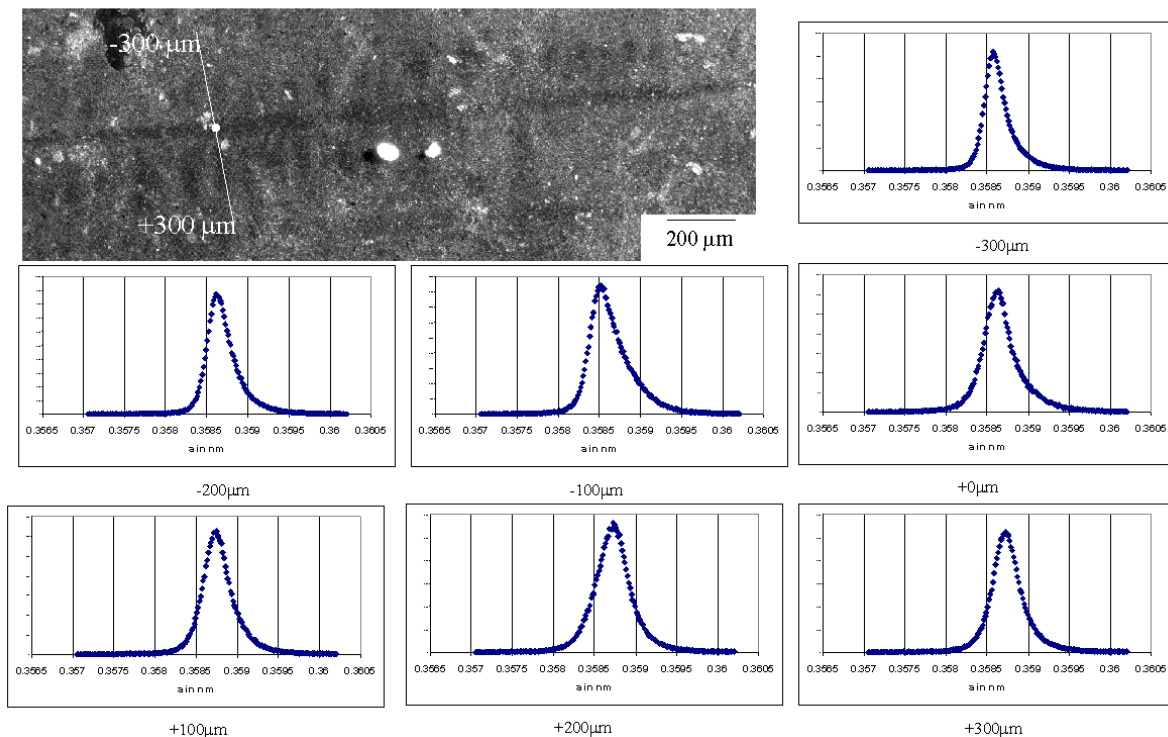
Figure 1. The measurement situation in the investigated specimen is shown in the upper left corner. The dot shows the position where the 0 μm pattern was recorded. All other measurements were performed along the white line with distances of 100 μm between two subsequent measurement positions. The X-ray profiles recorded at different measurement positions between dendritic core, secondary dendrite arms and interdendritic regions are also shown in the figure.

References:

[1] U. Brückner, A. Epishin, T. Link and K. Dressel, The influence of the dendritic structure on the γ/γ′-lattice misfit in the single-crystal nickel-base superalloy CMSX-4, Material Science and Engineering **A247**, 23-31 (1998).
[2] R. Völkl, U. Glatzel and M. Feller-Kniepmeier, Measurement of the lattice misfit in the single crystal nickel based superalloys CMSX-4, SRR 99 and SC 16 by convergent beam electron diffraction, Acta mater. **46**, 4395-4404 (1998).

STRUCTURE DISTURBANCES OF NEAR-SURFACE AREAS
IN IMPLANTED SILICON PLATELETS FOR SOLAR CELLS

J.T. Bonarski[1], Z. Swiatek[1], I. Kopacz[2], M. Zehetbauer[2] and S. Bernstorff[3]

1.) Institute of Metallurgy and Materials Science, Polish Academy of Sciences, Ul.Reymonta 25, PL-30-059 Kraków, Poland
2.) Institute of Materials Physics, Vienna University, Strudlhofgasse 4, A-1090 Wien, Austria
3.) SAXS Group, Synchrotron ELETTRA, Basovizza, I-34012 Trieste, Italy

Synchrotron experiments have been concerned to the analysis of a diffraction "response" of modified Si-single crystal (001) solar cell element with the *n-p* junction and the *Back Surface Field* (BSF). The modification consisted in generating of a so called buried amorphized layer due to implantation of P^+ ions, followed by thermal treatment, and by creating a subtle porosity layer on the top of ca. 50% of area of the PV element surface. Two particular areas (with porous layer, and with amorphized and porous layers) of the modified structure have been investigated by means of synchrotron radiation of 8 keV. Rocking curves as well as line profiles have been registered. A part of the collected data is presented in Figs.1 and 2. As a result of data processing by means of standard procedures [1,2], the following informations on the structure investigated have been obtained:

- The implantation did induce local as well as extended deformation fields in sub-surface areas of the Si crystal. They result from a significant decrease of structural order in those regions due to implantation of P^+ ions;

- Fourier analysis applied to the experimental rocking curves enabled the quantitative evaluation of the effective size of the structure disturbances L_{eff}, the mean lattice deformation $\bar{e} = (\Delta d/d)$, and the mean-square deformation of it. From calculations, maximum mean deformation of the damaged layer amounts to $\varepsilon_{max} \sim 4.0 \times 10^{-3}$. The radiation defects in the crystalline-amorphous transition area (below the amorphized layer) induced a lattice deformation of order $\varepsilon \sim 3\text{-}5 \times 10^{-4}$. The thicknesses of transition area, and that of amorphised layer, were found to be $\sim$300nm, and $\sim$100nm, respectively.

- The largest lattice damages are located at an effective depth of 400 to 800nm below the crystal surface. The values are about two times higher than the penetration range of P^+ ions at applied energy and doze. Moreover, the identified area of elastic deformations reached depths in between 1000 to 1300 nm.

The obtained values of parameters inform us on the structure perfection of the tested photovoltaic element. As it has been shown above, the structural changes and/or disturbances in the sample area with amorphized and porous layers are much larger than those in the second area (with porous layer only). The dislocation density obtained from the ions' doze applied was found to reach up to $\sim 10^{15} m^{-2}$ which is almost two orders more than the value found for the reference (non-implanted) crystals.

As for the sample area with porous layer, the identified spreading of the diffraction reflections indicates the presence of strain gradients in the bulk of sample. The lattice deformation has been estimated as $\Delta d/d = 3\text{-}9 \times 10^{-5}$. FWHM parameters of experimental rocking curves reached a maximum of 12'', being ca. 50% higher than their theoretical value. The "tails" of the registered curves have been non-symmetrically extended above the background level which proves diffuse scattering from the structure inhomogeneities as well as from the pores.

A more detailed analysis of the results will be prepared for presentation at the ECM' 2001 conference in Krakow.
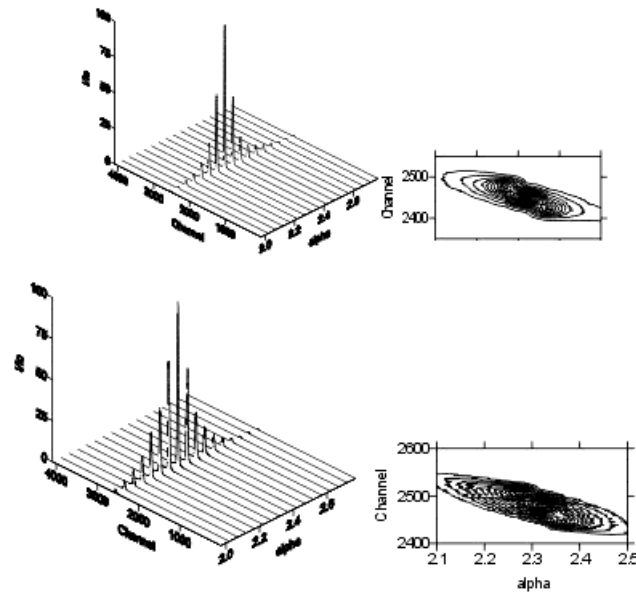
Figure 1. Experimental line profiles at different sample tilt angles *alpha* (as a part of pole figure) for Si (001) after structure modification by porous Si layer formation (top) and additional previous ion implantation (bottom).
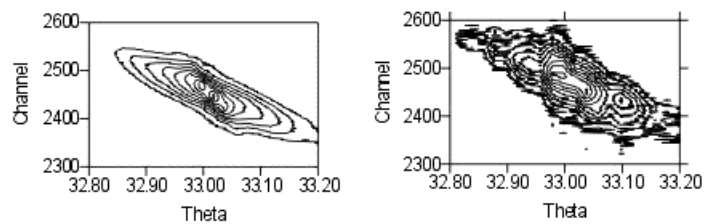

Figure 2. Experimental rocking curves registered by means of a linear position-sensitive detector, for Si (001) after structure modification by porous Si layer formation (left) and additional previous ion implantation (right).

References:

[1] Z. Swiatek, J.T. Bonarski, R. Ciach, I.M. Fodchuk, M.D. Raransky and O.G. Guminsky; X-ray diffracting investigation of strain distribution in silicon implanted by phosphorous, Opto-Electronics Review **8**, 421-425 (2000)

[2] J.T. Bonarski, M.Zehetbauer, Z. Swiatek, I.M. Fodchuk, I. Kopacz, S.Bernstorff and H.Amenitsch; Structural Disturbances of Near-Surface Areas in Silicon Solar Cell Modified by P$^+$ Ion Implantation and Thermal Treatment, Opto-Electronics Review **8**, 323-327 (2000)

TIME DEPENDENT STRUCTURAL STUDIES ON HYDRATING CEMENT CLINKER PHASES AND PORTLAND CEMENT BY SAXS AND WAXS

F. Häußler[1], J. Tritthart[2], H. Amenitsch[4] , S. Palzer[1], A. Eckart[3] and P. Laggner[4]

1.) Institut für Massivbau und Baustofftechnologie der Universität Leipzig, Marschner Straße 31, Leipzig, Germany.
2.) Technische Versuchs- und Forschungsanstalt (TVFA) der Technischen Universität Graz, Stremayrgasse 11, Graz, Austria
3.) F.A. Finger-Institut für Baustoffkunde der Bauhaus-Universität Weimar, Coudraystraße 11, Weimar, Germany
4.) Institut für Biophysik und Röntgenstrukturforschung/ ÖAW, Steyrergasse 17/VI, Graz, Austria

Introduction

The objective of these experiments was to investigate the hydrating process of the clinker minerals tricalcium silicate (C_3S) and tricalcium aluminate (C_3A) as well as of ordinary Portland cement (OPC) in the early stage of hydration (several hours after the onset of hydration). It should be given new information about the complex hydration process within the first day. The non-hydrated clinker mineral phases and the OPC were partly converted into hydration products (e.g. C-S-H-phases, pseudo-hexagonal Portlandite crystals). Using the 16 keV setting of the SAXS beamline SAXS and WAXS patterns caused by microstructural objects (nm and μm range) as well as crystalline phases were observed (i) at room

Experimental Results

Combined and time resolved SAXS and WAXS studies in the early stage of hydration (until ~ 21 hours) were realized [1]. Here the results of SAXS and WAXS investigations concerning the time dependent changes in the microstructure of hydrating C_3S in dependence on the temperature are discussed exemplarily. Hence the microstructural changes of the amorphous phases (via SAXS) could be correlated with that one in the crystalline phases (via WAXS). – The samples were prepared and put into a sample holder allowing the measurement of up to four samples successively. The sample thickness was 0.3 mm. The water-solid ratio was about 0.40 (exactly 0.43 and 0.41 for hydration at room temperature and 40°C, respectively). The C_3S hydration was studied between 14 and 930 minutes at room temperature as well as between 14 and 1304 minutes at 40°C.
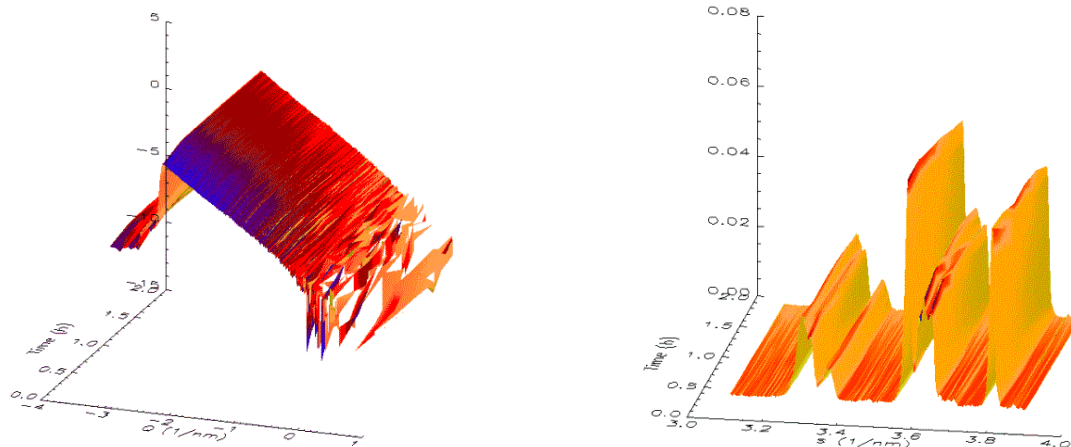

Figures 1a-1b: SAXS (left) and WAXS (right) scattering pattern of hydrating C_3S, w/s=0.43, at room temperature.
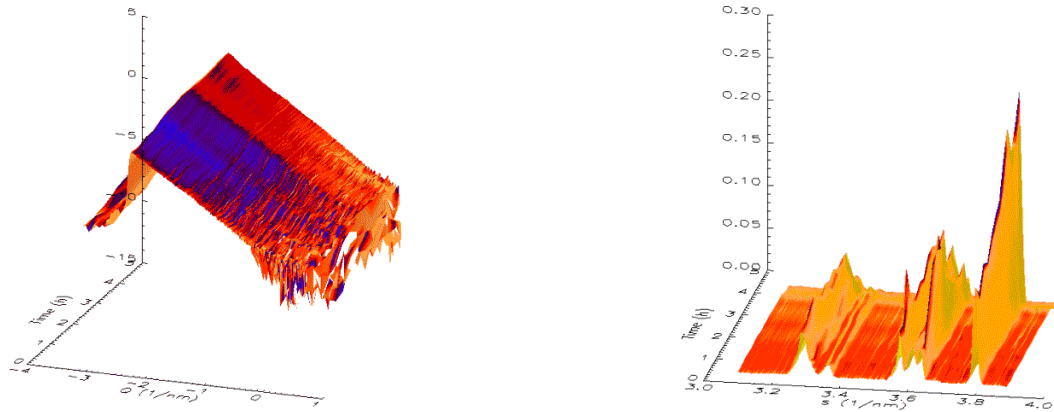
Figures 2a-2b: SAXS (left) and WAXS (right) scattering pattern of hydrating C$_3$S, w/s=0.41, at 40°C. Here an increased rate of structural changes is evident.

In figures 1a to 2b a set of time dependent SAXS- and WAXS curves are shown. In figures 3 and 4 the time dependent behaviour of the SAXS and WAXS patterns covering total data acquisition time range are shown. In fig. 3 the power law behaviour of the scattering curve quantified by $I(Q) \sim \dfrac{d\Sigma}{d\Omega}(Q) = A(1) \cdot Q^{-A(2)} + A(3)$ is characterized to discuss the results in terms of fractality. Here two regions are visible. The first one points at surface fractal structures (4>A(2)>3) whereas the second one is very short and might allow to apply the Porod law (A(2)=4). The changes in the microstructure are visible in the changed SAXS pattern (A(2) is marked at the upper lines with 3.1, 3.5, and 4.0).
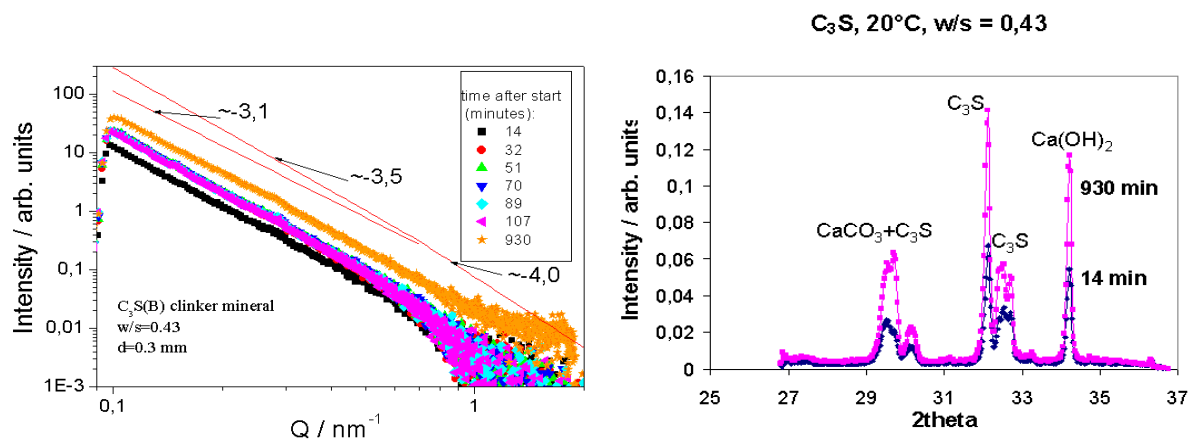
Figures 3-4: Several SAXS (left) and WAXS (right) curves of hydrating C$_3$S (w/s=0.43, at room temperature) covering the time range of 14 till 930 minutes after start. During the hydration process the power law behaviour (left, exponents) is changed.

The small 2θ range in the WAXS curves (fig. 4) limits the observable crystalline phases. The C$_3$S phases and Portlandite phases could be monitored. Calcite crystals emerging by carbonation (reaction of C$_3$S with CO$_2$ in air) are evident. Their relevant peak is superposed by a C$_3$S peak (at 2θ = 29.4). Some crystalline peaks of Portlandite as one hydration product and C$_3$S are shown.

References:

[1] F. Häußler and J. Tritthart, SANS und SAXS zur Untersuchung der Zementsteinmikrostruktur – SAXS/WAXS-Studien zur Hydratationsfrühphase am Synchrotron Triest, Seminarvortrag, TVFA der TU Graz, 20.06.2000

CORRELATION OF DEGREE OF MINERALIZATION AND MINERAL CRYSTAL SIZE IN DIFFERENTLY MINERALIZED TISSUES

W. Tesch[1,2], P. Roschger[2], O. Paris[1], R. Puxkandl[1], J. Keckes[1], S. Bernstorff[3], H. Amenitsch[4], P. Fratzl[1]

1.) Erich Schmid Institute of Material Science, Austrian Academy of Sciences, and Institute of Metal Physics, University of Leoben, Jahnstr. 12, 8700 Leoben, Austria

2.) Ludwig Boltzmann Institute of Osteology, 4th Medical Department, Hanusch Hospital, Heinrich Collin Str. 30, Vienna, Austria

3.) Sincrotone Trieste, Area Science Park, Trieste, Italy

4.) Institute of Biophysics and X-Ray Structure Research, Austrian, Academy of Sciences, Schmiedlstraße 6, 8042 Graz, Austria

Bone has a varying arrangement of structures at many length scales which work in concert to perform diverse mechanical, biological and chemical functions. Discussing bone architecture, scale is of importance as the structure is hierarchically organized and complex. The basic building block is the mineralized collagen fibril. The fibrous protein collagen constitutes the main component of a three-dimensional matrix into which the mineral dahllite, also known as carbonated apatite ($Ca_5(PO_4,CO_3)_3(OH)$) forms. The degree of mineralization of the collagenous matrix as well as the size, shape and arrangement of the mineral crystals are crucial parameters which influence the stability and properties of the whole structure. During bone remodeling, new bone is formed onto older, matured bone. These new formed bone areas are less mineralized at the beginning. Therefore there is a gradient of degree of mineralization from new formed to matured bone areas. Especially in bone diseases with disturbed mineralization, alterations of the volume fraction might occur. A change in volume fraction can happen due to a change of the *number* of mineral particles per unit volume or by change of the *particle size*. Therefore it is indispensable to understand how these parameters change with the degree of mineralization.

In order to correlate the crystal size with the bone mineral density distribution (BMDD), small angle x-ray scattering (SAXS) and quantitative backscattered electron imaging (qBEI) studies were performed on identical bone areas. After embedding, the bone samples were first investigated by qBEI. The BMMD was determined and regions of interest for the SAXS measurements defined. Afterwards, 20 µm thick bone sections were prepared for SAXS containing the same surface as investigated with qBEI.

A SAXS setup with a beam size of 20 µm, developed by our working group [1,2] was used at the SAXS beamline at ELETTRA. Two-dimensional x-ray transmission scans with a spatial resolution of 20 µm, performed within the corresponding qBEI regions, provided the quantitative positional link between qBEI and the following SAXS measurement. Linear scans containing 20-40 frames (steps of 20 µm) were taken at several positions. Special care was taken to monitor the primary beam intensity. In all measurements, the so called T-parameter increases from new formed to matured bone (Fig. 1). The T-parameter is defined by $T=4\,\Phi\,(1-\Phi)/\sigma$, were Φ is the volume and σ the specific surface of mineral particles. The quantitative correlation with qBEI is still in work.

In order to find out how the basic collagen-mineral structure is altered in the case of bone diseases (Paget, Zöliakie and Osteomalazia), measurements on the pathologically new formed bone areas were done also. As an example, we were able for the first time to monitor severe disturbances of the size and shape-distribution of the mineral particles within one part (trabecula) of the bone (Fig. 2). This was due to the fact, that diseased new bone has been laid down on former formed healthy bone.

This outstanding results show the importance of position resolved SAXS measurements using synchrotron-radiation, not only in the field of material science, but also in the field of medical research.

References:

[1] I. Zizak, O. Paris, P. Roschger, S. Bernstorff, H. Amenitsch, K. Klaushofer and P. Fratzl, Investigation of bone and cartilage by synchrotron scanning-SAXS and –WAXD with micrometer resolution, J Appl Cryst 33, 820-823 (2000)

[2] P. Paris, I. Zizak, H. Lichtenegger, P. Roschger, K. Klaushofer and P. Fratzl, Analysis of the hierarchical structure of biological tissues by scanning X-ray scattering using a micro-beam, Cellular and Molecular Biology 46, 993-1004 (2000)

[3] P. Fratzl, S. Schreiber, P. Roschger, M.H. Lafage, G. Rodan and K. Klaushofer, Effects of sodium fluoride and alendronate on the bone mineral in minipigs: a small-angle X-ray scattering and backscattered electron imaging study, J Bone Miner Res, 11 [2], 248-253 (1996)
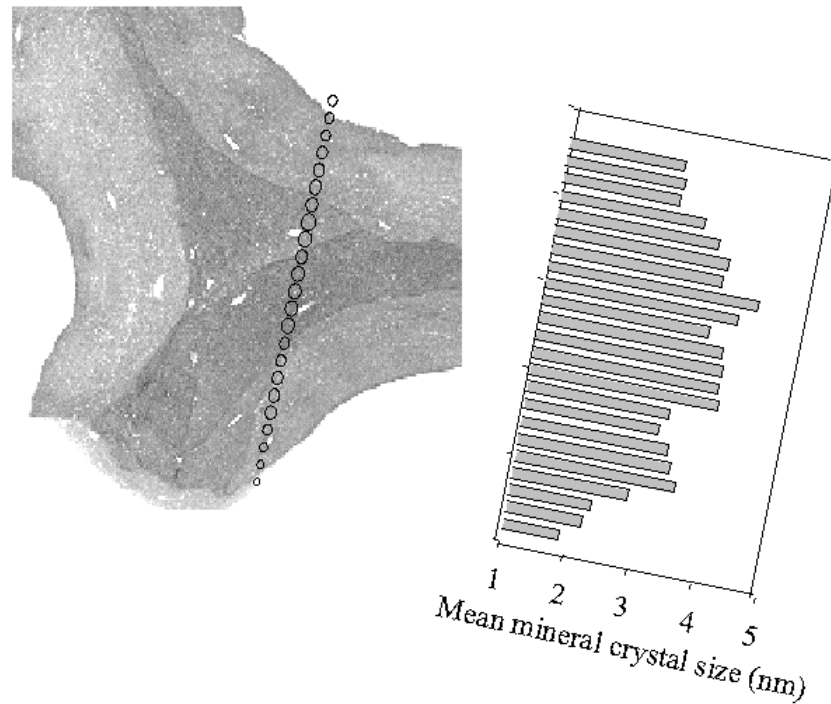
Figure 1: Quantitative backscattered electron image with SAXS line scan overlaid (black circles). Different gray levels indicate different mineral density, i.e., dark = high mineral density; bright = low mineral density. The size of the black circles and the bar diagram show how the mean mineral particle size is increasing within matured bone (dark gray area).
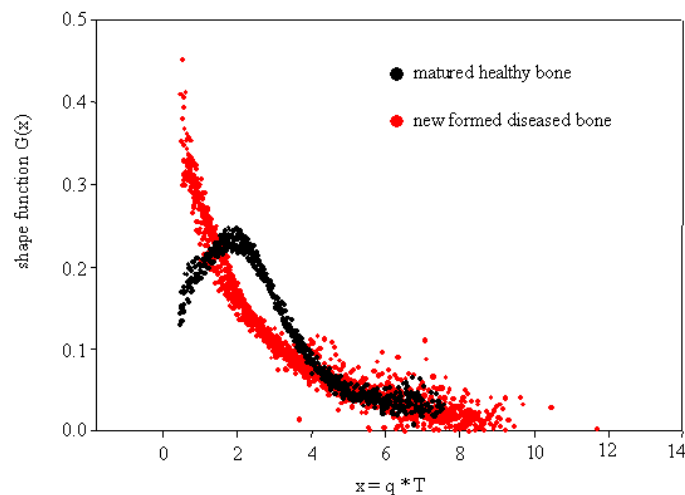
Figure 2: The shape function G(x) [3] of the mineral particles in matured healthy bone (black) and new formed diseased bone (gray) is shown (q....scattering vector; T... T-parameter). The data stem from a line scan of 500 µm (step 20µm) of an trabecula, which runs from healthy into new formed diseased bone.

IN-SITU SYNCHROTRON BRAGG PEAK PROFILE ANALYSIS OF MICROSTRUCTURAL PARAMETERS DURING DISCONTINUOUS PLASTIC DEFORMATION OF FCC METALS

M. Zehetbauer[1], T. Ungar[2], R. Pippan[3], E. Schafler[1], P. Hanak[2], I. Kopacz[1, 3], K. Simon[2], S. Bernstorff[4] and H. Amenitsch[5]

1.) Institute of Materials Physics, Vienna University, Strudlhofg. 4, A-1090 Wien, Austria
2.) Institute of General Physics, Eötvös University, Pazmany Peter Setany 1/A, H-1518 Budapest, Hungary
3.) Erich Schmid Institute for Materials Science, Austr.Acad.of Sciences, Jahnstr.12, A-8700 Leoben, Austria
4.) SAXS Group, Synchrotron ELETTRA, Basovizza, I-34012 Trieste, Italy
5.) Institute of Biophysics and X-Ray Structure Research, Austr.Acad.of Sciences, Schmiedlstr. 6, A-8042 Graz, Austria

Time resolved in-situ Synchrotron line profile analyses have been started by the preceding project [1] in order to measure for the first time the evolution of lattice defect (dislocation) density and internal stresses *during* plastic deformation of metals. Due to the great importance of experimental results for plasticity research in general this proposal aimed to reproduce the first results [1] and to add investigations on the effects of load relaxation and removal to the quantities mentioned, not only in polycrystals but also in single crystals.
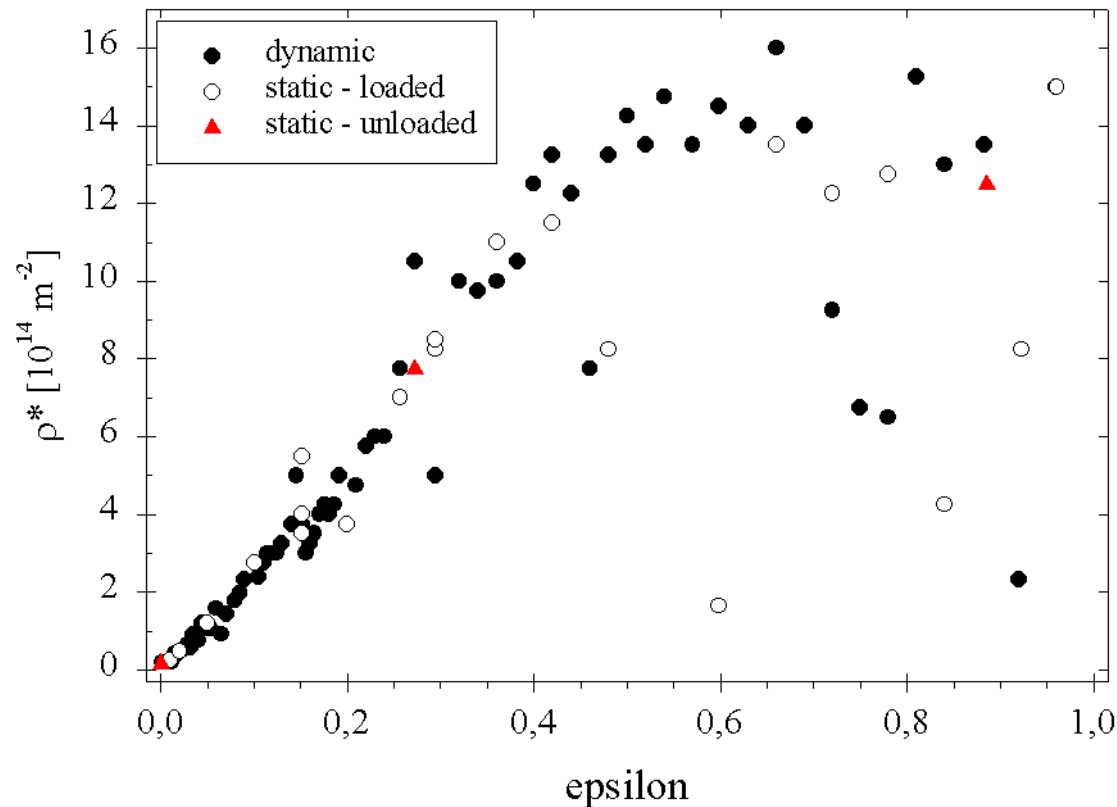
Fig. 1 shows the evolution of dislocation density ρ^* in a Cu polycrystal, as a function of plastic compression ε, for different loading conditions. It can be concluded that the difference of dislocation density during deformation (full circles, dynamic case) and after load relaxation or unloading (empty circles and triangles, for static loaded and unloaded case, respectively) is little (if any) after small amounts of plastic deformations, but gets increasingly large when a critical strain of about $\varepsilon = 0.4$ is exceeded: Similar to the observations reported in [1], fluctuations of the dislocation density as well as of the long range internal stresses occur

which are particularly significant in the dynamic case. They can be attributed to the transformation of cell walls from a dipole to a tilt arrangement being observed in previous independent experiments by the authors [2, 3].
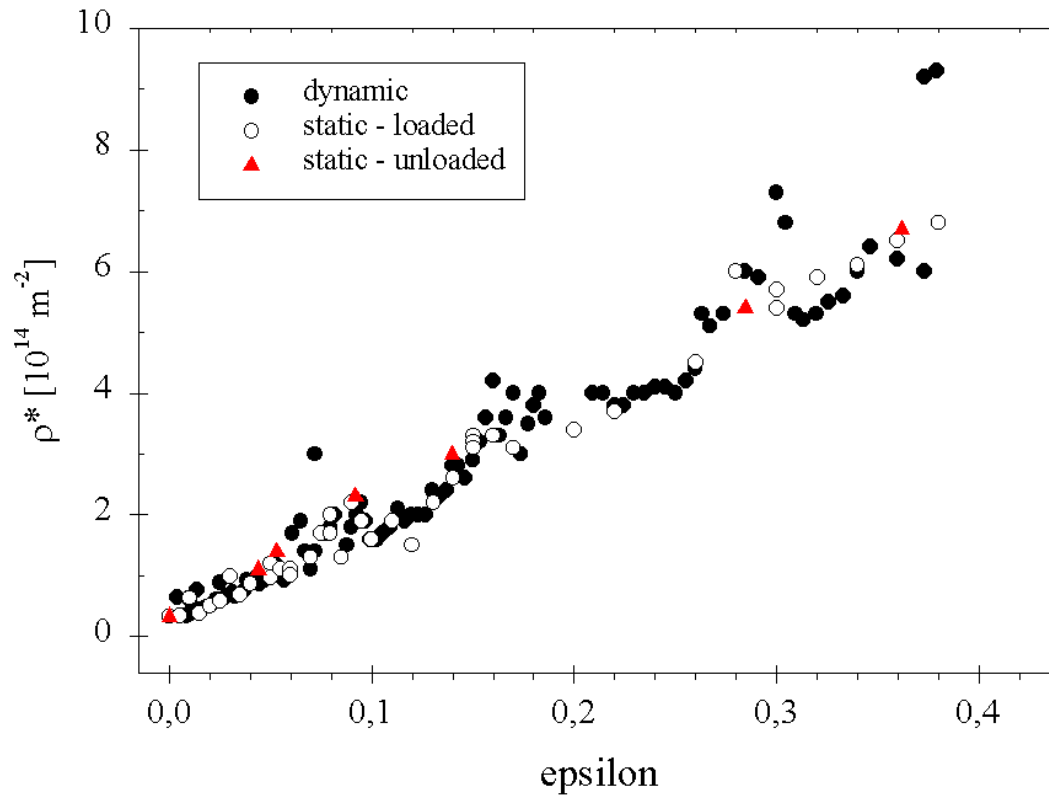
In **Fig. 2** the evolution of dislocation density ρ^* dependent on deformation ε from first experiments of Cu (100)-oriented single crystals are demonstrated. Analogous to the behaviour of polycrystals, the differences between the dislocation densities and internal stresses measured in dynamic and static case are almost within the measuring error up to a deformation strain of ≈ 0.4. Besides the well known fact that the dislocation density evolving in single crystals is about a factor 10 lower than in polycrystals, there form relative maxima of dislocation density after certain intervals of strain which may be the consequence of the propagation of deformation fronts instead of a homogeneous deformation taking place in polycrystals. This effect has been recently documented by strain measurements of single metal crystals which exhibit a marked single slip behaviour in the initial stages of deformation [4]. Such effect never has been reported before for local dislocation density evolution which is, for the first time, shown to be accessible by the in-situ synchrotron X-ray line profile analysis introduced by actual proposals.

References:
[1] M.Zehetbauer, T.Ungar, R.Pippan, E.Schafler, P.Hanak, I.Kopacz, S.Bernstorff, H.Amenitsch Microstructural Parameters During Plastic Deformation of FCC Metals As Observed by In-Situ Synchrotron Bragg Peak Profile Analysis; Annual Report 1999 of Austrian SAXS Beamline at ELETTRA, p. 96 (2000)
[2] T.Ungar, M.Zehetbauer; Stage IV Work Hardening in Cell Forming Materials, pt.II: A New Mechanism; Scripta metall.mater. 35, 1467-1473 (1996)
[3] M.Zehetbauer, T.Ungar, R.Kral, A.Borbely, E.Schafler, B.Ortner, H. Amenitsch and S. Bernstorff, Scanning X-Ray Diffraction Peak Profile Analysis in Deformed Cu-Polycrystals by Synchrotron Radiation, Acta mater. 47, 1053-1061 (1999)
[4] L.B.Zuev, V.I.Danilov, A Self-Excited Wave Model of Plastic Deformation in Solids, Phil.Mag. A 79, 43-57 (1999)

SPATIAL DISTRIBUTION OF DEFORMATION INDUCED LATTICE DEFECTS IN ULTRAFINE-GRAINED AND NANOSTRUCTURED METALLIC MATERIALS

M.Zehetbauer[1], T.Ungar[2], R.Pippan[3], E.Schafler[1], P.Hanak[2], I.Kopacz[1, 3], K.Simon[2], and S.Bernstorff[4]

1.)Institute of Materials Physics, Vienna University, Strudlhofg. 4, A-1090 Wien, Austria
2.) Institute of General Physics, Eötvös University, Pazmany Peter Setany 1/A, H-1518 Budapest, Hungary
3.) Erich Schmid Institute for Materials Science, Austr.Acad.of Sciences, Jahnstr.12, A-8700 Leoben, Austria
4.) SAXS Group, Synchrotron ELETTRA, Basovizza, I-34012 Trieste, Italy

Because of very interesting results from the preceding proposal [1] it has been decided by the authors to check whether the wavy character of dislocation density increase $\Delta\rho$ in monocrystalline Cu holds for reproductional measurements, and whether the fluctuations of ρ in (deformation) time come from fluctuations of ρ in space, too. This basic effect should be of fundamental meaning for inhomogeneities of dislocation densities/-arrangements of plastically deformed polycrystals, too, even with grain sizes in micrometer as well as in nanometer scale. The fluctuations measured in the preceding proposal (see Fig. 2 of [1]) were strongly confirmed. The numerous and highly pointed profiles allowed for a reliable evaluation of the dislocation arrangement parameter M as a function of compression strain ε, too (M is a measure of the internal strain level connected to a certain dislocation arrangement with dislocation density ρ, [2]): Fig. 1 does not exhibit fluctuations of M in parallel to ρ which means that the fluctuations in ρ are due to a local change of ρ with the same basic dislocation arrangement. On the other hand, the general decrease of M with increasing time and/or deformation ε indicates the formation of dislocation dipoles from single dislocations having a quite lower strain field than the same number of single dislocations. M reaches a minimum at a total strain of $\varepsilon = 0.08$ when all the single dislocations have arranged to dipoles which themselves arrange to dislocation dipole walls. The minimum of M indicates that such a wall represents a local minimum of strain energy.

The slight increase of M at higher deformation may be better understood when one compares the results of spatial scans, too (Fig.2). It indeed seems that the fluctuations in (deformation) time have a correspondence to those in space what fits to Zuev's et al. [3] observations of propagating strain fronts in metallic single crystals instead of a homogeneous deformation. While up to deformations $\varepsilon = 0.08$ (Figs. 2a – c) the fluctuations of ρ are not stationary, they get it for deformations $\varepsilon \geq 0.08$ (Figs. 2 d, e). This result can be interpreted in such a way that the dislocations are still mobile when they have been paired to dislocation dipoles, but that they get sessile when the dipoles have mutually trapped to whole dislocation dipole walls. Inspecting the height of peaks at deformations $\varepsilon \geq 0.08$ shown in Figs. 2d, e, it can be recognized that the peaks of dislocation density - although keeping stationarity - increase and decrease with continued deformation. Together with the finding from above that M slightly increases for $\varepsilon \geq 0.08$ one may conclude that the dipole walls have formed a network of cells; "free" ends of dipole walls do not exist anymore, thus the attractive forces to absorb new mobile free dislocations and/or dislocation dipoles into the wall will be markedly smaller than with the microstructure at smaller ε. Mobile dislocations will move across the network, will get loosely pinned by some wall but also easily unpinned, resulting in a mutually fluctuating dislocation density in neighbouring walls, and slight increase of M due to incomplete screening of strain fields during this temporary pinning event.

The results fit to numerous investigations from Transmission Electron Microscopy (TEM) of dislocation microstructure developing during early plastic deformation (see, e.g. [4]). However, neither it has been possible up to now to measure the microstructural evolution

under load during deformation nor could be obtained quantitative informations on dislocation density and particularly the strain field of dislocation arrangements as a function of (deformation) time and space.
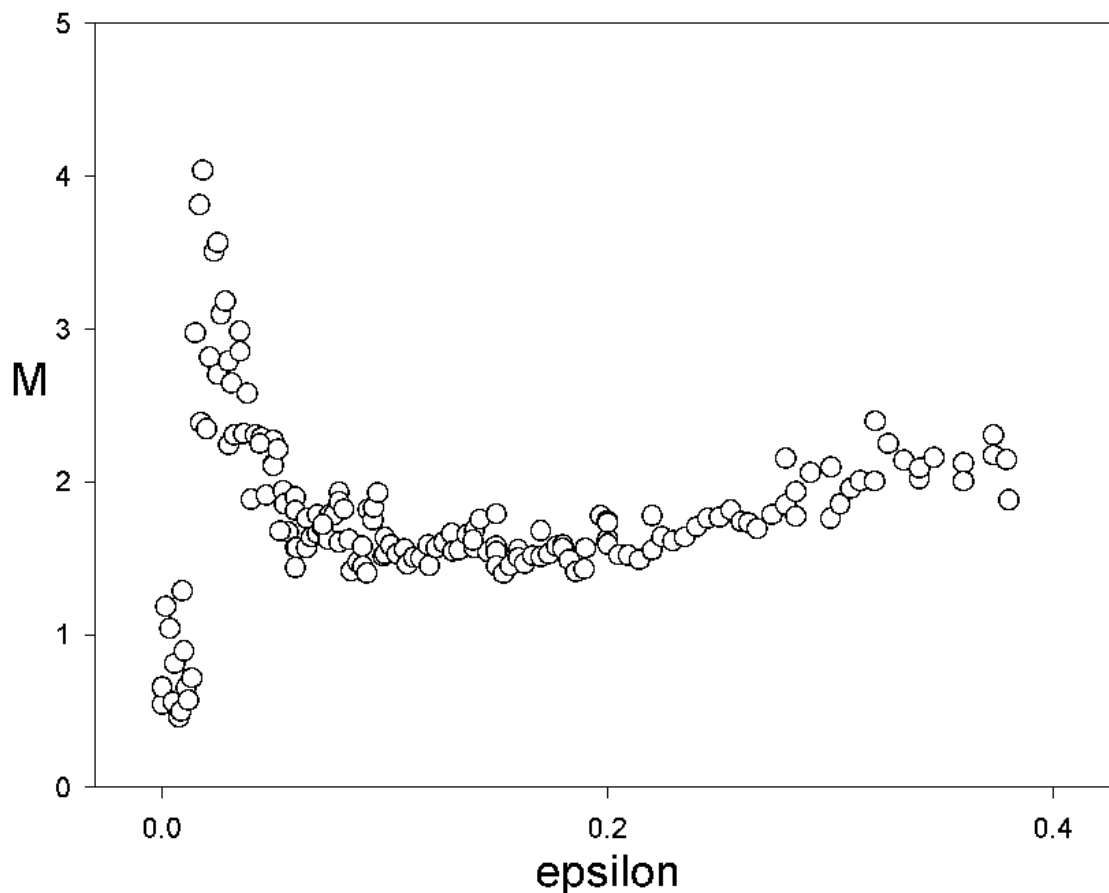

Figure 1. Deformation dependent evolution of dislocation arrangement parameter M, measured during compression of an (100) oriented Cu single crystal. The measuring error is $\Delta M = \pm 0.1$.

Figure 2 (next page). Spatial variation of dislocation density ρ in an (100) oriented Cu single crystal being compressed to increasing certain amounts of true plastic strain ε.(a) $\varepsilon = 0.02$, (b) $\varepsilon = 0.04$, (c) $\varepsilon = 0.08$, (d) $\varepsilon = 0.12$, (e) $\varepsilon = 0.16$. The measuring error is $\Delta \rho = \pm 0.9 \times 10^{11} \, m^{-2}$.

References

[1] M.Zehetbauer, T.Ungar, R.Pippan, E.Schafler, P.Hanak, I.Kopacz, K.Simon, S.Bernstorff, H.Amenitsch; In-situ Synchrotron Bragg Peak Profile Analysis of Microstructural Parameters During Discontinuous Plastic Deformation of fcc Metals; see previous report

[2] M.Zehetbauer, T.Ungar, R.Kral, A.Borbely, E.Schafler, B.Ortner, H. Amenitsch and S. Bernstorff; Scanning X-Ray Diffraction Peak Profile Analysis in Deformed Cu-Polycrystals by Synchrotron Radiation, Acta mater. 47, 1053-1061 (1999)

[3] L.B.Zuev, V.I.Danilov, A Self-Excited Wave Model of Plastic Deformation in Solids, Phil.Mag. A 79, 43-57 (1999)

[4] A.S.Argon; Mechanical Properties of Single-Phase Crystalline Media: Deformation at Low Temperatures, ch.21 in: R.W.Cahn and P.Haasen (eds.), Physical Metallurgy, Vol.III, North-Holland, Amsterdam/Tokyo, p.1877-1955 (1996)
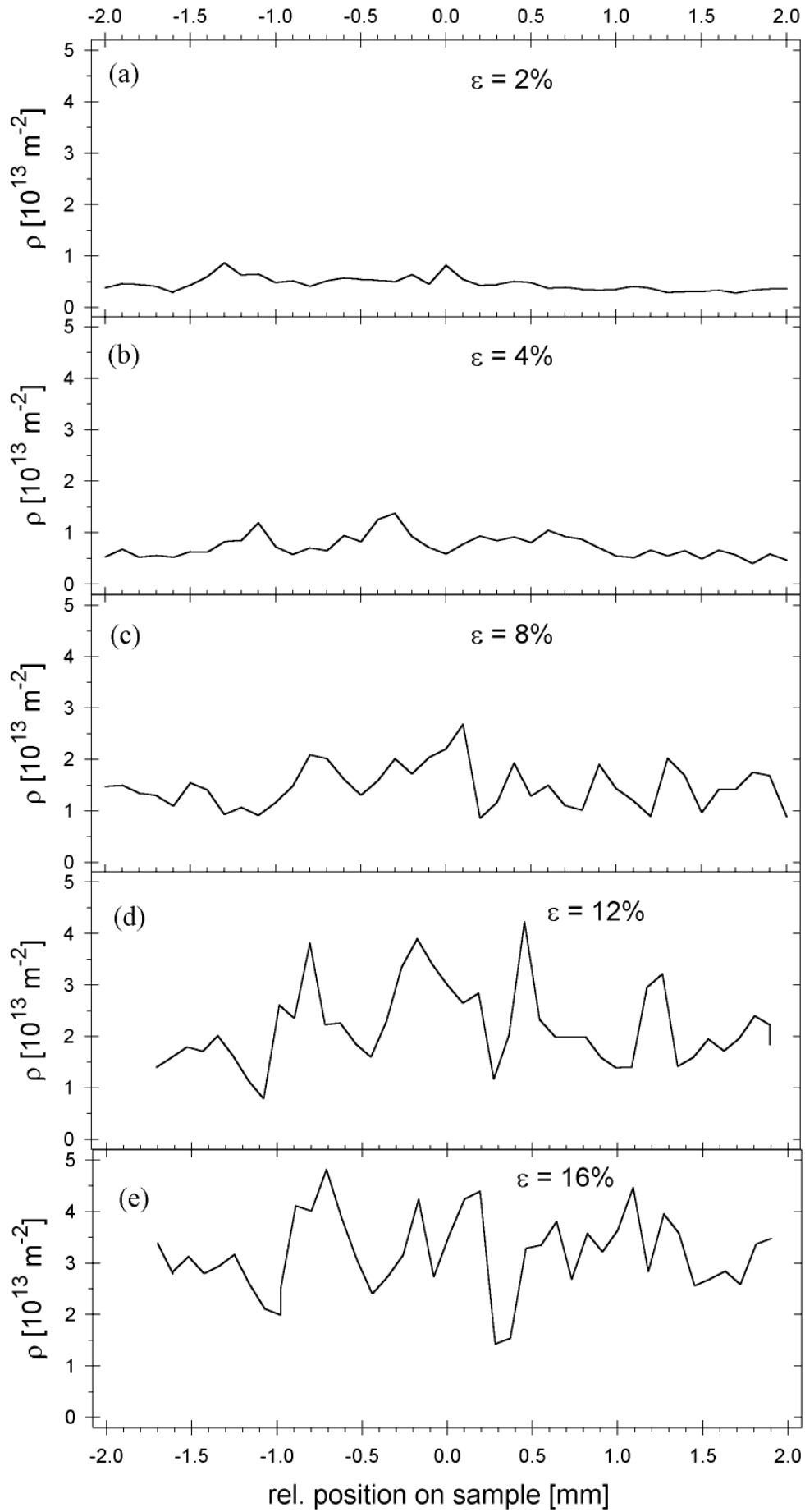
2. Life Sciences

HIGH PRESSURE X-RAY SURFACE DIFFRACTION ON HIGHLY ALIGNED LIPID SYSTEMS UNDER EXCESS WATER CONDITIONS

H. Amenitsch[1], M. Kriechbaum[1], M. Steinhart[2], M. Rappolt[1], S. Bernstorff[3] and P. Laggner[1]

1.) Institute of Biophysics and X-ray Structure Research, Austrian Academy of Sciences, Graz, Austria
2) Institute of Macromolecular Chemistry, Academy of Sciences of the Czech Republic, Prague, Czech Republic
3) Sincrotrone Trieste, Basovizza, Italy

Recently a hydrostatic high pressure cell [1] was modified to allow the studies on highly aligned lamellar lipid systems. This experimental set-up allows simultaneously wide and small angle scattering studies to elucidate the complex morphology of these systems. In contrast to isotropic bilayer systems (usually liposomal preparations also called "powder samples") highly aligned bilayer membrane systems have enabled to derive additional structural information by diffraction. Aligned samples allow the clear differentiation of in-plane and out-of-plane correlation as well as the unique identification of the Miller indices in higher (>1) dimensional phases. However, aligning them under physiological conditions (i.e. excess water, ionic strength and physiological pH) has turned out to be a difficult task, e.g. the "vapour pressure paradox"[2],[3].

This new high pressure cell allows to study these systems under physiological conditions and pressures between 0 - 3000 bar. Additionally the temperature can be varied between 0 and 80 °C. Furthermore the cell offers the possibility to perform p-jump experiments on these systems with jump amplitudes of up to 3 kbar/10 ms.

In Fig. 1 the diffraction pattern of the aligned phospholipid (DMPC) is shown at a temperature of 20 °C and ambient pressure giving clear evidence of the in-plane reflection from the $P_{\beta'}$ Phase after cooling down from the L_{α} Phase, which is lamellar and has no in-plane reflections (see e.g. [4-6]). The real space model of the $P_{\beta'}$ Phase is given in Fig. 2. For the first time the set-up allowed to perform the L_{α} - $P_{\beta'}$ phase transition on aligned lipids using pressure as the thermodynamical variable increasing the pressure from 0 to 1080 bar and at a temperature of 30 °C. To compare the results the d-spacings obtained at different temperatures and pressures are given in Table 1.

Table 1. Liquid crystalline and stable ripple phase of DMPC.

Phase of DMPC	Temperature/°C	Pressure/bar	d-spacing/nm
L_{α}	30	1	6.47
$P_{\beta'}$ cooling from 30 °C	20	1	7.06
$P_{\beta'}$ pressurizing from 1 bar	30	1080	7.38

References:

[1] Steinhard, M., Kriechbaum, M., Pressl, K., Amenitsch, H., Laggner, P. and Bernstorff, S.(1999), Rev.Sci.Instrum. 70, 1540-1545.
[2] Rand, R.P., Parsegian, V.A. (1989), Biochim. Biophys. Acta 988, 351.
[3] Katsaras, J., Watson, M.J. (2000), Rev. Sci. Instrum. 71, 1737.
[4] Tardieu, A., Luzzati, V., Reman, F.C. (1973), J.Mol.Biol. 75, 711.
[5] Wack, D.C., Webb, W.W., (1989), Phys.Rev. A 40, 2712.
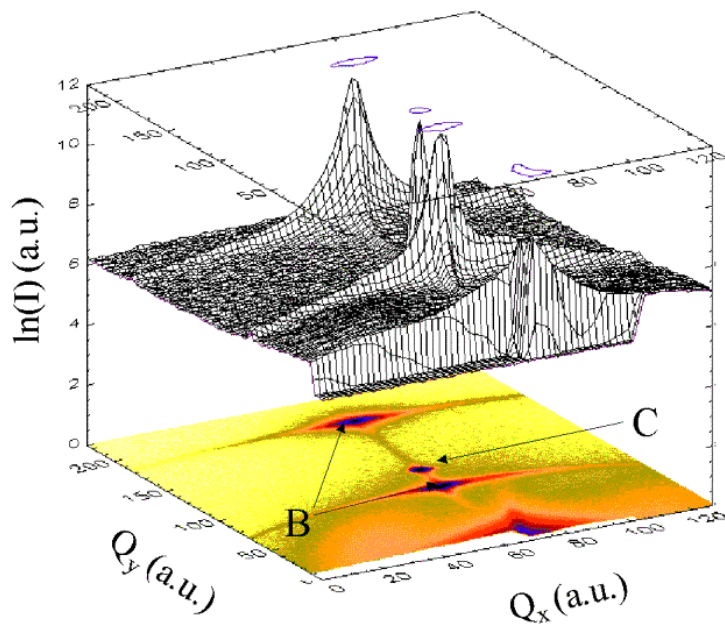[6] Katsaras, J., et.al. (2000), Phys.Rev. E 61, 5668.

Figure 1. Diffraction pattern of a highly aligned lipid (DMPC) in the L$_\alpha$ (top) and in the P$_{\beta'}$ phase (bottom) at constant grazing angle at 30°C and 20 °C. Letter A shows the in-plane reflections due to the ripple structure (distance λ), Letter B gives the off-plane reflections due to the lamellar repeat distance d (see fig 2). C denotes the specular reflectivity peak.
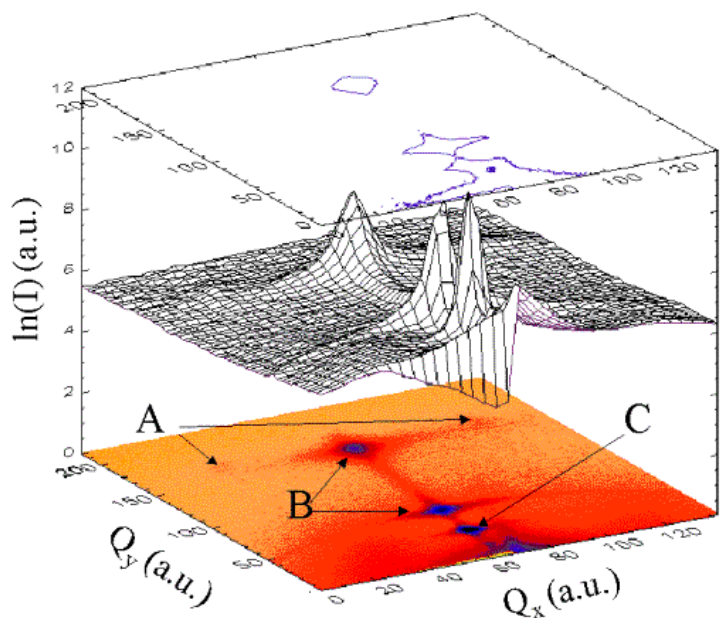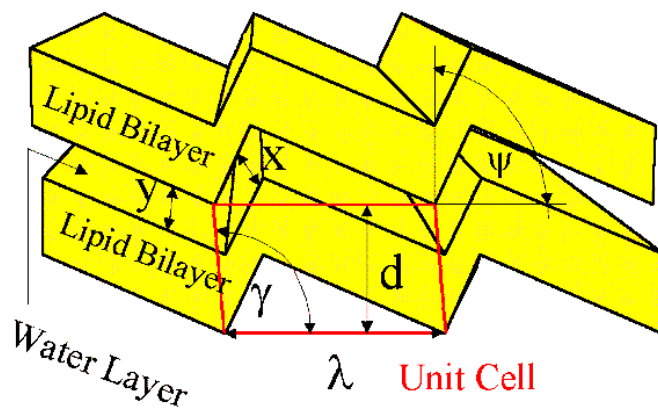

Figure 2. Schematic sketch showing asymmetric rippled bilayer, separated by a layer of water. The unit cell, shown in red, is given by the dimensions d and λ and the monoclinic angle γ.

TEMPERATURE EFFECTS ON THE INTENSITY CHANGES OF THE MERIDIONAL 14.5 NM X-RAY REFLECTION FROM TETANISED SKELETAL MUSCLE FIBRES DURING SINUSOIDAL OSCILLATIONS

M.A. Bagni[1], G. Cecchi[1], B. Colombini[1], P.J. Griffiths[2], C.C. Ashley[2], H. Amenitsch[3] and S. Bernstorff[4].

1) Dip. Scienze Fisiologiche, Università degli Studi di Firenze, I-50134 Firenze, Italy
2) University Laboratory of Physiology, Parks Road, Oxford, OX1 3PT, UK
3) Institut für Biophysik und Röntgenstrukturforschung, Graz, Austria
4) Sincrotrone Trieste, Area Science Park, I-34012 Basovizza / TS, Italy

Work generation by contracting muscle results from interaction between the S1 moiety of the motor protein, myosin II, and actin. Both filaments are arranged as highly structured, filamentous aggregates, which are axially aligned and overlapping. Contraction results from sliding of these filaments, powered by ATP hydrolysis at the S1 ATP binding site. The 'power stroke' structural change of actin-bound S1 (termed cross-bridges), which produces work, was proposed to be a rotation of part of S1 [1, 2] generating a torque at its point of attachment to the myosin filament. Skeletal muscle structure is highly ordered, and gives rise to a strong X-ray diffraction pattern. S1 projects from the myosin filament at regular intervals of 14.3 nm, and the X-ray reflection at this spacing (M3) samples its structure. Therefore, the behaviour of this reflection should be related to the structural basis of the power stroke.

Step length changes cause a synchronised power stroke, due to the change in load on the cross-bridges. Both step stretch and release cause a fall in intensity of M3 (I_{M3}), but while the fall in I_{M3} is instantaneous for a stretch, it is delayed for a release [3]. The instantaneous nature of the response to a stretch suggests that I_{M3} is sensitive not only to the power stroke distortion of S1, but also to its elastic distortion by the change in axial load. It has been proposed that if actin-bound S1 were disposed at an angle to the fibre axis such that maximum I_{M3} was reached for a release of ca. 2 nm, this could account for the delay in the I_{M3} release response [4, 5]. We have examined whether the I_{M3} response to sinusoidal length changes (where X-ray time resolution can be very much higher than for steps) is consistent with its behaviour during step length changes.

Sinusoidal length oscillations at high frequency (3 kHz) in activated muscle fibres produced changes in I_{M3} of roughly sinusoidal shape, and in phase with length changes. At lower frequency (100-400 Hz), intensity changes were not sinusoidal, but showed a strong distortion, forming a double peak during the release phase of the sinusoids. These results are consistent with the proposal that I_{M3} changes are due to both elastic distortion by the applied force and to the power stroke: at high frequencies I_{M3} is mainly due to elastic distortion, while at lower frequencies the power stroke proceeds further, and contributes more to I_{M3}. The presence of the double peak permits calculation of the mean disposition of S1 during the oscillations, and hence comparison with crystallised S1 structures obtained *in vitro*. Frog muscle fibres develop higher tension as the temperature increases above 0-2 °C. Since it is thought that this increased tension is due to an increased force per cross-bridge rather than an increase in cross-bridge number, we examined the effect of temperature on I_{M3} distortion. Experiments were performed on single fibres or small bundles of frog muscle fibres at temperatures between 2 and 24 °C by applying oscillations at 1 kHz. The experimental procedure was similar to that previous described [6]. The results indicate that a more pronounced distortion does become apparent as temperature increases. If, at higher temperatures, tetanic tension increases without recruitment of new S1 moieties, then this implies a less angled disposition of bound S1, which should increase the distortion of I_{M3} signals during the release phase of sinusoidal oscillations. Static patterns showed a 10% reduction in intensity in activated fibres at the higher temperature, and not an increase as would be expected if S1 disposition approached that of maximum I_{M3} at the higher temperature. In addition, if S1 disposition were significantly displaced toward I_{M3} (max, the disposition of S1 at which I_{M3} is maximal), the total intensity change would become smaller during oscillations, since part of the I_{M3} change in the release phase would pass through I_{M3} (max) and thus cause a fall in intensity. I_{M3} changed on average by 30-33% peak to peak (as a percentage of minimum intensity during oscillation) at all temperatures in the range 2-24 °C. It therefore seems likely that the increased distortion of I_{M3} at

higher temperature results chiefly from an increased contribution of the power stroke structural change to this signal rather than a changed disposition of S1.
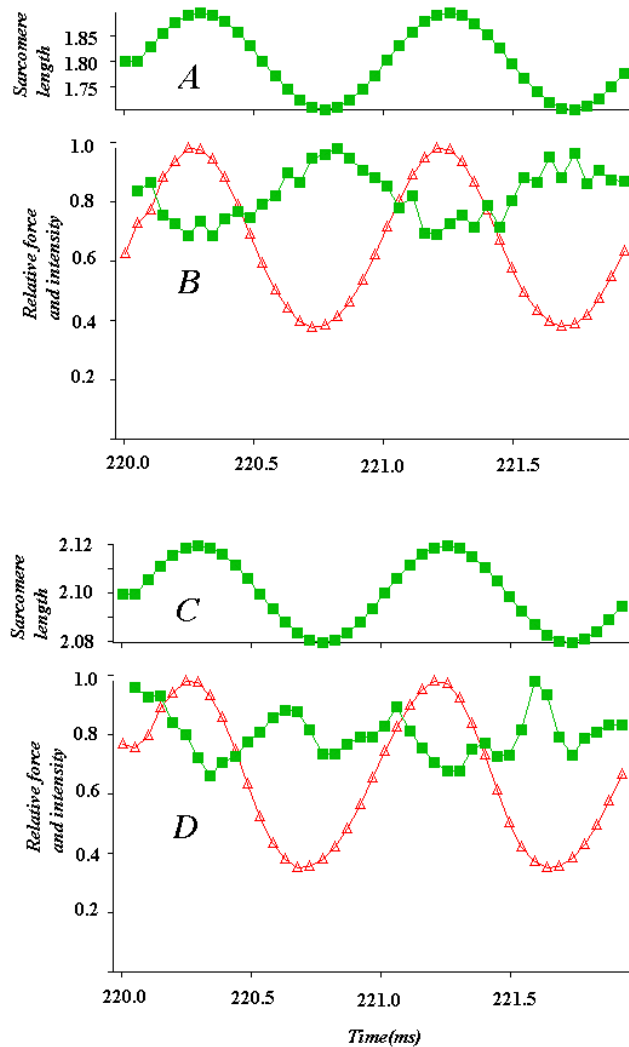

Figure 1: sarcomere length (μm, panels A and C), and force ($\triangle$) and I_{M3} (■) (panels B and D) during 1 kHz oscillations at 4 °C (A and B) and 18 °C (C and D). Time axis divisions 0.5 ms. Length oscillation amplitude adjusted to give a constant force oscillation amplitude (0.8-1.1 P_0 peak to peak) at all temperatures. The position of the intensity minima is delayed with respect to the maxima and minima of both the sarcomere length and force signals at the higher temperature, due to the greater progress of the power stroke, which causes the system to emulate the response of a damped compliance.

References:

[1] Huxley, H.E. 1969. The mechanism of muscle contraction. *Science* **164**: 1356-1366.

[2] Huxley, H.E. and M. Kress. 1985. Crossbridge behaviour during muscle contraction. *J. Muscle Res. Cell Motil.,* **6**: 153-161.

[3] Huxley, H.E., R.M. Simmons, A.R. Faruqi, M. Kress, J. Bordas, and M.H.J. Koch. 1983. Changes in the X-ray reflections from contracting muscle during rapid mechanical transients and their structural implications. *J. Mol. Biol.* **169**: 469-506.

[4] Irving, M., V. Lombardi, G. Piazzesi and M.A. Ferenczi. 1992. Myosin head movements are synchronous with the elementary force generating process in muscle. *Nature*. **357:** 156-158.

[5] Piazzesi, G., V. Lombardi, M.A. Ferenczi, H. Thirlwell, I. Dobbie and M. Irving. 1995. Changes in the X-ray diffraction pattern from single, intact muscle fibers produced by rapid shortening and stretch. *Biophys. J.* **68**: 92s-98s.

[6] Bagni, M.A., B. Colombini, H. Amenitsch, S. Bernstorff, C.C. Ashley, G. Rapp and P.J. Griffiths. 2001 Frequency dependent distortion of meridional intensity changes during sinusoidal length oscillations of activated skeletal muscle. *Biophys. J. in press.*

MECHANISM OF MEMBRANE DISRUPTION BY HUMAN ISLET AMYLOID POLYPEPTIDE

J. P. Bradshaw[1], R. H. Ashley[2], T. A. Harroun[1]

1.) Department of Preclinical Veterinary Sciences, R.(D.)S.V.S., University of Edinburgh, Summerhall, Edinburgh, EH9 1QH, Scotland, UK.
2.) Department of Biomedical Sciences, University of Edinburgh, George Square, Edinburgh, EH8 1XD, Scotland, UK.

How do amyloidogenic peptides, like islet amyloid polypeptide (IAPP), Alzheimer's β peptide (Aβ) and prion proteins, interact with cell membranes to disrupt their structural integrity and normal functions? Improved molecular understanding will lead to advances in knowledge concerning (self-directed) protein folding and membrane/protein interactions, and to new therapies. We are currently engaged in a study of islet amyloid polypeptide (IAPP), a 37-residue peptide of unknown function that is co-secreted with insulin from pancreatic beta cells. A number of lines of evidence have converged to suggest that IAPP is causally related to the development of non insulin-dependent diabetes mellitus, possibly through the formation of amyloid fibres, similar to those seen in Alzheimer's disease (AD). Although amyloid formation and beta cell dysfunction might both be secondary to an unrecognised defect that results in abnormal IAPP processing in affected individuals, there is a substantial amount of evidence to support the idea that once islet amyloid can form, the protein is „toxic" to cells. At the level of the cell membrane, IAPP increases ionic permeability by forming discrete ion channels [1]. In excitable cells, such as pancreatic beta cells, this could lead to cell death following Ca^{2+} entry through plasma membrane Ca^{2+} channels activated by IAPP channel-induced membrane depolarisation, or cell death following direct Ca^{2+} entry through IAPP channels themselves.

We have shown that membrane disruption is caused by a transitory, quaternary form of IAPP, called intermediate-sized toxic amyloid particles (ISTAPs) [2]; monomeric IAPPs and mature amyloid are both inert. Our working model for the membrane toxicity of ISTAPs predicts that while IAPP forms amyloid fibrils and fibres in solution via β-sheet intermediates, it can also insert into accessible membranes as transbilayer α-helices. This behaviour would not be unique, and we have previously described two other peptides that display spontaneous self-directed environment-dependent conformational switching of this type [3, 4, 5].

As part of these studies, we used SAXS to probe the molecular structure of IAPP fibrils and membrane-associated complexes. Over a period of several hours, we monitored the formation of quaternary structures under a number of different conditions, the main variables being: peptide concentration; lipid presence or absence; presence or absence of the inhibitors of membrane-activity, congo red and rifampicin. The data are currently being analysed.

References:

[1] Mirzabekov, T.A., Lim, M. & Kagan, B.L. Pore formation by the cytotoxic islet amyloid peptide Amylin. J. Biol. Chem. 271 (1996) 1988-1992.
[2] Janson, J., Ashley, R.H., Harrison, D., McIntyre, S. & Butler, P.C. The mechanism of IAPP toxicity is membrane disruption by intermediate-sized toxic amyloid particles (ISTAPs) causing apoptosis and necrosis. Diabetes 48 (1999) 491-498
[3] Bradshaw, J.P. Phosphatidyl glycerol promotes bilayer insertion of salmon calcitonin. Biophys. J. 72 (1997) 2180-2186.
[4] Davies, S.M.A., Bradshaw, J.P. & Epand, R.M. Modulation of lipid polymorphism by the feline leukaemia virus fusion peptide: implications for the fusion mechanism. Biochemistry 37 (1998) 5720-5729.
[5] Gilchrist, P.J., & Bradshaw, J.P. Amyloid formation by salmon calcitonin. Biochim. Biophys. Acta 1182 (1993) 111-114.

PROTEIN FOLDING AND PROTEIN-PROTEIN INTERACTIONS

Michael Forstner

Department of Molecular Biology, Biomedical Center, SLU Uppsala, S-75124 Uppsala, Sweden

The work of our group during the year 2000 was centered around two main topics – the study of the kinetics of protein folding and unfolding, and the investigation of the formation of protein complexes. The experiments performed at the SAXS beamline at Elettra provided us with valuable information to design further experiments and will be an important part in the final interpretation of the results obtained in these studies.

1.) <u>Kinetics of protein folding</u>: Based on previous work on creatine kinase (CK), we investigated the unfolding of the CK holoenzyme and the isolated domains by time-resolved small-angle x-ray scattering, using guanidinium hydrochloride (GdnHCl) as a denaturing agens. The protein and the denaturant were mixed in a stopped flow cell to create different final concentrations of GdnHCl and the change in the scattering function was observed as a function of time. We could detect different species of folding intermediates that show characteristics similar to the intermediates found in thermodynamic equilibrium unfolding. Currently we are trying to employ different other unfolding methods (e.g., acid unfolding) that might not suffer from the significant absorption effects observed when using GdnHCl. These studies also provide the basis for our investigation of the thermal unfolding behavior of proteins from hyperthermophilic organisms compared to those from mesophiles.

2.) <u>The formation of the ADF-actin complex</u>: *Toxoplasma gondii* is one of the leading causes of death from opportunistic infections in patients suffering from immunodeficiency disorders, especially AIDS. The parasite enters the host cell by protruding a rod of F-actin, penetrating the membrane of the host cell and quasi pulling itself into the host cell by depolymerizing the actin rod on the proximal end. Depolymerization has been shown to be controlled by a small protein of 115 amino acids, termed actin-depolymerizing factor (ADF). While this protein shows some sequence homology to related yeast proteins like cofilin or profilin, the sequence identity is very low and it is generally believed that blocking the infection pathway of *T. gondii* could be blocked by inhibiting the action of ADF.

ADF has recently been cloned and expressed as a recombinant protein in *E. coli* .We have improved the expression and purification scheme and are now routinely purifying 50-100 mg amounts of the recombinant protein. Crystallization trials have been performed and we have obtained crystals with a maximum diameter of 0.3 mm recently (Forstner and Söderberg, unpublished). In parallel, we have been trying to obtain crystals of the complex with actin, which, however, has not yielded any diffraction quality crystals so far. Additionally, we have started to perform site-directed mutagenesis experiments to identify putative active site residues important for the control of actin dynamics.
In the experiments performed at Elettra, we tried to investigate the actin turnover dynamics controlled by recombinant *T. gondii* ADF. While we could not use a stopped-flow mixing cell to rapidly add wild-type or mutant ADF to solutions of F-actin and study the kinetics of actin depolymerization upon addition by time-resolved small-angle scattering as planned. We could, however, investigate the low-resolution structure of the complex of globular G-actin with ADF and are currently using our model of the ADF structure and the crystal structure of actin to create a plausible model for the complex.

TIME RESOLVED TRANSITIONS OF THE pH-DENATURED STATES OF FERRICYTOCHROME-c BY SAXS

P. Mariani[1], F. Spinozzi[1], F. Corsi[1], S. Cinelli[2] and G. Onori[2], H. Amenitsch[3] S. Bernstorff[4]

1) Istituto di Scienze Fisiche and INFM, Università di Ancona, Via Ranieri 65, I-60131 Ancona, Italy
2) Dipartimento di Fisica and INFM, Università di Perugia, Via Pascoli, I-06123 Perugia, Italy
3) Institute of Biophysics and X-ray Structure Research, Austrian Academy of Sciences, Schmiedlstraße 6, A-8042 Graz, Austria
4) Sincrotrone di Trieste S.C.p.A. Strada Statale 14 Km 163.5, 34016 Basovizza (Trieste), Italy

The molten globule is a compact denatured protein form, with a significantly native-like secondary structure, but a largely flexible and disordered tertiary structure. On the basis of structural and kinetic studies, the molten globule has been proposed as the major intermediate in globular protein folding [1]. Horse cyt-c is a well characterised globular protein both in the crystalline and in solution states and it represents a very useful model for protein folding studies. In particular, cyt-c has been shown to exist in three stable states in acidic pH region, corresponding to the native (N), unfolded (U_1) and compact intermediate or molten globule (A) forms [2,3]. Acid-unfolding of cyt-c occurs substantially under conditions of low salt at pH 2 (U_1 state); the subsequent addition of Cl^- ion from either HCl or NaCl induces the partial refolding to a molten globule state (A_1 and A_2 respectively), indicating that the chloride anion should play a key role in acid-salt induced refolding. Recently SAXS results [4] showed that in the acidic-unfolded U_1 form the protein assumes a worm-like conformation while the refolded states induced by adding HCl or NaCl to U_1 appear structurally different: in the A_1 state cyt-c is dimeric and less compact, while in the A_2 form the protein reverts to a globular-like conformation.

In order to study the dynamics of the three transition processes $N \rightarrow U_1$, $U_1 \rightarrow A_1$ and $U_1 \rightarrow A_2$ we have performed time resolved measurements at the ELETTRA's SAXS beamline. Samples have been prepared with the stopped-flow apparatus (mixing time 100 ms) by using three stock solutions of cyt-c (50 g l^{-1}), HCl (550 mM) and NaCl (670 mM). The SAXS patterns (Fig. 1) were recorded at room temperature for 250 s, by changing the frequency form 0.05 s/frame to 1 s/frame. The sample-detector distance was 2.5 m and the X-ray wavelength 1.54 Å.

From a preliminary Guinier analysis of the four states of cyt-c in equilibrium condition we have determined the gyration radii reported in the Table 1.

Table 1. Guinier analysis of static SAXS data from cyt-c in the native (N), acid-denatured (U_1), acid-induced refolded (A_1) and salt-induced refolded (A_2) states.

Sample	PH	[HCl] (mM)	[NaCl] (mM)	R_g (Å)
N	7	0	0	14.0±0.5
U_1	2	27	0	21±2
A_1	0.5	440	0	27±3
A_2	2	27	400	14±1

The results are in perfect agreement with the radii of gyration previously measured [4]. Dynamic measurements have been then analysed by studying the variation of R_g after the mixing of cyt-c with the solutions of HCl or NaCl. In order to improve statistics, each experiment has been repeated 10 times. Moreover time-averaged R_g values have been

calculated by defining a suitable time grid and by combining all the frames measured in the same time range. The experimental R_g of the three transition processes $N{\rightarrow}U_1$, $U_1{\rightarrow}A_1$ and $U_1{\rightarrow}A_2$ are reported in Fig. 2 as a function of time. Those curves were interpreted by assuming a parametric function

$$R_g(t) = (R_{g1}+R_{g2})/2 + (R_{g2}-R_{g1}) \tan^{-1}[(t-\tau_0)/\tau]/\pi, \qquad\qquad (1)$$

where R_{g1} and R_{g2} are the gyration radii before and after the transition, τ_0 is the half-time and τ the transition time. The fitted parameters are given in the Table 2.

Table 2. Fitting results of time resolved SAXS patterns from cyt-c during the native / acid-denatured ($N{\rightarrow}U_1$), acid denatured / acid-induced refolded ($U_1{\rightarrow}A_1$) and acid denatured / salt-induced refolded ($U_1{\rightarrow}A_2$) transitions.

Transition	R_{g1} (Å)	R_{g2} (Å)	t_0 (s)	t (s)
$N{\rightarrow}U_1$	12±1	16.1±0.2	59±8	23±9
$U_1{\rightarrow}A_1$	19±5	23.9±0.1	2±1	13±5
$U_1{\rightarrow}A_2$	17±3	14.2±0.2	7±2	8±3

In the frame of experimental errors, the first transition, i.e. from native to acid unfolded states is the slowest process, while the formation of the two molten globule A states takes place in a few seconds.
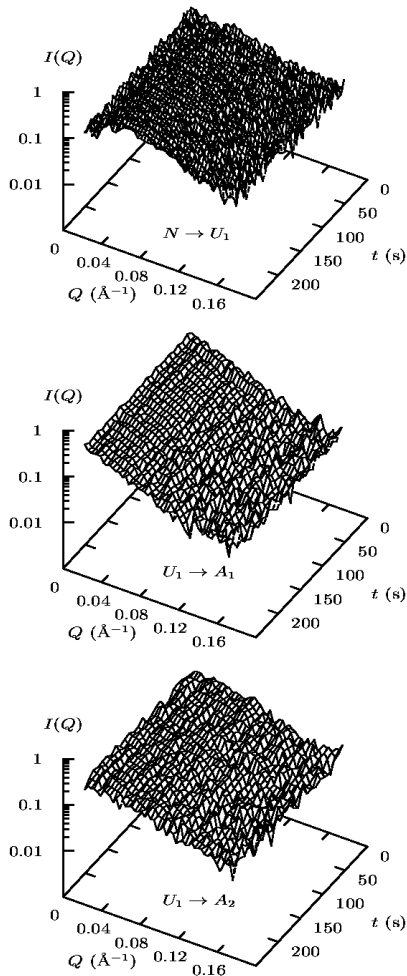
Figure 1. Time resolved scattering patterns from cyt-c during the native / acid-denatured ($N{\rightarrow}U_1$), acid denatured / acid-induced refolded ($U_1{\rightarrow}A_1$) and acid denatured / salt-induced refolded ($U_1{\rightarrow}A_2$) transitions. The corresponding time resolutions are 4, 10 and 10 s/frame.
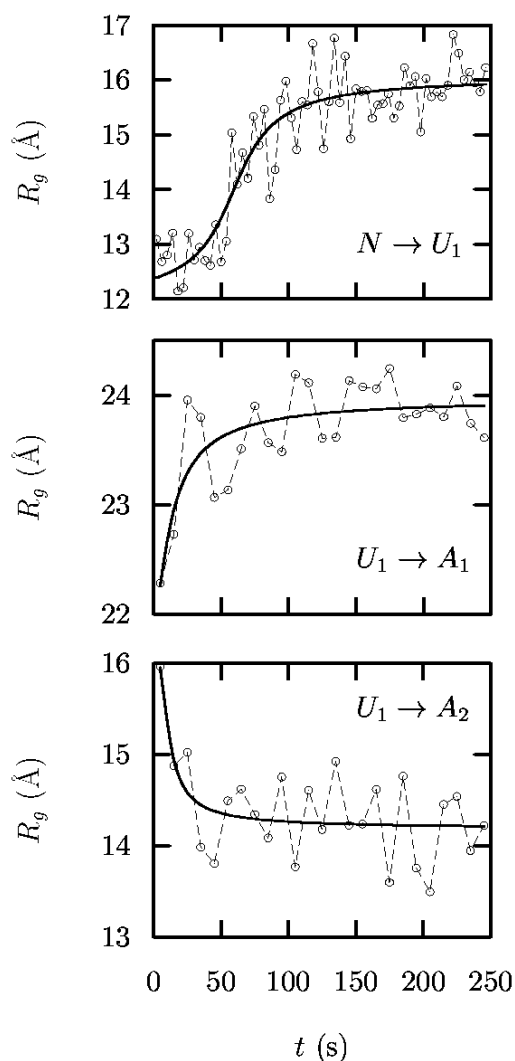
Figure 2. Time resolved radii of gyration from cyt-c during the native / acid-denatured ($N{\to}U_1$), acid denatured / acid-induced refolded ($U_1{\to}A_1$) and acid denatured / salt-induced refolded ($U_1{\to}A_2$) transitions. Continuous line correspond to best fits calculated from the Eq. (1).

References:

[1] Y. Goto, N. Takahashi and A. L. Fink. Mechanism of acid-induced folding of proteins. *Biochemistry* **29**, 3480-3488 (1990).

[2] A. L. Fink, L. J. Calciano, Y. Goto, T. Kurotsu and D. R. Palleros. Classification of acid denaturation of protein: intermediates and unfolded states. *Biochemistry* **33**, 12504-12511 (1994).

[3] L. Pollack, M. W. Tate, N. C. Darnton, J. B. Knight, S. M. Gruner, W. A. Eaton and R. H. Austin. Compactness of the denatured state of a fast-folding protein measured by submillisecond small angle x-ray scattering. *Proc. Natl. Acad. Sci. USA* **96**,:10115-10117 (1999).

[4] S. Cinelli, F. Spinozzi, R. Itri, F. Carsughi, G. Onori and P. Mariani, Structural characterisation of the pH-denatured states of ferricytochrome-c by synchrotron small angle x-ray scattering. *Biophys. J.*, submitted (2001).

CRYSTALLIZATION IN MILK FAT GLOBULES AFTER QUENCHING

M. Ollivon, C. Lopez and F. Artzner

Equipe physico-Chimie des systèmes polyphasés.
UMR 8612 du CNRS. 5, rue J.B. Clément, France.

Milk is one of the rare biological fluid that exist as an emulsion in its native state. In native milk, fat which is mainly composed of triacylglycerols (TAGs) is present in the form of globules (0.2-20μm). Cream is the oil in water emulsion resulting from the concentration of milk. As a major food and as a model for milk, the examination of the physical properties of cream is of particular importance. Thus, it is of interest to study crystallization of TAGs in natural milk fat globules.

A concentrated cream (500g/l) was loaded in a thin glass capillary. The sample was heated at 50°C for 10 min. in order to melt all existing crystals and nuclei. Hot sample was quenched by rapid introduction of the capillary into the calorimeter pre-cooled to –8°C, in order to study the formation of the less stable crystalline structures of TAGs within fat globules of cream. The quenching temperature was chosen low enough to study crystallized TAGs structures and high enough to avoid water crystallization during the experiments. X-ray patterns had been recorded in isothermal conditions at –8°C for 20 minutes.
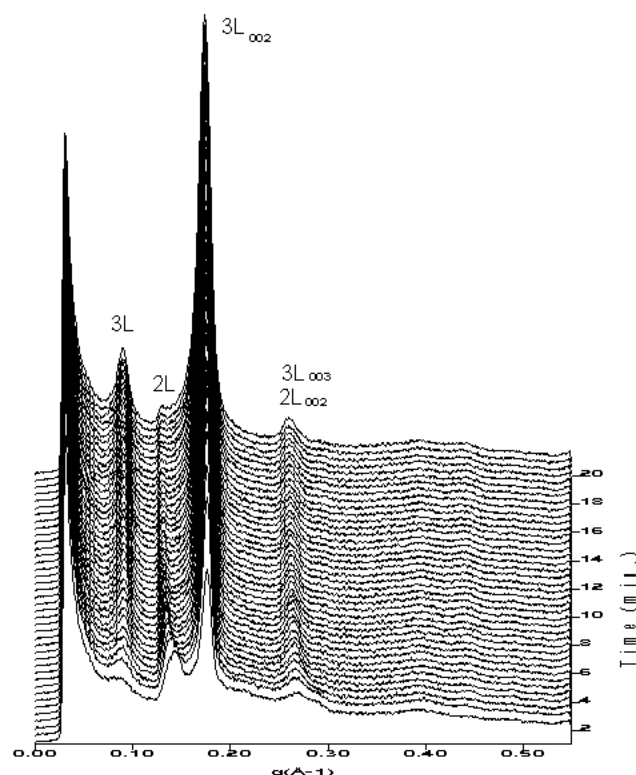
Small-angle X-ray diffraction shows the unstable forms resulting from cream quenching correspond to two lamellar phases corresponding to a two-length chain ($2L = 0.139\text{Å}^{-1}$) and a three length chain ($3L=0.089\text{Å}^{-1}$) arrangements of TAGs. The line at $q=0.268\text{Å}^{-1}$ is attributed to both the third order of the 3L structure and the second order of the 2L packing.

The X-ray pattern evolution consists in both progressive vanishing of 2L and development of 3L organizations. The destabilization of the 2L structure is due to the metastable character of the structure.

ANOMALOUS SWELLING IN PHOSPHOLIPID BILAYERS

G. Pabst[1,2], M. Rappolt[1], H. Amenitsch[1], S. Bernstorff[3] and P. Laggner[1]

1.) Institute of Biophysics and X-ray Structure Research, Austrian Academy of Sciences, Schmiedlstraße 6, A-8042 Graz, Austria.
2.) Neutron Program for Materials Research, National Research Council of Canada, Chalk River Laboratories, Station 18, Chalk River, Ontario, K0J 1J0, Canada (present address).
3.) Synchrotron Trieste (ELETTRA), SS 14, Km 163.5, I-34012 Basovizza (TS), Italy.

Biomimetic membrane systems composed of certain single component phospholipid bilayers are known to exhibit increased fluctuations as the main transition temperature, T_m, is approached from above T_m in the L_α phase. Although the main transition is clearly first order, the build up of fluctuations is understood theoretically on the grounds that the main transition occurs in the vicinity of a critical temperature T_c [1]. Since the main transition pre-empts the critical transition, strictly speaking, the system cannot be said to be exhibiting critical behaviour and has therefore been alternatively described as displaying "pretransitional critical" or "pseudocritical" characteristics near T_m. A further theory has been recently proposed based on so-called heterophase fluctuations, i.e., nuclei of the emerging $P_{\beta'}$ phase are statistically created and dissipated, resulting in the observed swelling [2]. Thus it may be that the system may not even be close to a critical point.

Despite contradicting theories, attention has focused on the non-linear temperature dependence of the lamellar repeat distance, d, in multilamellar vesicles (MLV's) of diacyl phosphatidylcholines such as DPPC, DMPC and DLPC where d shows a marked, non-linear increase as the temperature is decreased towards T_m. This behaviour has been described as "anomalous swelling" and various groups have attempted to reveal its structural origins as the d spacing being measured is the sum of the bilayer thickness, d_B, and the water layer thickness, d_W, of adjacent bilayers. Nagle and co-workers [3] could show by high resolution x-ray diffraction experiments that most of the swelling is due to the increase of bilayer thickness, which disagrees with previous conclusions relating the increase in d spacing to the water layer (see references in [3]).

We have tried to tackle the problem through a recently developed analysis method, which - in contrast to previous methods - allows to analyze the full q range of powder diffraction data from MLV's [4]. This method enables us to obtain much more accurate results for structural parameters as well as bilayer fluctuations. The experiments carried out so far look very promising, however, one more run will be needed to obtain a complete data set.

References:

[1] O.G. Mouritsen; Theoretical Models of Phospholipid Phase Transitions; Chem. Phys. Lipids **57,** 179 - 194 (1991).
[2] D. P. Kharakoz and E.A. Shlyapnikova; Thermodynamics and Kinetics of the Early Steps of Solid-State Nucleation in the Fluid Lipid Bilayer; J. Phys. Chem. **104,** 10368 - 10378 (2000).
[3] J.F. Nagle, H.I. Petrache, N. Gouliaev, S. Tristram-Nagle, Y. Liu, R.M. Suter and K. Gawrsich; Multiple Mechanisms for Critical Behavior in the Biologically Relevant Phase of Lecithin Bilayers; Phys. Rev. E. **58,** 7769 – 7776 (1998).
[4] G. Pabst, M. Rappolt, H. Amenitsch and P. Laggner; Structural Information from Multilamellar Liposomes at Full Hydration: Full q-range Fitting with High Quality X-ray Data; Phys. Rev. E. 62, 4000 – 4009 (2000).

PHASE BEHAVIOR, MOLECULAR CONFORMATION AND COMPRESSIBILITY OF INVERSE LIPID SYSTEMS

M. Pisani[1], H. Amenitsch[2], S. Bernstorff [3] and P. Mariani[1]

1.) Istituto di Scienze Fisiche and INFM, Universita' di Ancona, Via Ranieri 65, 60131 Ancona, Italy.
2.) Institute of Biophysics and X-ray Structure Research, Austrian Academy of Sciences, Schmiedlstraße 6, A-8042 Graz, Austria
3.) Sincrotrone di Trieste S.C.p.A. Strada Statale 14 Km 163.5, 34016 Basovizza (Trieste), Italy

Amphiphilic lipid molecules display a variety of polymorphic states, depending on their molecular structure and on environmental conditions, such as water content, pH, temperature and pressure. A peculiar interest concerns the bicontinuous cubic phases (named *Ia3d*, *Pn3m*, *Im3m* according to their symmetry), which consist of curved membranes (*e.g.*, lipid bilayers) that fill up the space in a regular pattern, forming a complicated network of intertwined and unconnected water regions [1,2]. The structure of the cubic phases can be described in terms of Infinitely Periodic Minimal Surfaces (IPMS). This approach involves analytic generation of ordered surface morphologies and quantification of the effect of topology and symmetry on geometrical characteristics. The IPMS are mathematical surfaces that are periodic in 3-D and which have zero mean curvature at every point on the surface. In the inverse bicontinuous cubic phase, the lipid monolayers are draped across either side of the minimal surface, touching it with their terminal methyl groups; this results in a three-dimensional periodic bicontinuous structure, formed by distinct water and lipid volumes [1].

It is interesting to resume the lyotropic phase behavior of the monoolein [2]. The temperature-concentration phase diagram is characterized by the presence of a lamellar structure *La*, where lipid molecules assemble into stacked sheets, an inverted (type II) hexagonal phase H_{II}, which consists of cylindrical structure elements packed in a 2-D hexagonal lattice, and two bicontinuous inverted cubic phases with space group *Pn3m* and *Ia3d*. The two cubic phases are based on G (Gyroid) and D (Diamond) IPMS surfaces, respectively (Figure 1) and their properties have been investigated for a long time [2,3]. However, it should be noticed that a cubic-to-cubic phase transition occurs when the monoolein is left to equilibrate in excess solution of cytochrome C: the protein induces the formation of another bicontinuous inverted cubic phase, with space group *Im3m* and which is based on the P (Primitive) IPMS surface (see Figure 1). The structural characteristics of the *Im3m* phase occurring in the monoolein-cytochrome C-water ternary system are not completely solved and also the role of the protein on the phase transition still remains unclear [2]. Indeed, the narrow range of existence of the *Im3m* phase in the concentration-temperature phase diagram precludes fine structural investigations. Pressure can be used as a suitable thermodynamic variable to obtain information on the structure, energetic and stability of lipid phases: therefore synchrotron X-ray diffraction experiments have been performed under hydrostatic pressure to investigate the structural properties of the *Im3m* bicontinuous cubic phase in the monoolein-cytochrome C-water system.

The system we investigated is monoolein in cytochrome C solutions from 10 to 100 mg/ml. Samples were prepared in excess solution by mixing the lipid with the appropriate cytochrome C solution in small bottles and were equilibrated in the dark for one week at ambient temperature and pressure. For pressure experiments, we used the pressure-control system designed and constructed by M. Kriechbaum and M. Steinhart (see description on page 27 in this issue). The pressure cell has two diamond windows (each 0.5 mm thick) and allows to measure diffraction patterns at hydrostatic pressures up to 2.5 kbar. X-ray diffraction measurements were performed on the SAXS beamline at 25°C for different

pressures, from 1 bar to 2.5 kbar, with steps of about 100 bar. Particular attention has been devoted to check for equilibrium conditions and for radiation damage. A gently compression of the sample, at a rate of 0.5-2 bar/s, was observed to ensure the establishment of equilibrium conditions, also in the regions of phase coexistence. In each experiment, a number of sharp low angle reflections were observed (Figure 2). Low angle diffraction profiles were indexed using equations which define the spacing of reflections for the different symmetry systems usually observed in lipid phases [2]: the indexing problem was easy to solve, because in no case extra peaks, which can be ascribed to the presence of unknown phases or to crystalline structures, were observed. In the present experimental conditions, three different series of low-angle Bragg reflections were observed and indexed according to the *Im3m* space group (spacing ratios $\sqrt{2}$: $\sqrt{4}$: $\sqrt{6}$: $\sqrt{8}$: $\sqrt{10}$...), to the *Pn3m* space group (spacing ratios $\sqrt{2}$: $\sqrt{3}$: $\sqrt{4}$: $\sqrt{6}$: $\sqrt{8}$...) and to the lamellar 1-D symmetry (spacing ratios 1:2:3...). Once the symmetry of the lipid phase was found, the dimension of the unit cell *a* was calculated.

At atmospheric pressure and room temperature, the protein is detected to induce the formation of the *Im3m* cubic phase. The unit cell dimension is 128 Å, independently on the solution protein concentration. Increasing the pressure, the *Im3m* phase transforms in the *Pn3m* cubic phase at about 1 kbar. However, the two cubic phases coexist until 2.5 kbar. The lattice periodicities depend on pressure, ranging from about 128 Å to 150 Å for *Im3m* and from 105 Å to 113 Å for *Pn3m.* The lamellar phase forms at about 2.5 kbar and the unit cell is of 50 Å. The unit cell pressure dependence (Figure 3) can be understood in terms of simple molecular packing arguments, based on changes in the molecular wedge shape of monoolein. Increasing pressure, increases the lipid chain order parameter, and then decreases the molecular wedge shape. This results in an enlargement of the unit cell size of the two cubic phases because of a decreased curvature of lipid bilayer. The more cylindrical molecular shape also leads to the formation of the lamellar *Lα* phase, whose unit cell increases as a function of pressure, as the chain order parameter increases. The underlying mechanisms for the phase transition is based on the analysis of the relationships between the structural data (such as area-per-lipid at the lipid-water interface, mean curvature, monolayer thickness, position of the pivotal surface) on the two phases. Since the external pressure increases the cell sizes, reducing the curvatures, the present data appear also suitable for a tentative analysis of the curvature elastic parameters to prove theoretical models for the energetic of bicontinuous cubic structures and to understand the pressure-induced phase behavior [3].
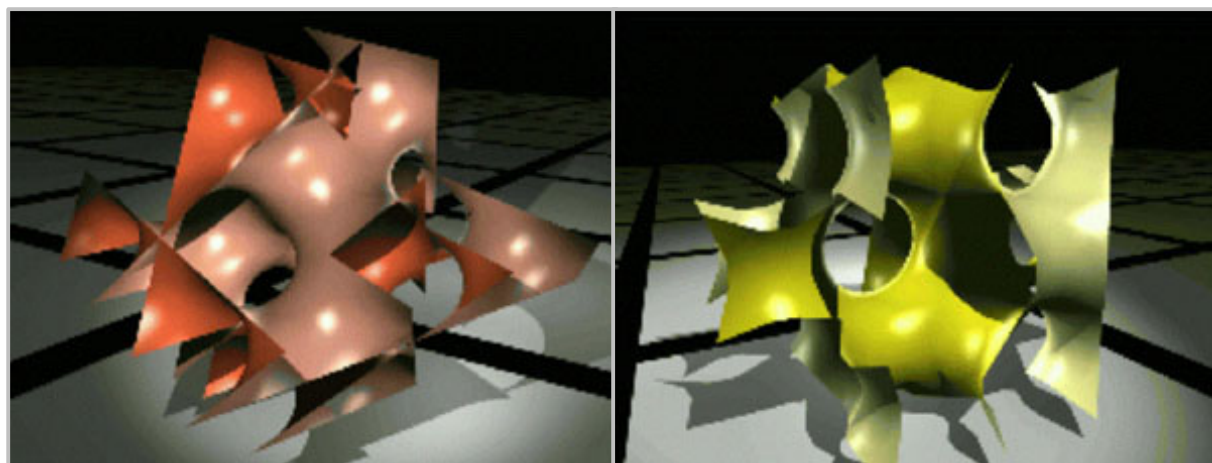

Figure 1. Representation of the unit cell structure of the *Pn3m*, symbol Q[224] (left frame) and of *Im3m*, symbol Q[229] (right frame) cubic phases.
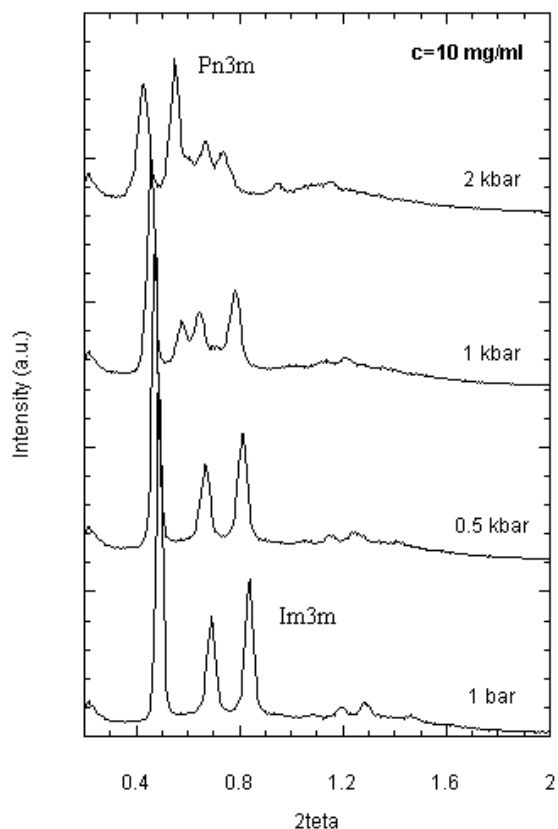
Figure 2. Diffraction patterns at different pressure for a sample in cytochrome c solution of 10 mg/ml.
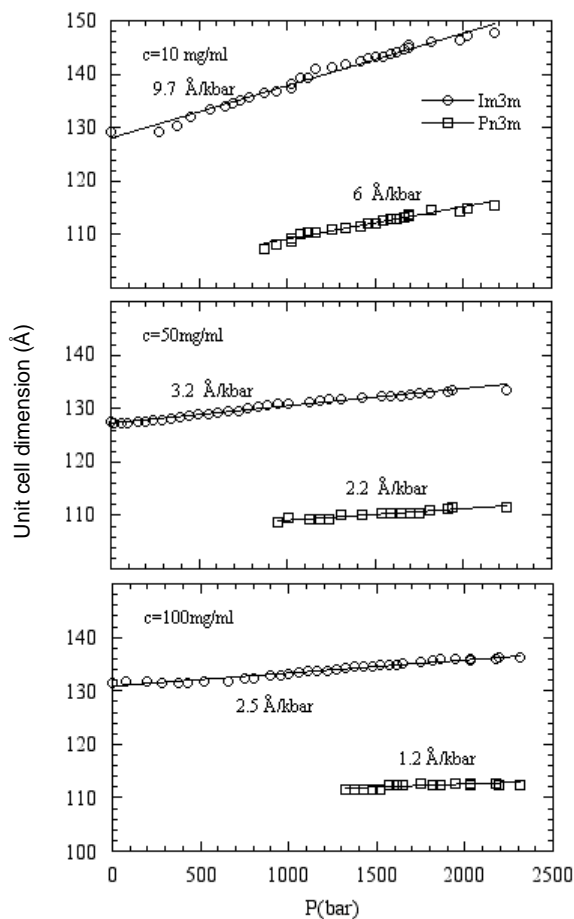
Figure 3. Pressure dependence of the unit cell dimension for samples of fully hydrated monoolein in cytochrome c solution of 10, 50, 100 mg/ml.

References:

[1] V. Luzzati, R. Vargas, P. Mariani, A. Gulik, and H. Delacroix: "Cubic phases of lipid-containing systems. Elements of a theory and biological connotations"; J. Mol. Biol. **229**, 540-551 (1993).

[2] P. Mariani, V. Luzzati, and H. Delacroix: "Cubic phases of lipid-containing systems. Structure analysis and biological implications"; J. Mol. Biol. **204**,165-189 (1988)

[3] M. Pisani, S.Bernstorff, C.Ferrero and P. Mariani: "Pressure induced cubic-to-cubic phase transition on the monoolein hydrated system"; will be published in J. of Physical Chemistry April 2001.

SALT-INDUCED PHASE SEPARATION IN THE LIQUID CRYSTALLINE PHASE OF PHOSPHATIDYLCHOLINES

M. Rappolt[1], G. Pabst[1,2], H. Amenitsch[1], S. Bernstorff[3] and P. Laggner[1]

1.) Institute of Biophysics and X-ray Structure Research, Austrian Academy of Sciences, Schmiedlstraße 6, A-8042 Graz, Austria.
2.) Neutron Program for Materials Research, National Research Council of Canada, Chalk River Laboratories, Station 18, Chalk River, Ontario, K0J 1J0, Canada (present address).
3.) Synchrotron Trieste (ELETTRA), SS 14, Km 163.5, I-34012 Basovizza (TS), Italy.

The effects of alkali chlorides on multilamellar vesicles of various phosphatidylcholines in the lamellar liquid crystalline L_α-phase were investigated by using small-angle X-ray scattering. At alkali chloride concentrations above 70 mM (LiCl) a phase separation in the liquid crystalline phase of POPC is induced. The splitting of the first and second order diffraction peaks into two major discrete components indicates a separation into different lamellar liquid crystalline (smectic A) phases. Detailed data-analysis applying the modified Caillé theory proves that the phases mainly differ in the interbilayer water thickness by about two hydration layers. The lipid bilayer profile itself remains essentially the same in all liquid crystalline phases. A comparison of differently prepared samples and rapid mixing experiments in combination with simultaneous time-resolved X-ray diffraction suggest that the phase separation is osmotically driven.
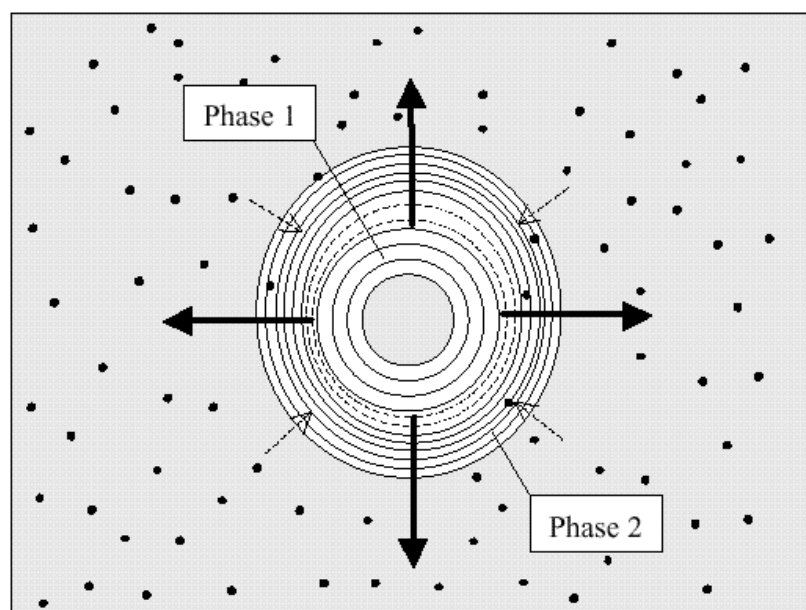
Figure 1. Sketch of the proposed phase separation in a liposome. Solid lines represent bilayers in phase 1 and phase 2, respectively. Throughout osmosis the water flux (bold arrows) is directed outwards the liposome, while the very slow salt flux (dashed arrow) is directed inwards. Between phase 1 and phase 2 a disordered bilayer region is presented by dashed lines.

References:

[1] M. Rappolt, K. Pressl, G. Pabst, and P. Laggner, Biochim. Biophys. Acta 1372 (1998)
[2] M. Rappolt, G. Pabst, H. Amenitsch, and P. Laggner, Colloids and Surfaces A, (2001), in press.

STRUCTURAL INVESTIGATION OF THE SUB-MAIN TRANSITION IN DISTEAROYLPHOSPHATIDYLCHOLINE

M. Rappolt[1], M. Strobl[1], H. Amenitsch[1], S. Bernstorff[2] and P. Laggner[1]

1.) Institute of Biophysics and X-ray Structure Research, Austrian Academy of Sciences, Schmiedlstraße 6, A-8042 Graz, Austria.
2.) Synchrotron Trieste (ELETTRA), SS 14, Km 163.5, I-34012 Basovizza (TS), Italy.

Saturated Phosphatidylcholines display several thermotropic phases. The biological most relevant phase transition is the main transition in which the system changes from a gel-phase (ordered chains) to a fluid like phase [1,2]. However, in addition to the main transition some few tens of degree below, thermodynamic measurements have identified a low enthalpie transition: the sub-main transition [3,4]. This transition is highly cooperative, and a model has been presented [5,6] interpreting the transition to be due to decoupling of the acyl-chain melting from the disappearing of the primer lattice of the ripple-phase $P_{\beta'}$. Nevertheless, a detailed understanding of the molecular mechanism is still missing, therefore we carried out highly angular and thermal resolved small angle X-ray diffraction on distearoylphosphatidyl-choline (DSPC) in the near "full hydration" range. The calculation of density maps around the sub-main transition using reflections up to the 4th order (Fig. 1) are on the way.
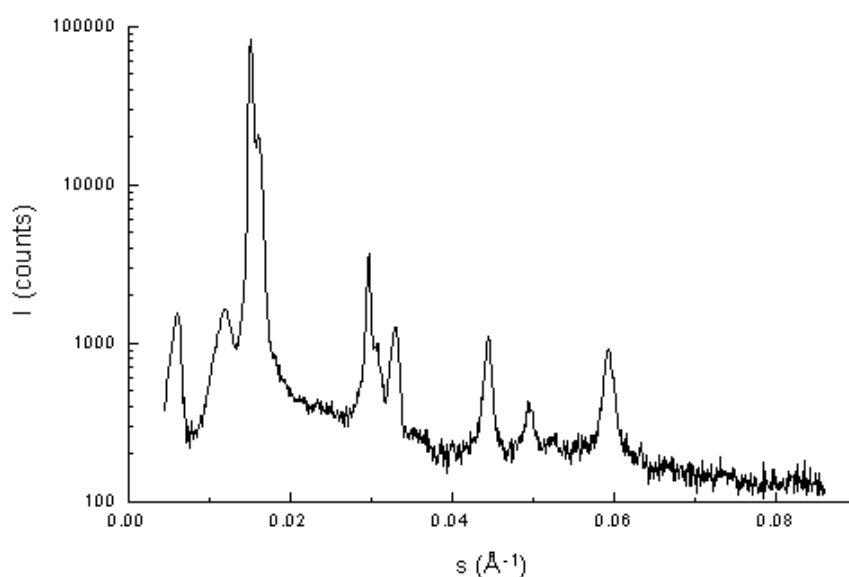
Figure 1. X-ray diffraction pattern of 75 wt% DSPC at 54.4 °C (a = 170 Å, b = 66.4 Å, γ = 89 °).

References:

[1] G. Cevc; Phospholipids Handbook; M. Decker, New York, Basel, Hong Kong (1993)
[2] P. Laggner; Progr. Colloid Polymer Sci. **93**, 112 (1994)
[3] K. Jørgensen; BBA **1240**, 111 (1995)
[4] K. Jørgensen and O.G. Mouritsen; Thermochim. Acta **328**, 81 (1999)
[5] M. Nielsen, L. Miao, J.H. Ipsen, K. Jørgensen, M.J. Zuckerman and O.G. Mouritsen; BBA **1283(2),** 170 (1996)
[6] K. Pressl, K. Jørgensen and P. Laggner, BBA **1325(1)**,1 (1998)

IN-SITU DYNAMICS OF PHASE TRANSIONS OF TREHALOSE POLYMORPHIC FORMS INVOLVED IN CRYPTOBIOSYS

F. Sussich[1], A. Cesaro[1], F. Princivalle[2] and H. Amenitsch[3]

1.) Dept. Of Biochemistry, Biophysics and Macromolecular Chemistry, Univ. of Trieste, I-34127 Trieste, Italy
2.) Dept. Of Earth Sciences, Univ. of Trieste, I-34127 Trieste, Italy
3.) Austrian Academy of Science-Inst. of Biophys. and X-ray Structure c/o Sincrotrone Trieste, SAXS-beamline, Basovizza, I-34012 Italy

Nature shows many examples of strategies for long term survival of organisms. Among those of most interest is the life protection (cryptobiosis) against low-humidity in extreme temperature conditions, far from the ambient. Sugars are the most well known chemicals that nature and man use as stabilizers for complex biostructures and foods preservatives Among all the sugars, trehalose [1, 2] has received the greatest attention, both because of its wide role in nature and its potential use as a highly efficient natural preservative. Experiments have revealed that all these organisms are able to induce the production of trehalose as they desiccate, and the dried organism is able to survive in a dormant state and then to "resuscitate" when environmental humidity permeates the cell, restoring the original conditions; this state can also be induced in non-adapted cells through the addition of exogenous trehalose There are no doubts that the solid state stability of trehalose at different temperatures and relative humidity conditions has to be fully known and taken into account for the assessment of its protection. If trehalose is involved in the preservation of organisms under thermal stresses, it seems obvious that a global knowledge of all the transformations is needed. In order to improve the understanding of trehalose metamorphism, it is of fundamental importance to systematically study the thermodynamics and the structural pattern of the polymorphic transformations with the final goal the elucidation of the mechanism behind the protection imparted by trehalose.

By means of calorimetric measurements [3,4,5] we have obtained qualitative and quantitative information about trehalose polymorphs interconversion. With time-resolved simultaneous small and wide angle X-ray scattering measurements (SWAXS) carried out at the SAXS beamline at ELETTRA new insight was gained into the system: using the on-line DSC we could performed simultaneously calorimetric and SWAXS measurements and the output was structural and thermodynamic data for the same sample. In Figure 1 is reported the results of a typical experiments: the thermogram of the trehalose polymorph under study and the corresponding SWAXS profile, still as a function of increasing temperature.

The reflected lines of diffraction patterns for the different polymorphs were indexed and the unit cell parameters were determined for two polymorphs, dihydrate trehalose (Th) and trehalose beta (Tβ) (see Table 1 and 2). Thermal expansion of this two crystalline form were then evaluated: the expansion coefficient along the *a* and *c* axes of dihydrate trehalose is quite larger than that observed for the *b* axis of beta trehalose, as well as the volume expansion of Th is bigger than that of Tβ. These findings are very important because dehydration is the key process for the protective action imparted by trehalose and the fact that dihydrated crystals expand easily as the temperature is increased is seen as a facility for the water molecules to be gently removed without the need of an high amount of energy; the anhydrous form Talpha (Tα) is then formed.The new proposed mechanism based on these results is that in nature with the decrease of water activity dihydrate trehalose is produced and afterwards water molecules can be reversibly removed form the crystals forming Tα without disrupting the native structure of the biological systems. The life-safe protection is guaranteed by the reversible path Th-Tα-Th.
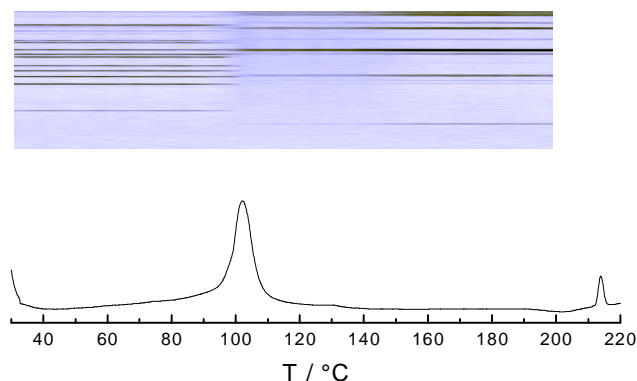
Figure 1. DSC trace and the corresponding SAXS profile for a sample of dihydrate trehalose (Th) heated at a scan rate of 10 K min^{-1}.

Table 1. Experimental data for dihydrate trehalose (Th)

Crystallographic axes	Unit cell parameter (nm)	Expansion coefficient
a	1.807	$6.1 \cdot 10^{-5}$
b	1.227	$1.6 \cdot 10^{-5}$
c	0.766	$6.6 \cdot 10^{-5}$
V	1.703	$1.41 \cdot 10^{-4}$

Table 2. Experimental data for trehalose beta (Tβ)

Crystallographic axes	Unit cell parameter (nm)	Expansion coefficient
a	1.313	$2.34 \cdot 10^{-5}$
b	0.861	$3.5 \cdot 10^{-5}$
c	0.695	$4.3 \cdot 10^{-5}$
V	0.766	$1.05 \cdot 10^{-4}$

References:

[1] S. Nkawa and H. Holzer in Moldave K. (Ed) Progress in Nucleic Acid Research and Molecular Biology, Academic Press 1997, 197-237

[2] L.M. Crowe, R. Mouradian,J.H. Crowe, S.A. Jackson, C. Womersley, Effects of carbohydrates on membrane stability at low water activity; Biochimica et Biophysica Acta, **769**, 141-150 (1984)

[3] F. Sussich, R. Urbani, F. Princivalleand A. Cesàro, Polymorphic amorphous and crystalline forms of trehalose. J. Am. Chem. Soc. **120**, 7893-7899 (1998).

[4] F. Sussich, F. Princivalle, A. Cesàro, The interplay of water removal in the dehydration of α,α-trehalose; Carbohy. Res. **322**, 113-119 (1999)

[5] F. Sussich, A. Cesàro, Transition and phenomenolgy of α,α-trehalose polymorphs inter-conversion, J.Thermal Analysis and Calorimetry, **62**, 757-768 (2000)

NON-LINEAR CONCENTRATION EFFECTS OF CHOLESTEROL ON LIPID BILAYERS STUDIED BY PRESSURE SCANNING

M.F. Vidal[1], M. Kriechbaum[1], M. Steinhart[2], H. Amenitsch[1], S. Bernstorff[3] and P. Laggner[1]

1.) Institute of Biophysics and X-Ray Structure Research, Austrian Academy of Sciences, Schmiedlstrasse 6, A-8042 Graz, Austria.
2.) Institute of Macromolecular Chemistry, Academy of Sciences of the Czech Republic, Heyrovsky Sq. 2, 162 60 Prague, Czech Republic.
3.) Sincrotrone Trieste, Strada Statale 14 - Km. 163.5 in AREA Science Park 34012 Basovizza, Trieste, Italy.

Hydrostatic pressure is an important thermodynamic variable for the structural phase behaviour of phospholipid membrane systems.

PC phospholipids exhibit thermotropic and barotropic lamellar phase transitions: a gel to liquid-crystalline (L_β/L_α) main transition, at a transition temperature T_m or at a transition pressure P_m respectively. Upon compression, the lipids adapt to volume restriction by changing their conformation and packing mode.

In our studies we used POPC (1-Palmitoyl-2-Oleoyl-*sn*-glycero-3-Phosphatidylcholine) in excess water which undergoes a phase transition from the lamellar gel phase to the lamellar fluid (liquid crystalline) phase at about –5°C at ambient pressure (1 bar) associated with a decrease of the lamellar d-spacing of about 1 nm.

The influence of cholesterol on the barotropic phase transitions of POPC was studied in pressure-scans by small-angle X-ray scattering at the SAXS beamline at ELETTRA.
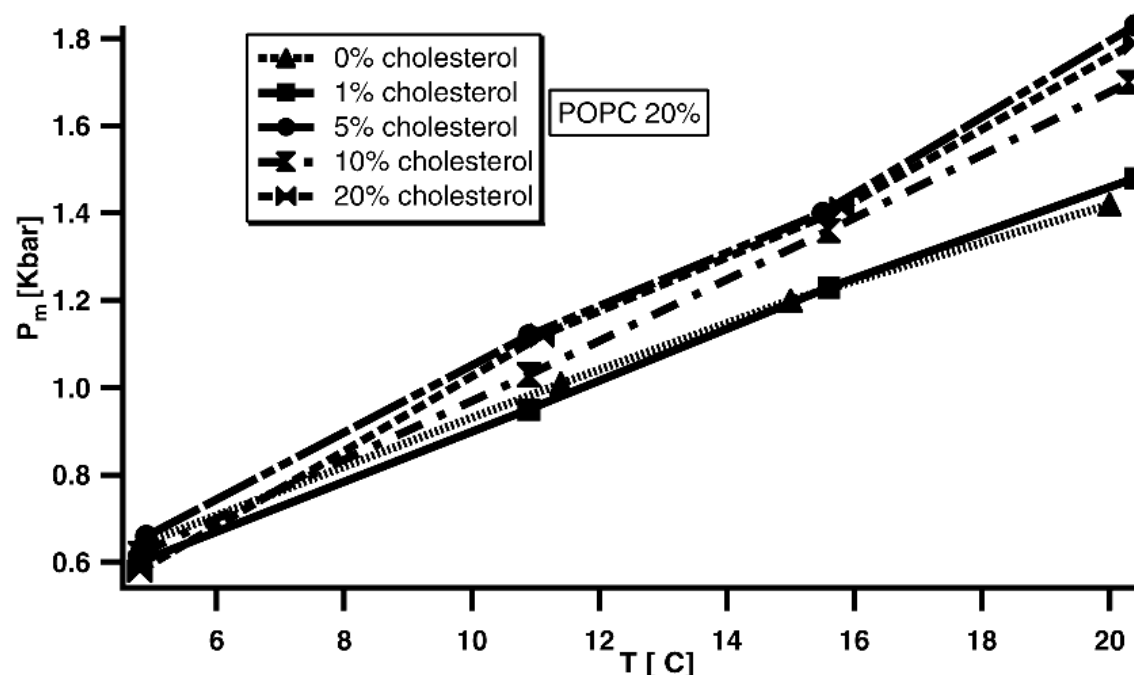
Figure 1. Transition pressure P_m of 20% POPC at different molar cholesterol concentrations (0-20%) as a function of temperature obtained from pressure-scans followed by SAXS.

Using the setup of the hydrostatic high-pressure X-ray cell [1,2] we have performed slow pressure scans in the range from 1-2000 bar at constant temperatures (5, 10, 15, 20°C) respectively, on various POPC/cholesterol dispersions in excess water and followed the

changes of the lattice parameters (i.e. lamellar repeat spacing) by SAXS in real-time, taking a single diffraction pattern typically every 2 s.

Increasing the temperature raises the transition pressure P_m for POPC 50 bar/°C. Adding cholesterol also induces a shift of the transition pressure to higher values. Using the Clausius – Clapeyron relation $dT_m/dP = T_m\Delta V_m/\Delta H_m$ the positive slope can be explained by an endothermic enthalpy change, ΔH_m, and a volume increase, ΔV_m ($265*10^{-7}$ m^3/mol), for the gel-fluid transition. Taking this value we have calculated the enthalpy: $\Delta H_m = 38$ kJ/mol, which agrees, within the errors limits, with published data. Additionally when studying the dependency of d-spacing as a function of pressure in slow p-scans (compression and decompression scan), we observed a significant hysteresis effect of the transition pressure P_m when adding cholesterol, reaching a maximum at 5% mol cholesterol.

Pressure scans studies of the lipid system POPC/cholesterol allow us to obtain structural and thermodynamic parameters. We have observed a significant hysteresis effect of the transition pressure when adding cholesterol, as well as an increase of the slope in the Clausius – Clapeyron relation, reaching in both cases a maximum at about 5% mol cholesterol. These results are in good agreement with measurements of the elastic properties of POPC bilayers obtained by T-jump experiments [3], where also a maximum at 5% mol cholesterol was observed. This can be interpreted as a softening of the bilayer at low cholesterol contents (<5%), whereas a higher cholesterol amount induces a rigidification of the bilayer. Furthermore, this indicates a domain structure of laterally separated POPC/cholesterol complexes and free POPC.

Figure 2. Hysteresis for POPC 20% and different molar concentrations of cholesterol at 20°C (d-spacing as a function of pressure during a p-scan, com-pression and decompression).

References:

[1] K. Pressl, M. Kriechbaum, M. Steinhart and P. Laggner; Rev. Sci. Instrum. **68**, 4588-4592 (1997)

[2] M. Steinhart, M. Kriechbaum, K. Pressl, P. Laggner and S. Bernstorff; Rev. Sci. Instrum. **70**, 1540-1545 (1999)

[3] G. Pabst, M. Rappolt, H. Amenitsch, S. Bernstorff and P. Laggner; Langmuir **16**; 8994-9001 (2000)

3. Physics

CRYSTALLIZATION OF PEO-PPO/PEO BLENDS

J. Baldrian[1], M. Horky[2], M. Steinhart[1], H. Amenitsch[3] and S.Bernstorff[4]

1.) Institute of Macromolecular Chemistry, Academy of Sciences of the Czech Republic, Heyrovsky Sq.2, 162 06 Prague, Czech Republic
2.) Faculty of Nuclear Sciences and Physical Engineering, Czech Technical University, V Holesovickách 2, 180 00 Prague 8, Czech Republic
3.) Institute of Biophysics and X-ray Structure Research, Austrian Academy of Sciences, Schmiedlstraße 6, 8042 Graz, Austria
4.) Sincrotrone Trieste, Basovizza, 34012 Trieste, Italy

The intensive research studies in the last years were devoted to the important family of polymer blends, namely block copolymer/homopolymer mixtures, where the homopolymer is identical with one block of the copolymer used. Prevailing part of these studies was devoted to blends with amorphous homopolymer admixture. However very little is known about the blends with homopolymeric crystalline component. The aim of this work was to study real-time development of the structure of such blends during isothermal melt-crystallization, to contribute to deeper knowledge of these technologically important systems.

Binary mixtures of two narrow-molecular-weight fractions 3000 (P3) and 4000 (P4) of PEO with triblock copolymer PEO-PPO-PEO (F) (Pluronic FP68, FLUKA, Mw ~ 3340-1760-3340) of 8/2, 5/5 and 2/8 compositions were studied by time-resolved SAXS/WAXS method. The copolymer was choosen because it has similar Mw of PEO tails (P33) as P3 and P4. The midle PPO block is amorphous. Measurements were performed during isothermal melt-crystallization (jump from 80 °C to T_C 35, 40 and 45 °C) in 256 frames, 10s each.

It has been shown that low-molecular fractions of PEO crystallize in stable lamellae with extended (EC) and integrally folded (IF) chains and in transient unstable lamellae with an intermediate thickness, which corresponds to the lamellae with nonintegrally folded (NIF) chains [1,2].

During isothermal crystallization two different lamellar systems LP1 (with thicker lamellae) and LP2 are simultaneously formed in neat copolymer and in the blends with predominant content of copolymer. This tendency faints with decreasing content of copolymer and in blends with majority of neat PEO components the only one lamellar system is developed. In the blend with 80 % of P4 a small part of this polymer crystallize in EC structure. Thicknesses of lamellae do not change during crystallization in prevailing part of blends. Only in the FP3 5/5 and FP4 2/8 5/5 blends the thicknesses of LP1 lamellae increase and thicknesses of LP2 lamellae decrease during crystallization.

A crystallization temperature strongly influence development of lamellar systems in blends as the crystallization rate decreases with increasing T_C. With growing T_C increases thickness of lamellae in both lamellar systems (Fig.1) and increases also content of lamellar system LP1. While in the blends with P3 are lamellar thicknesses of LP1 system greater than in neat copolymer, in blends with P4 are smaller one. In the case of LP2 system are these thicknesses smaller in both kinds of blends (Fig.1).

From the contents of LP1 and LP2 structures and their thicknesses of lamellae follows, that in all blends the cocrystal systems are formed during crystallization [1]. The LP1 lamellae in blends with P3 consist of extended chains of P3 and of copolymer PEO tails P33. The LP1 cocrystal structures developed in blends with P4 are probably formed by NIF chains of P4 and NIF and EC chains P33. The LP2 lamellar systems are, in both kinds of blends, cocrystals consisting in 1F and NIF chains of both components. The PPO part of the copolymer forms with chain ends and folds of PEO amorphous phase.
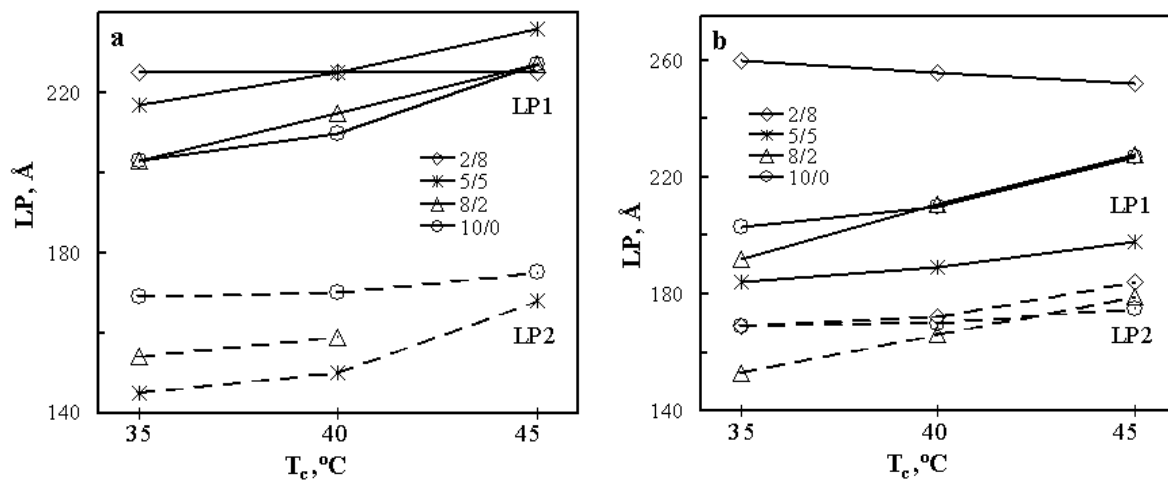
Figure 1. Changes of lamellar thickness LP1 and LP2 in F/P3 (a) and F/P4 (b) blends with crystallization temperature T_C

References

[1] J. Baldrian, M. Horky, M. Steinhart, A. Sikora, H. Amenitsch, S. Bernstorff S. and P. Laggner; Real-time microstructure development of PEO/PEO blends, 8th Users Meeting 'Sincrotrone' Trieste, Abstracts, p. 28

COCRYSTALLIZATION IN PEO/PEO BLENDS

J. Baldrian[1], M. Horky[2], M. Steinhart[1], A. Sikora,[1] H. Amenitsch[3], S. Bernstorff[4] and P. Laggner[3]

1.) Institute of Macromolecular Chemistry, Academy of Sciences of the Czech Republic, Heyrovsky Sq.2, 162 06 Prague, Czech Republic
2.) Faculty of Nuclear Sciences and Physical Engineering, Czech Technical University, V Holesovickách 2, 180 00 Prague 8, Czech Republic
3.) Institute of Biophysics and X-ray Structure Research, Austrian Academy of Sciences, Schmiedlstraße 6, 8042 Graz, Austria
4.) Sincrotrone Trieste, Basovizza, 34012 Trieste, Italy

This study was aimed at a better understanding of structure formation in crystalline/crystalline polymer blends during crystallization, attention being focused on the cocrystallization phenomena in these systems. Binary mixtures of two narrow-molecular-weight fractions 3000 (P3) and 4000 (P4) of poly(ethylene oxide) of 8/2, 5/5 and 2/8 compositions were studied by time-resolved SAXS/WAXS method and DSC. Measurements were performed during isothermal melt-crystallization (jump from 80 °C to 35 and 40 °C) and during cooling and heating (from melt to 35 °C and back).

It has been shown that low-molecular fractions of PEO crystallize in stable lamellae with extended (EC) and integrally folded (IF) chains and in transient unstable lamellae with an intermediate thickness, which corresponds to the lamellae with nonintegrally folded (NIF) chains [1,2]. Neat P3 forms EC and 1F lamellae while P4 can also form 2F lamellae [3].

At the beginning of isothermal crystallization, cocrystals are formed as a predominant structure. The single cocrystal system is developed in the blends 2/8, 5/5 and this structure does not change during crystallization (Fig.1a). In the 8/2 blend this starting cocrystal structure partly recrystallizes to the structures with lamellar thicknesses corresponding to the 1F (~10 nm) and EC (~20 nm) lamellae of P3.

The molten blends crystallize during continuous cooling also in cocrystal lamellae, the thickness of which grows with increasing content of P4. Similarly to the isothermal crystallization this structure in the blends 2/8, 5/5 does not change during cooling and in the 8/2 blend, a part of cocrystals recrystallize to the lamellae similar to 1F and EC structures of P3 (Fig.1b).

During heating, upon approaching melting points of the components, the structures of all blends recrystallize in the whole volume to the only one structure with EC/P3 thickness of lamellae, which means that the new more stable cocrystal system is formed.

A single cocrystal system or with a small amount of other lamellar systems are formed in the blends during both crystallization treatments. The components cocrystallize in a common crystal lattice. The thickness of cocrystal lamellae depends on the composition of blends, crystallization temperature and grows with growing concentration of P4. This thickening is caused by growing number of higher-molecular-weight chains (P4) incorporated in the cocrystal lamellae. The partial recrystallization of cocrystals to the 1F and EC structures in 8/2 blend during crystallization, probably consisting only of P3 chains, is caused by the higher content of the lower-molecular-weight component, which has lower melting temperature and higher chain mobility. Besides a lower molecular weight of component also a higher temperature facilitate this recrystallization. Our measurements are in accordance with DSC measurements.
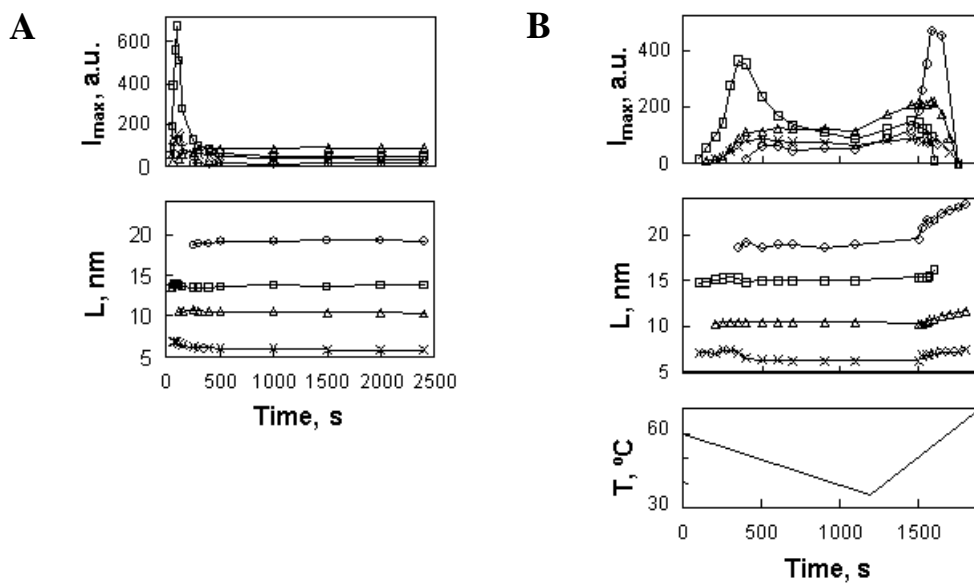
Figure 1 Time changes of SAXS peak intensities I_{max} and crystal thicknesses L of

a) P3/P4 5/5 blend during isothermal crystallization at 35 °C

b) P3/P4 8/2 blend during crystallization and melting

References:

[1] S.Z.D. Cheng, A. Zhang, J.S. Barley and J.Chen; Isothermal Thickening and Thinning Process in Low Molecular Poly(ethylene oxide) Fractions. 1. From Nonintegral-Folding to Integral-Folding Chain Crystal Transition; Macromolecules 24, 3937-3944 (1991)

[2] J. Baldrian, M. Horky, A. Sikora, M. Steinhart, P. Vleek, H. Amenitsch and S. Bernstorff; Time-resolved SAXS study of crystallization of poly(ethylene oxide)/ poly(methyl methacrylate) blends, Polymer **40**, 439-445 (1999)

[3] C.P. Buckley, A.J. Kovacs; Structure of crystalline Polymers, Ed. I.H. Hall, Elsevier, London, N.Y. (1984)

GISAXS STUDY OF CADMIUM SULFIDE QUANTUM DOTS

P. Dubcek[1], U.V. Desnica[2], I.D. Desnica-Frankovic [2], K. Salomon[2], S. Bernstorff[1], C.W. White[3], E. Sonder[3] and R.A. Zuhr[3]

1.) Sincrotrone Trieste, SS 14 km 163,5, 34012 Basovizza (TS), Italy
2.) Ruder Boskovic Institute, Bijenicka 54, 10000 Zagreb, Croatia
3.) Oak Ridge National Laboratory, P.O. Box 2008, Oak Ridge TN 37831, USA

The traditional method of preparing quantum dots in optical semiconductor devices is adding semiconductor components into glass melt. During the solidification process however, one has not sufficient control over the growth process, which results in non-ideal sample properties (defects, semiconductor surface states, dopant size fluctuations). Most of these drawbacks are overcome in a newly proposed technique of ion implantation into solid substrates.

In order to investigate the structure of films prepared by this new method, the grazing incidence small angle X-ray scattering (GISAXS) technique was applied on the films of CdS nanocrystals synthesized in SiO_2 by implanting separately constituent Cd and S atoms with a dose of $10^{17}/cm^2$ each and subsequently annealed at 700 °C. Due to the high concentration of nanocrystalline CdS, the scattered intensity is not following the distorted wave Born approximation.
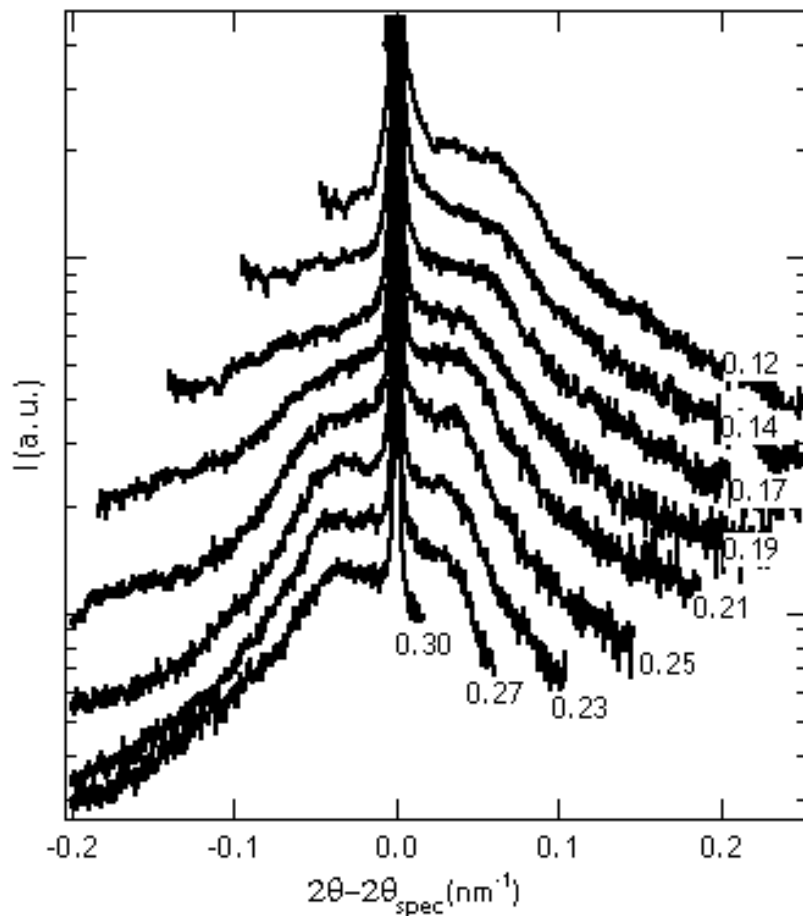
Figure 1. Inplane correlation part of GISAXS from ion (Cd and S) implanted SiO_2 vs. offset from specular angle, for diverse grazing incidence angles (in nm^{-1}, as indicated)

76

In addition to the surface scattering (surface roughness of 0.3 nm), additional contribution from nanoparticles, whose size varies with depth, is pronounced, particularly around the specular peak, where the correlation between the particles of similar sizes and at same depth is contributing with surface-like scattering. In figure 1. GISAXS from samples, with surface roughness contribution numerically deconvoluted, is plotted against offset from specular angle. The figure displays information about sizes of nanoparticles for different depth. The depth from which the scattering comes is controlled by grazing angle, which is indicated in the figure.
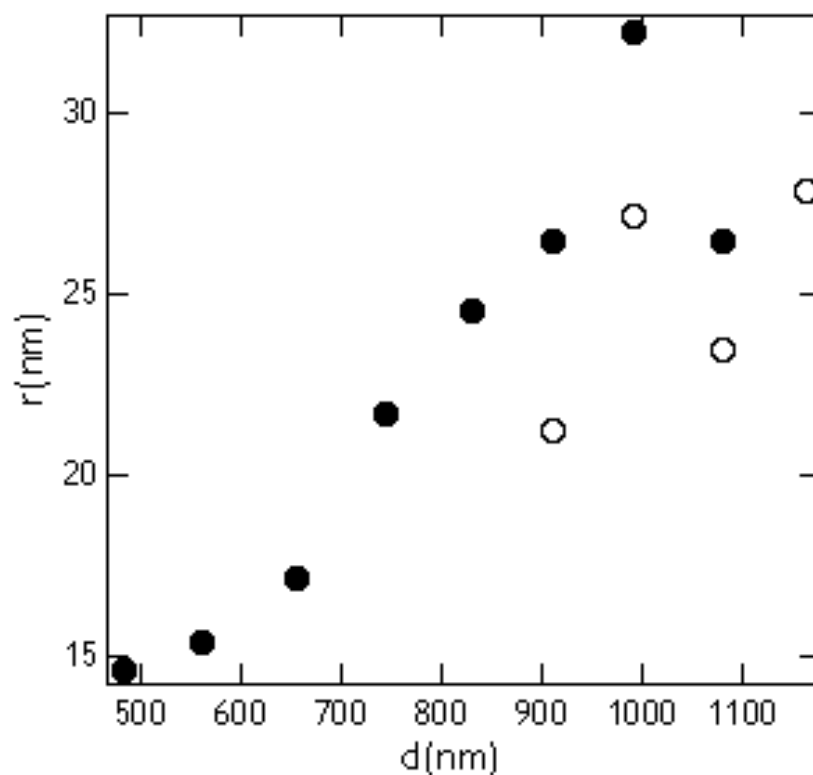
Figure 2. Quantum dots sizes vs. penetration depth

From calculated penetration depth, the depth size distribution is obtained, as displayed in figure 2. It is in good correlation with the results for depth distribution for constituent ions, revealing that this preparation method is a highly reliable one. The nanosizes can easily be controlled by the annealing parameters, since their growth is mainly influenced by difusion of constituent ions.

GRAZING-INCIDENCE SMALL-ANGLE X-RAY SCATTERINGON NANOSIZED VANADIUM OXIDE AND V/CE OXIDE FILMS

P. Dubcek[1], A. Turkovic[2], Z. Crnjak-Orel[3] and S. Bernstorff[1]

1.) Sincrotrone Trieste, SS 14 km 163,5, 34012 Basovizza (TS), Italy.
2.) Ruder Boskovic Institute, Bijenicka 54, 10000 Zagreb, Croatia
3.) National Institute of Chemistry, Hajdrihova 19, Ljubljana, Slovenia

Vanadium oxide, such as V_2O_5 tends to form layered structure that allows the intercalation/de-intercalation of different ions between its layers. Nanosize nature of its structure has also been found. Nanosize structure is making V_2O_5 and V/Ce oxides a good candidate for photoanodes in dye-sensitized solar cells.

To determine the grain size of sol-gel dip coating obtained vanadium/cerium oxide, grazing incidence small angle X-ray scattering (GISAXS) has been performed on them at SAXS beamline at Sincrotrone Trieste, using a Gabriel type, gas filled 1D detector. In order to precisely determine the film thickness, X-ray reflectivity was also measured: a sequence of GISAXS curves was recorded for a sequence of fixed grazing angles, and from these measurements, specular peak integral intensity was extracted, with diffuse intensity subtracted. The results are displayed in fig.1. together with the best fit obtained using distorted wave Born approximation (DWBA [1]). Because of the high intensity in specular peak interference fringes are clearly resolved here, and film thickness as well as film surface roughness is obtained.
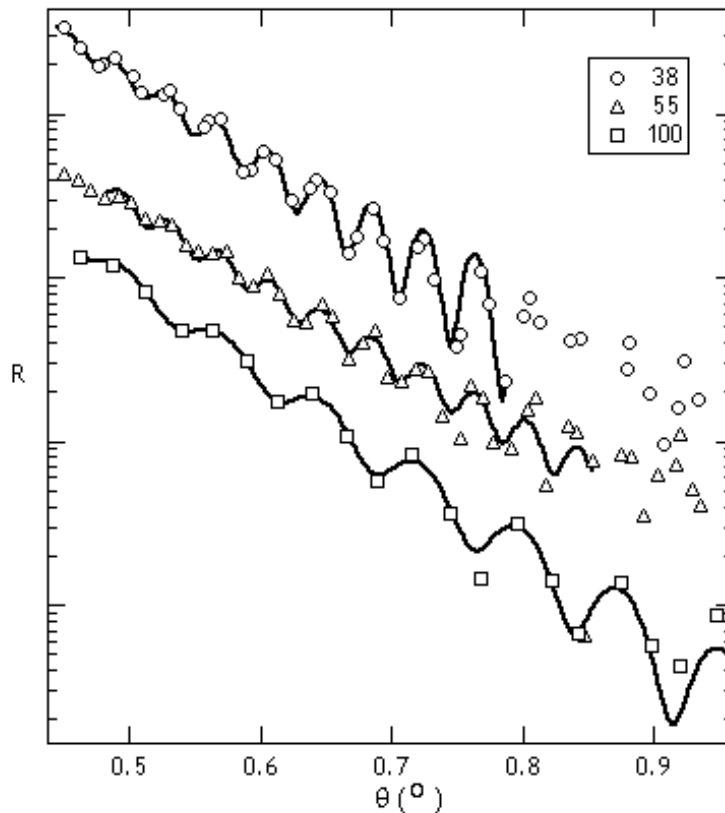
Figure 1. X-ray reflectivity of V/Ce oxide films together with best fits vs. grazing angle. The plots are offset vertically for clarity.

GISAXS results are displayed in figure 2. together with the best fits. These fits cannot reproduce the GISAXS results if only DWBA expression for a single film is used. When additional term, giving bulk scattering of Guinier type, corrected for absorption depending on grazing and scattering angle, is included the reproduction of experiment is much better. Due to the significant difference in electron density between cerium and vanadium oxides, nanoparticles contribution to the scattering is weakest (relative to surface scattering) in the highest vanadium concentration sample. On the other side, characteristic sizes for particles and porosity do not differ that much (see table 1.).
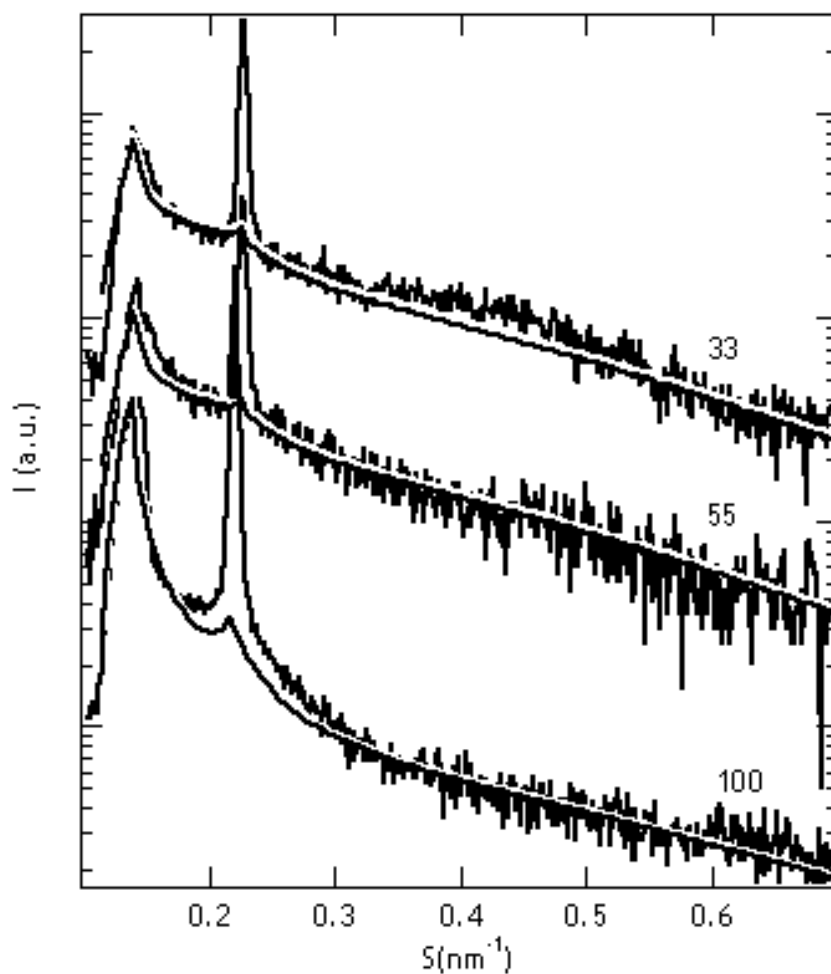
Figure 2. GISAXS of V/Ce oxide films together with best fits vs. scattering angle. The plots are offset vertically for clarity.

Table 1. Characteristic sizes in V/Ce oxide films obtained by different measurements.

Vanadium percent	Film thickness [nm]	Surface roughness Reflectivity [nm]	Surface roughness GISAXS [nm]	Guinier radius (nm)
33	55.3	0.72	1.0	0.61
55	54.9	0.63	1.1	0.65
100	28.6	0.78	1.5	0.50

[1] S.K. Sinha, E.B. Sirota, S. Garoff, *Phys Rev B,* **38** (1988) 2297.

X-RAY REFLECTIVITY STUDY OF DERELAXATION IN KRYPTON IMPLANTED MONOCRYSTALLINE SILICON

P. Dubcek[1,2], B. Pivac[1], O. Milat[3], S. Bernstorff[2], and I. Zulim[4]

1.) Rudjer Boskovic Institute, P.O. Box 180, HR-10000 Zagreb, Croatia
2.) Sinchrotrone Trieste, SS 14km 163.5, I-34012 Basovizza (TS), Italy
3.) Institute of Physics, P.O. Box 1010, HR-10000 Zagreb, Croatia
4.) Faculty of Electrical and Mechanical Engineering, and Naval Architecture, University of Split, R. Boskovica b.b. HR-21000 Split, Croatia

The amorphous silicon (a-Si) is considered to be a model system of a covalently bonded continuos random network [1], which makes it an ideal system to study the effect of structural disorder on various material properties. Annealing of such a systems produces changes in the structure, often called „structural relaxation", which include evolution of the system to lower free energies, while derelaxed state from relaxed one can be obtained by low dose ion implantation of relaxed state at room temperature.

We have investigated amorphous silicon layers produced by the Kr^+ ion implantation into (100) oriented Czochralski silicon wafers at room temperature. Multiple energy implants were performed to generate a 220 nm uniform amorphous layer. The implanted doses were 2.0×10^{15} at/cm^2 for a 250 keV beam energy and 5×10^{14} at/cm^2 for 100 keV (sample A). Then, samples were annealed in a vacuum furnace (residual pressure ~5×10^{-7} Torr) at 500°C for 90 min to fully relax the amorphous structure and to remove the damaged layer at the crystal/amorphous interface (sample B). Partially relaxed, i.e. derelaxed states, have been obtained by reimplanting the fully relaxed a-Si layer with the Kr^+ ions with the same energies to doses ranging between 6×10^{11} and 2×10^{14} at/cm^2 to produce 0.003, 0.006, 0.012 and 0.024 displacements per atom (samples 1 to 4 respectively).

X-ray reflectivity has been measured using Gabriel type, gas filled 1-D detector at fixed position, while the grazing angle has been changed from below the critical angle, up to 2° approximately. From these measurements, specular peak integral intensity has been extracted, with diffuse intensity subtracted, and it is shown in figure 1. The results have been fitted according to distorted wave Born approximation (DWBA)[2] for single film on thick substrate.

Slightly above the critical angle, the reflectance drops from 1, following the exponential law for top surface, since the reflected radiation from lower surface is attenuated in the film. For the as-implanted sample (A) it continues to fall smoothly. For relaxed sample, on the other hand, a decrease after the critical angle is steeper and for higher values of angle exhibits oscillations. These are due to interference with the part of the beam reflected from the lower surface of the uneffected top film. Soon after the first and the lowest dose of 6×10^{11} at/cm^2 of Kr reimplantation observed oscillations completely disappear and spectrum resembles very much of as implanted one due to destroyed correlation between the two surfaces. Also a decrease after the critical angle becomes less steep similar to as-implanted case. Further implantation produced sudden drop after the critical angle and the appearance of oscillations that become more evident with increasing the dose of implanted ions.
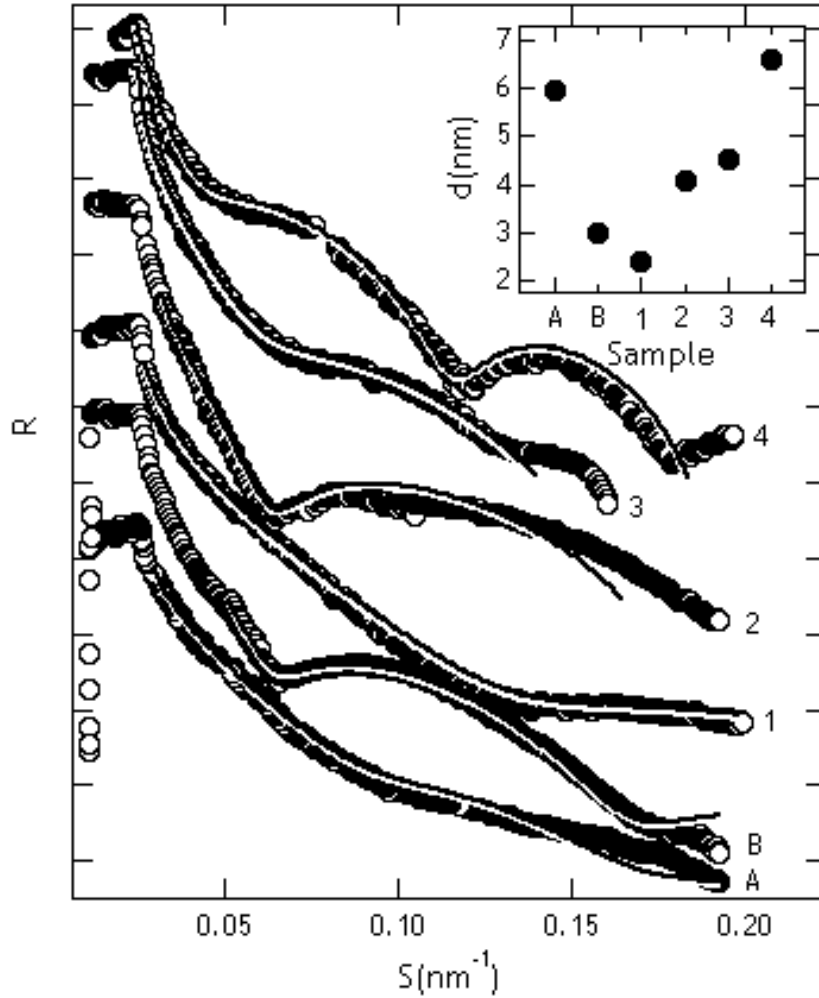
Figure 1. Figure shows X-ray reflectivity spectra together with the best fit obtained using DWBA. The spectra are offset vertically for clarity. Calculated film thickness is given in the inset of the figure vs. sample number.

From the reflectivity data it has been concluded that the structure of the samples comprises of thin film, mostly unaffected by the implantation, above the Krypton rich amorphous layer 220 nm thick. Upon annealing, the density of defects does not vary altogether smoothly with the depth. A relatively sharp change in density (of electrons) is formed few nanometers below the surface, which is resolved as oscillations in reflectance curves when the correlation between upper and lower surface is good. This correlation is more or less destroyed in the sample 1 after an additional implantation, but it is rebuilt in subsequent ones. Deeper through the sample, density of the electrons is varying smoothly (amorphous film), and no double film type contribution is detected. Oscillations due to lower edge of Krypton rich layer are not resolved due to poor surface to surface correlation. The relaxation/derelaxation dynamics is indicated by uneffected top film thickness, as displayed in figure 1. It is reduced after relaxation, because the transition from monocrystalline to amorphous silicon film is structurally relaxed, but reimplantation (derelaxation) slowly rebuilds the same film thickness and surface roughness. Only the surface to surface correlation does not resemble the one of as implanted sample, which is attributed to top surface changes caused by implantation process.

[1]D.E. Polk and D.E. Bourdreaux, Phys. Rev. Lett. **31**, 92 (1973).
[2] S.K. Sinha, E.B. Sirota, S. Garoff, Phys Rev B, **38** (1988) 2297.

DEPTH-INFLUENCED STRUCTURE THROUGH PERMEATING POLYMER MEMBRANE

H.Grigoriew[1], S.Bernstorff[2], A.Wolinska-Grabczyk[3], J.Domagala[4], A.G.Chmielewski[1]

1.) Institute of Nuclear Chemistry and Technology, Warsaw, Poland
2.) Sincrotrone ELETTRA, Trieste, Italy
3.) Institute of Coal Chemistry PAS, Gliwice, Poland
4.) Institute of Physics PAS, Warsaw, Poland

The studies of permeation through polymer membrane do not involve yet an experimental measurement of any parameter step by step in the range covering whole membrane thickness, during permeate transport. It is due to experimental difficulties. All information we obtain comes from outside of the membrane, on its supplying and\or expelling side, eventually we can register some parameters referring to the whole membrane volume. Numerous theories and models of permeation were verified experimentally only indirectly by comparison of values of ingoing and outgoing parameters.

Synchrotron application using the SAXS method gave new possibilities in the subject. The question was: in which way we can measure a polymer structure step by step in the whole range of membrane thickness during solvent permeation. The main goal of this work was to find this way. We have chosen measurements in transmission mode, step by step, through model sample of greater dimensions.

The sample for SAXS measurements dependent on the membrane depth represented a section through an permeating membrane, which bottom surface is in a contact with solvent, and the top one with air. Therefore we made from a polyurethane foil a model sample, in a 10:1 scale, of dimensions 5mm x 20mm which represents the section of 5mm thick membrane. The foil was of proper thickness for X-ray measurements in transmission (0.3mm). To avoid evaporation in all directions above solvent level, the both sides of the sample (20 x 5mm) were covered by thin (1μm) layer of aluminium deposited in vacuum. The deposited aluminium bands were 3 mm wide, so the edges of the sample remained uncovered and accessible for sorption or/and evaporation. The continuity of the aluminium bands was tested using a microscope. Just before SAXS measurement the lower part of the 5mm thick membrane was dipped in benzene to reach saturation (Fig.1a). This resulted in a slight change of the sample shape from rectangular to half-moon (Fig.1b). After taking out of the benzene bath, the sample was immediately put in the aluminium pocket and measured in the same vertical position.
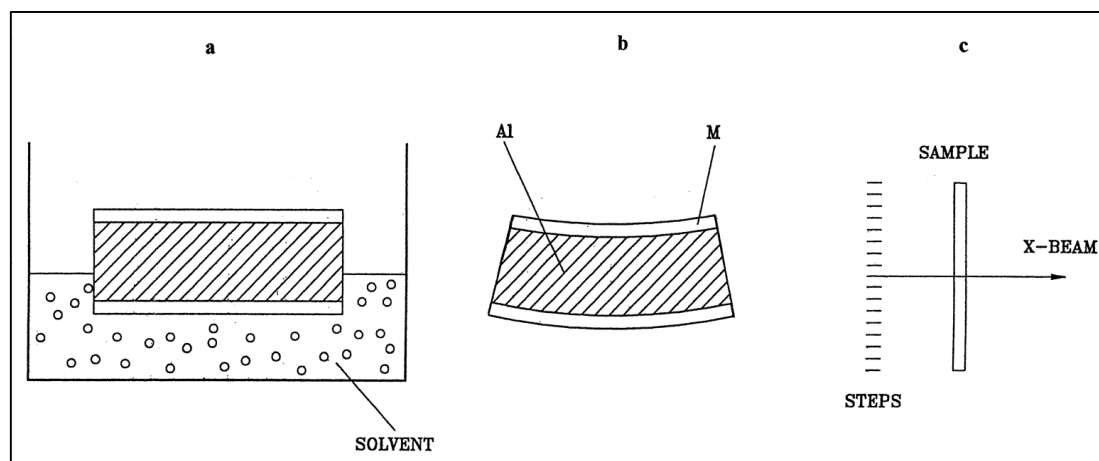
Figure 1. Experimental set-up.

The SAXS measurements were carried out at the Austrian SAXS beamline of the synchrotron ELETTRA. All measurements were done in transmission, at room temperature. The depth-dependend measurements were performed for subsequent vertical shifts of the sample table, in steps of 0.2mm each, from supplying to expelling side of the sample (Fig.1c).

The measurements data were subjected to a preliminary treatment and displayed using the OTOKO program. The SAXS curves measured step by step from supplying to expelling side of the sample height are displayed in the Fig.2 after initial treatment.
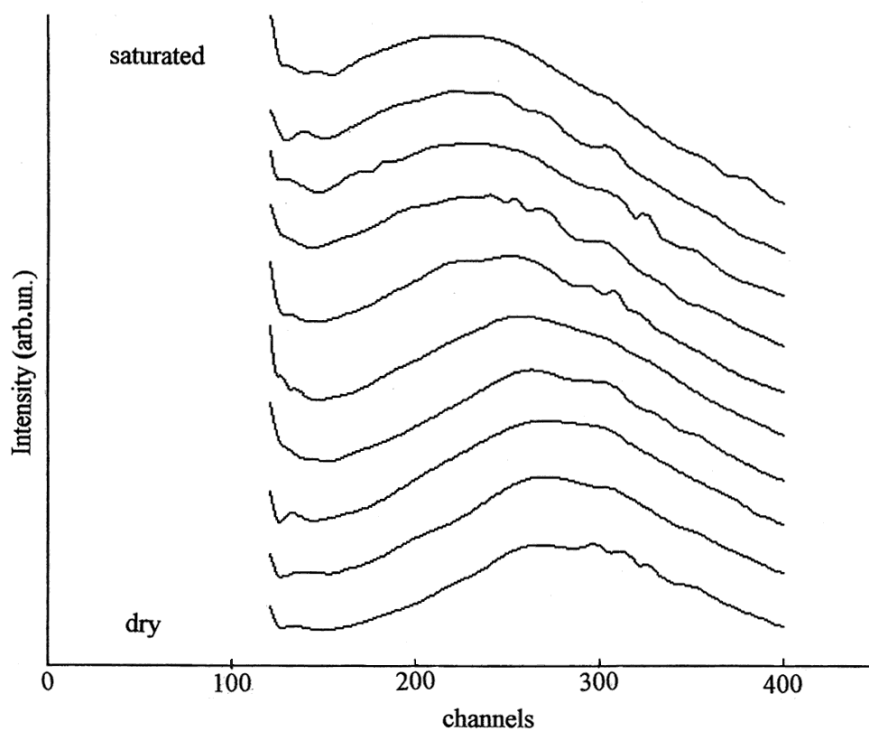
Figure 2. SAXS curves for subsequent steps of the sample height.

A comparison of the SAXS maxima positions for our previous measurements of dry and saturated-in-benzene polyurethane sample (6.4 and 7.4nm) with maxima positions for depth-dependend measurements (Table I) shows that the top part of „ the section" was fully dry and its bottom part was fully saturated with benzene. This is an evidence of the correct way of the sample preparation. The continous change of the SAXS maximum position through the sample means,that for dry sample the maximum is not generated by a form factor, but by repeated distances between lamellae.

Table I. Interlamellar distances, L [nm], for subsequent steps (after Lorentz correction).

L	7.4	7.2	6.9	6.7	6.6	6.5	6.5	6.4	6.4
L_S	11.8	11.6	11.2	10.8	9.9	8.3	7.0	-	-

Positions of the maxima give us interlayer distances - L- in lamellar structure of the polymer. The L values decrease monotonically from bottom to top of the sample (Table I). This decrease is associated with decreasing amount of the solvent in the swollen polymer, going from bottom to top of the sample. This monotonic change does not agree with commonly used model of permeation, with phase-transition (from liquid to vapor solvent) inside the membrane.

As one can see from Fig. 2, the slope of the SAXS maximum on the side of greater s is the same for all curves. The shift of the maximum in subsequent curves is caused only by the

shift of the slope on the side of smaller s. The one-sided change in the maximum shape inclined us to subtract the SAXS curve for the dry membrane from the curve for the saturated one. It occures that the difference has the form of a second peak. Next, we repeated the operation for curves from other steps and found that there is visible formation of a peak that emerges from experimental noises at steps nearly of the top and becomes greater and more close at steps near to the bottom of the sample (Fig.3). Simultaneously its position shifts from about 7 nm to nearly 12nm (Table I, values L_s).
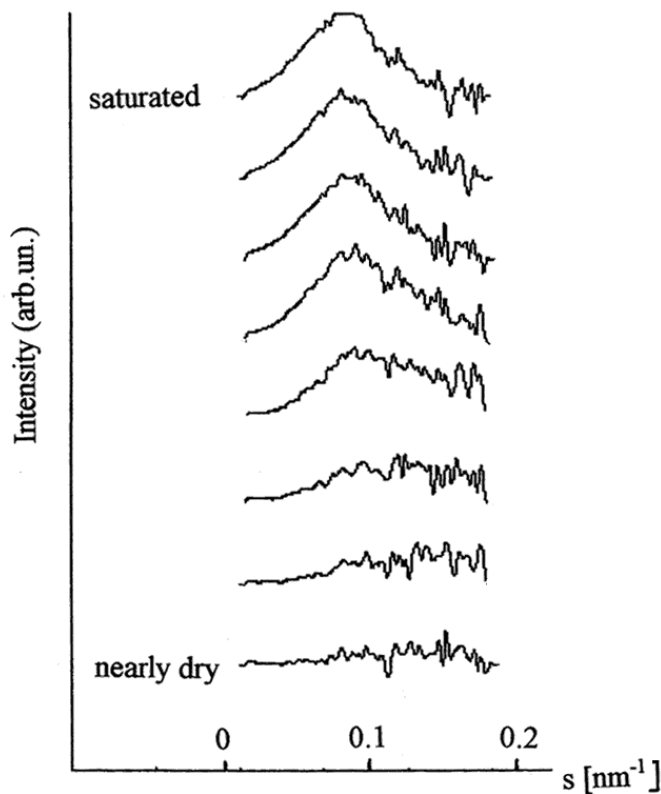
Figure 3. The results of subtraction the SAXS curve for dry membrane from subsequent ones (Lorentz corrected).

This second peak indicates the formation of new kind of aggregates as a result of an interaction between polymer and solvent, assuming that the structure of dry polymer is invariable. Nature of these aggregates is not clear. Because of close connection of the rising peak with the first one at the beginning stage, we may suppose that the aggregates are also of lamellar structure. But in contrary to the initial lamellar phase, the aggregates are very susceptible to the solvent amount (Fig.3 and Table I). Maybe it is a general phenomen that solvent conducives to the formation of a new kind of the aggregates in polymer matrix.

Reference.

H.Grigoriew, S.Bernstorff, A.Wolinska-Grabczyk, J.Domagala and A.G.Chmielewski
„Depth-influenced structure through permeating polymer membrane using SAXS synchrotron method.“,
Journal of Membrane Science 186, 1-8 (2001).

IN-SITU STUDY OF NANOCRYSTALLIZATION IN AMORPHOUS FeCuNbSiB ALLOY: EFFECT OF ANNEALING CURRENT DENSITY ON THE MICROSTRUCTURE

Ajay Gupta[1], Neelima Paul[1], B.A. Dasannacharya[1], G. Principi[2], A. Maddalena[2], S. Bernstorff[3] and H. Amenitsch[4]

1.) Inter-University Consortium for DAEF University Campus, Khandwa Road, Indore-452 017, India
2.) Settore Materiali, DIM and INFM, Universita di Padova, via Marzolo 9, I-35131 Padova, Italy
3.) Sincrotrone Trieste, SS 14, Km 163.5, I-34012 Basovizza, Trieste, Italy
4.) Institute for Biophysics and X-ray Structure Research, Austrian Academy of Sciences, Schmiedlstraße 6, A-8042 Graz, Austria

Nanocrystalline alloys produced by a controlled partial crystallization of amorphous transition metal-metalloid metallic glasses, containing small amounts of Cu, Nb, Ta, Zr are excellent soft magnetic materials, possessing high permeability and saturation magnetization [1,2]. Because of their great practical importance, extensive studies are being done on the mechanism of nanocrystalline phase formation as well as on the cause of their improved magnetic properties. Partial crystallization of such amorphous alloys results in formation of nanocrystals of a fcc Fe-Si phase dispersed in an amorphous matrix. Despite extensive studies using various microscopic and macroscopic techniques, the exact mechanism of nanocrystalline phase formation and the role played by Cu and Nb atoms has not yet been fully understood. A detailed understanding of the mechanism of nanocrystalline phase formation and the microstructure of the system is necessary in order to understand the improved soft magnetic properties of these alloys and also to optimize the alloy composition and annealing treatments for achieving the best soft magnetic properties.
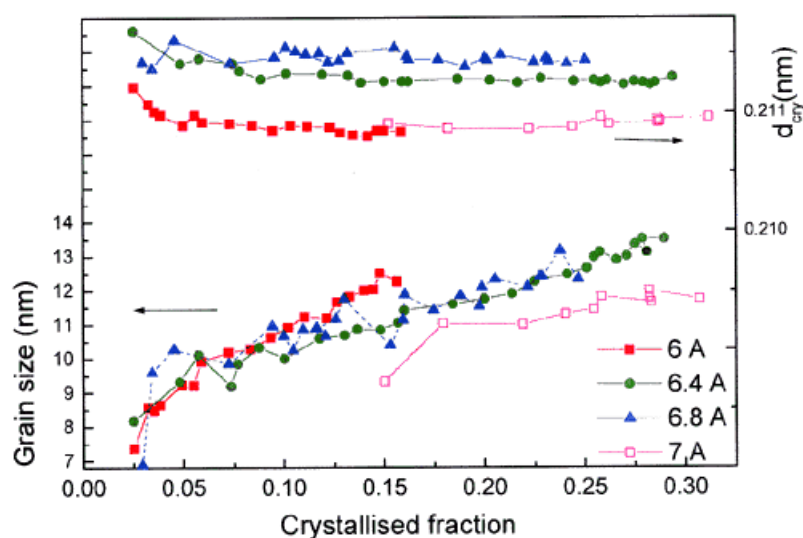
Figure 1. Variation of grain size and lattice constants as a function of crystallized fraction.

In the present experiment nanocrystallisation in the alloy FeCuNbSiB was studied using simultaneous wide-angle x-ray scattering (WAXS) and small angle x-ray scattering (SAXS) techniques. In-situ measurements were done during nanocrystallistaion induced by passing a dc current of sufficient strength through the sample. Figure 1 gives the variation of grain size as well as the lattice constant of the nanocrystalline phase as a function of crystallized fraction

for various values of current density. As seen earlier [3], the grain size increases with the amount of crystallization. However, with higher current density the average grain size at a given stage of crystallization is lower. Since the average crystallite size of nanoparticles effects the magnetic properties of the system, present studies suggest that the magnetic properties can be controlled by controlling the current through the sample during nanocrystallisation. The lattice constant of the nanocrystalline phase shows a non-monotonous variation with current density. Initially when the current is increased from 6 A to 6.4 A or 6.8 A, the lattice parameter increases. This is expected as higher current density would mean a higher specimen temperature and since the measurements are done in-situ, the thermal expansion would cause d value to increase with increasing current density. However, at 7 A the d value decreases. This decrease in d value at 7 A should be connected with a change in the composition of the grains. Analysis of the small angle x-ray scattering data (Figure 2) also shows that porod constant for a given degree of crystallization decreases with increasing current density. This again suggests some variation in the composition of the nanocrystalline phase.
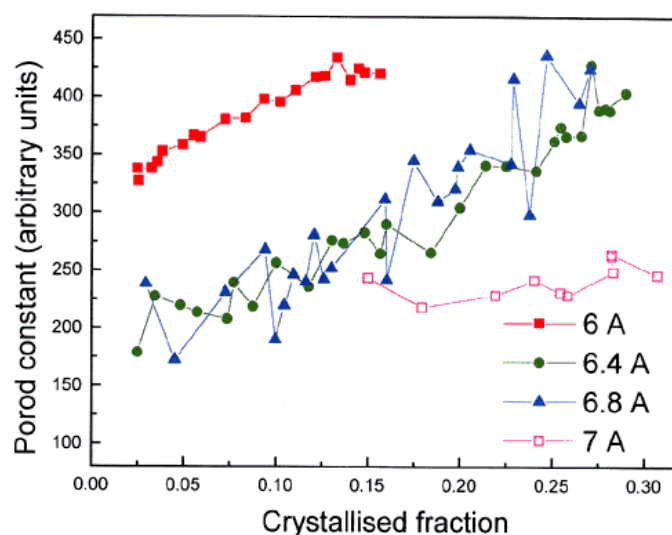
Figure 2. Porod constant as a function of crystallized fraction.

Recently, Hono et al. [4], using 3-dimentional field ion microscopy, have found that the on-set of nanocrystallization is preceded by formation of Cu clusters with size approximately 3 nm, and estimated number density from the analyzed volume to be of the order of 10^{24} m^{-3}. This is an important information for elucidating the role of Cu in nanocrystalline phase formation. However, since 3D FIM looks at a very small volume fraction (typically 40nmx10nmx10nm) of the material, it may not represent an average picture of the system.

In the present work we get a clear evidence of Cu cluster formation from the small angle scattering data. Figure 3 gives the small angle scattering as well as wide-angle scattering data for various annealing times at a current of 6 A. One may note that up to an annealing time of 2000s no nanocrystallisation occurs (as seen by WAXS measurements) while there is a large increase in the small angle scattering. This substantial increase in the small angle scattering before the onset of nanocrystallisation can be taken as an evidence for the formation of Cu clusters. A detailed study of the kinetics of Cu cluster formation will be done during the forthcoming beam time.

References:

[1] Y. Yoshizawa, S. Oguma and K. Yamauchi, J. Appl. Phys. 64 (1988) 6044.

[2] G. Herzer, IEEE Trans. Magn. 25 (1989) 3327.

[3] Ajay Gupta, N. Bhagat, G. Principi, A. Maddalena, N. Malhotra, B.A. Dasannacharya, P.S. Goel, H. Amenitsch, S. Bernstorff, Intermetallics 8 (2000) 287

[4] K. Hono, D. H. Ping, M. Ohnuma and H. Onodera, Acta Mater. 47 (1999) 997.
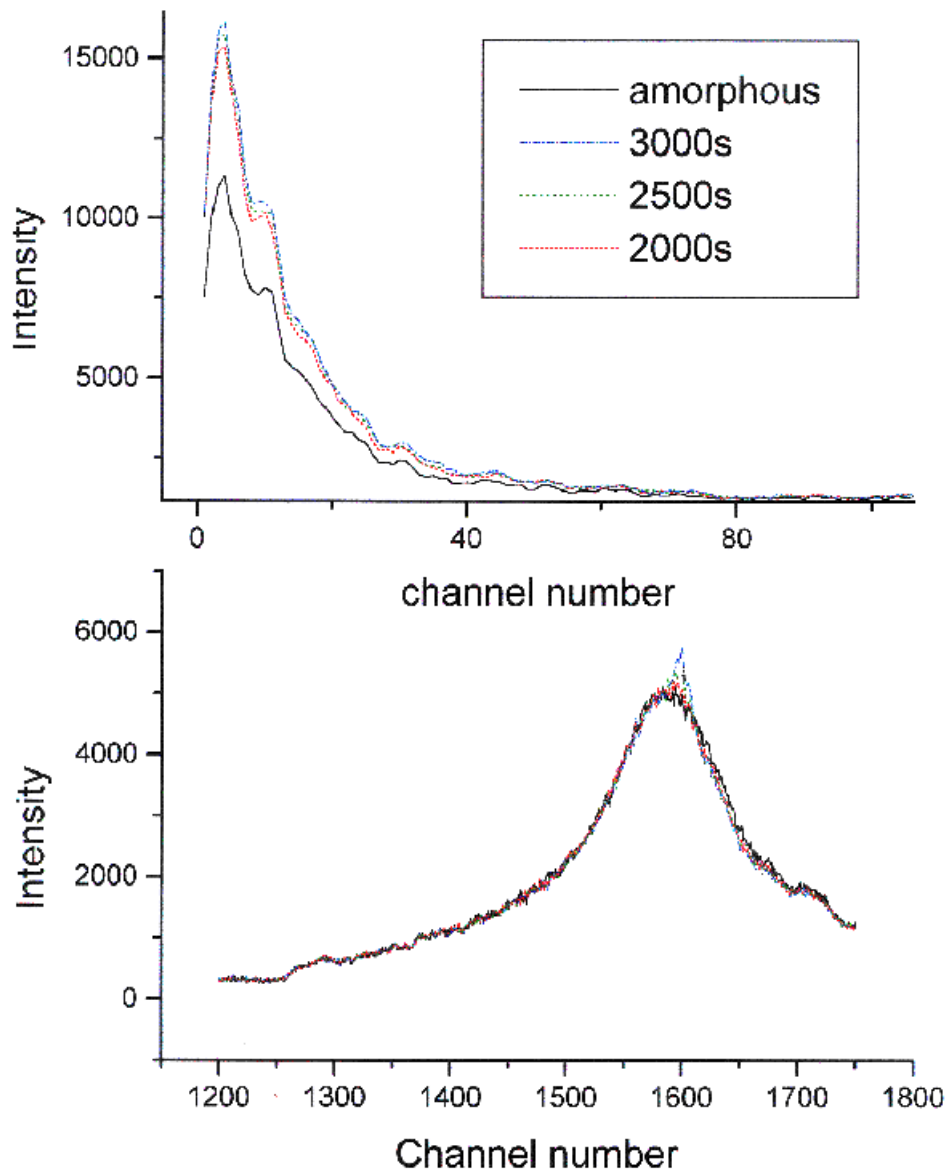
Figure 3. Small angle scattering and wide-angle scattering data for various annealing times at a current of 6 A.

SIZE SCALING OF DENDRITIC MICELLES FROM SOLUTION SAXS

R. Kleppinger[1], E.W. Meijer[1], S. Bernstorff[2] and H. Amenitsch[3]

1.) Laboratory of Macromolecular and Organic Chemistry, Technical University Eindhoven, NL-5600 MB Eindhoven, The Netherlands
2.) Sincrotrone Trieste, ELETTRA, Strada Statale, 14 km 163.5, Trieste, Italy
3.) Institute of Biophysics and X-ray Structure Research, Austrian Academy of Sciences, Schmiedlstraße 6, A-8042 Graz, Austria

Dendrimers are monodisperse macromolecules, build via step-wise addition of branched subunits to a multifunctional core. Due to their large number of endgroups these sysstems are able to complex various types of metals allowing for the preparation of new types of staining agents for magnetic resonance imaging. On the other hand, their ability to act as hosts for low molar mass guest molecules is of great significance for pharmaceutical applications where they might act as well-defined synthetic drug delivery systems.[1] The typical structure of a dendrimer that might be suited for these type of applications is displayed in figure 1.

The unique behavior of dendritic macromolecules is related to the distribution of their subsegments. This issue has been adressed in a number of modelling studies which gave in part contradicting results and suggested either a "dense-core" or a "dense shell" structure.[2,3] Experimentally this aspect is difficult to evaluate since such systems do not form crystals that can be analyzed via X-ray crystallography. Therefore, structural studies were based on small angle scattering from dilute solutions of these macromolecules where structure factor contributions are negligible. In this case, scattering pattern reflect the form factor contributions only.[4] Using SAXS, the scattering from a series of oligoethyleneoxy-terminated poly(propyleneimine)dendrimers[5] with molar mass varying between 3 and 54kgMol^{-1} had been evaluated. The ratio among the forward scattering intensities are related to their different molar mass. In combination with the invariant this yields an estimate for the particle volume which -except for the smallest dendrimer- agreed rather well with calculated values for the single molecules. The radius of gyration of the systems is displayed in figure 2 as a function of the molar mass of the system. In addition to the dendrimers evaluated in the
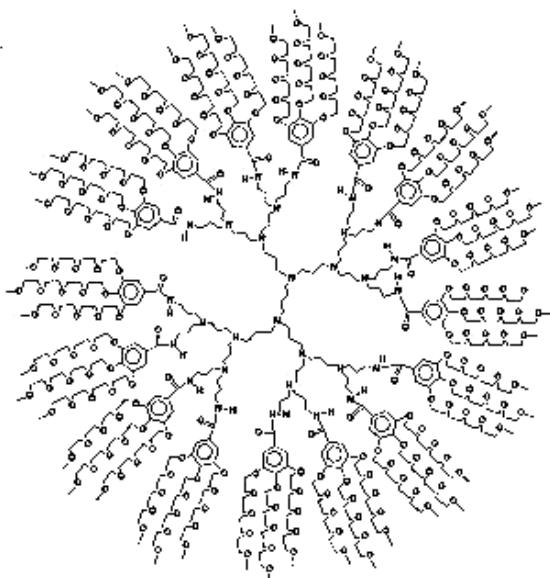
Figure 1. Structure of oligo(ethyleneoxy) terminated poly(propyleneimine) dendrimer, displayed is a dendrimer of generation three
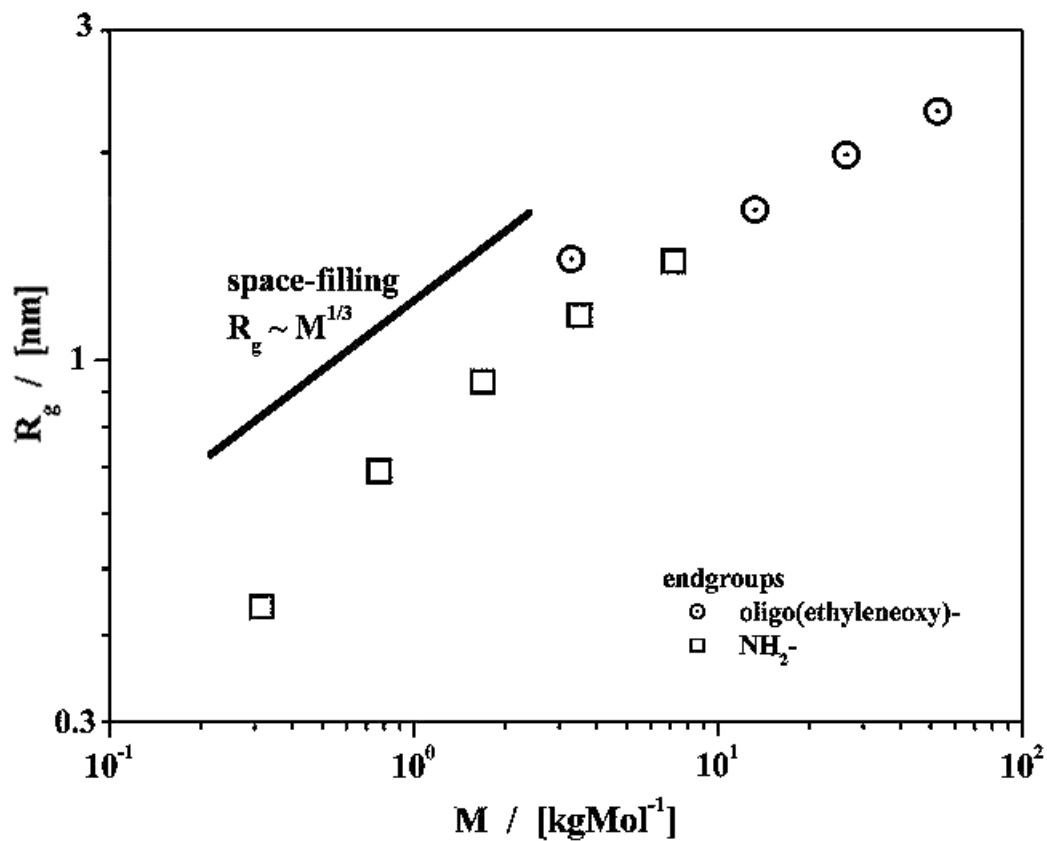
Figure 2. Scaling of the radius of gyration of the dendrimers with molar mass

References:

[1] Jansen, J.F.G.A.; de Brabander-van den Berg, E.M.M.; Meijer, E.W. Science **266**, 1226 (1994)

[2] de Gennes, P.G.; Hervet, H. J. Phys. (Paris) **44**, L351 (1983)

[3] Lescanec, R.L.; Muthukumar, M. Macromolecules **23**, 2280 (1990)

[4] Kleppinger, R.; Reynaers, H.; Desmedt, K.; Forier, B.; Dehaen, W.; Koch, M.H.J.; Verhaert, P. Macromol. Rapid Commun. **19**, 111 (1998)

[5] Baars, M.W.P.L., Kleppinger, R.; Yeu, Koch, M.H.J.; S.H. Meijer, E.W. Angew. Chemie Int. Ed. **39**, 1285, (2000)

4. Chemistry

INCREASING THE OIL SOLUBILIZATION CAPACITY OF M41S MATERIALS THROUGH THE USE OF CO-SURFACTANTS

J. Andersson[1], P. Ågren[2], P. Bussian[2], H. Amenitsch[3] and M. Lindén[1]

1.) Dept. Phys. Chem., Åbo Akademi University, Porthansgatan 3-5, 20500 Åbo, Finland
2.) MPI Kohlenforschung, Kaiser-Wilhelm-Platz 1, D-45470 Mülheim a.d. Ruhr, Germany
3.) Institute of Biophysics and X-ray Structure Research, Austrian Academy of Sciences, Schmiedlstr. 6, 8042, Graz, Austria

Introduction

The solubilization of toulene in mesoscopically ordered silica of type M41S [1] was studied by *in situ* XRD at the Elettra beam-line. Here, silicate oligomers and surfactants, normally CTAB, self-assemble to form a mesoscopically ordered hybrid material. An earlier study [2] revealed that toluene is solubilized to a much larger extent than saturated alkanes due to its relatively high water solubility and that a large amount of the toluene is solubilized after the inorganic-organic mesophase has formed.[3] It is well known that the use of co-surfactants may increase the solubilization capacity of ionic surfactant micelles quite dramatically, due to their influence on the preferential interfacial curvature of the mixed surfactant-co-surfactant aggregates formed. The scope of the present study was to investigate if the use of co-surfactants has a similar influence on the solubilization capacity of mesoscopically ordered silica. The experimental setup and synthesis conditions have been described elsewhere.[4] Several chemically different co-surfactants were used, including fatty acids, fatty amines and fatty alcohols.

Results

Addition of co-surfactants to the synthesis resulted in a much more efficient solubilization of toluene by the silicate-surfactant mesophase. An example of a measured time-resolved X-ray diffraction pattern is shown in fig 1, for the addition of decanoic acid, da, to the synthesis.
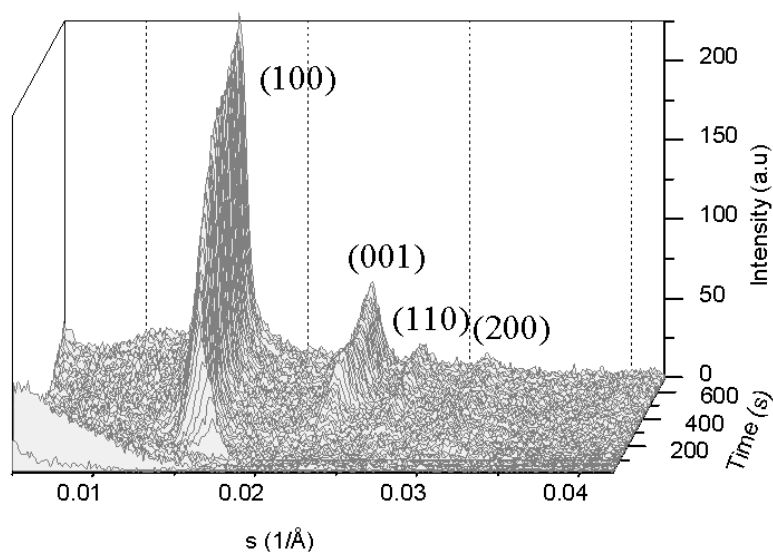
Figure 1. *In situ* XRD of the formation of a toluene swollen mesophase in the system SiO_2-CTAB-decanoic acid.

As seen in the figure 1, the initially formed hexagonal mesophase takes up a lot of oil after it has formed, as manifested by the pronounced swelling up to about 175 s after initiation of the reaction. A co-existing lamellar phase is formed after a reaction time of 400s. All in all, the results clearly show that the addition of an oppositely charged co-surfactant leads to the formation of microemulsion droplets which will serve as the pore building template in these materials. A summary of the results obtained for decanoic acid as the co-surfactant is shown in fig. 2. A continuous increase in the d-spacing is observed with increasing additions of da at a constant toluene content. Also included is the corresponding values obtained without addition of toluene. It can be seen that the mesophase is swelling slightly also with the addition of da only. Upon increasing the amount of da added, a transition from the hexagonal to the lamellar phase occurs. The transition to microemulsion templating occurs at a co-surfactant/surfactant ratio at which a lamellar phase is formed in the absence of toluene. In conclusion we have been able to show that the use of co-surfactants in the synthesis of M41S materials promises to be very useful in providing a means of modifying the mesoscopic ordering and porosity of organic-inorganic hybrid materials.
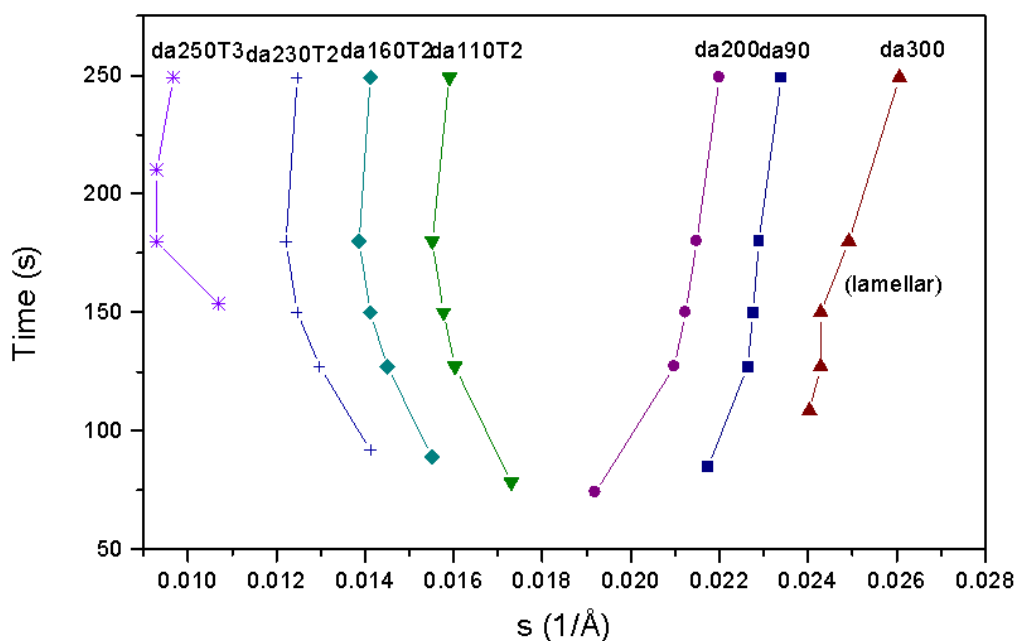
Figure 2. The position of the (100) reflection as a function of time for different additions of da (the number indicates the mass in mg of da/1.2 g CTAB) and toluene, T, in g.

The results will be discussed in more detail in forthcoming full papers.

[1] J.S. Beck, J.C. Vartuli, W.J. Roth, M.E. Leonowicz, C.T. Kresge, K.D. Schmitt, C.T-W. Chu, D.H. Olson, E.W. Sheppard, S.B. McCullen, J.B. Higgins, J.L. Schenkler, *J. Am. Chem. Soc.* **114**, 10834 (1992)
[2] P. Ågren, M. Lindén, J.B. Rosenholm, J. Blanchard, F. Schüth, H. Amenitsch, Langmuir, **16**, 8809 (2000)
[3] M. Lindén, P. Ågren, S. Karlsson, P. Bussian, H. Amenitsch, Langmuir, **16**, 5831 (2000)
[4] P. Ågren, M. Lindén, J.B. Rosenholm, R. Schwarzenbacher, M. Kriechbaum, H. Amenitsch, P. Laggner, J. Blanchard, F. Schüth, J. Phys. Chem, **103**, 5943 (1999)

LOCAL ORDER IN AMORPHOUS POLYMERS:
EFFECT OF SIDE CHAIN LENGTH

V. Arrighi[1], A. Triolo[2], I. J. McEwen[1] and P. Holmes[1]

1.) Department of Chemistry, Heriot-Watt University, Edinburgh EH14 4AS, UK
2.) BENSC – HMI Berlin Glienickerstr. 100 D-14109 Berlin, Germany

Poly(di-n-alkyl itaconate)s (figure 1) present unusual thermal behaviour as they exhibit two glass transitions when the length of the alkyl side chains varies between $7<n<11$ [1]. The high temperature glass transition, T_g^u has been identified with the usual polymer T_g due to co-operative movement of the main-chain whereas the lower temperature T_g, T_g^1, is believed to be associated with the independent relaxation of the long alkyl side chains. It has been postulated the side chains form discrete regions separated from the polymer core [2].

This hypothesis was successfully supported by a feasibility test run at the SAXS beam-line [3]. Analysis of the SAXS pattern revealed a direct correlation between the number of CH_2 units in the side chain and the peak position. Structural characterisation of these materials ($n = 1$-5, 8 & 10) was reported for the first time and resulted in a publication [4].

The aim of the current experiment is to complete room temperature measurements for the series $n = 1$ to 10 and to investigate the effect of temperature. We also intended to compare the poly(n-alkyl methacrylate) with $n = 1$ to 5 to study the effect of the chemical structure on the overall structural and thermal behaviour.

During the SWAXS allocated beam-time we were able to complete measurements on the series of poly(di-n-alkyl itaconate)s as shown in figure 2a. Two distinct peaks can be observed in the SWAXS patterns. „Equivalent Bragg" spacings were obtained by means of the Bragg equation and the results are shown in figure 2b. The dependencies of the two peaks are very different, peak 1 corresponding to $d \sim 5$ Å is independent of the side chain length. In contrast, peak 2 shows a strong correlation with the number of CH_2 units in the side chain. The temperature dependence of the SAXS profile for poly(didecyl itaconate) is reported in figure 3. Changes in peak position are observed and we are attempting to relate the T dependence of peak height, position and width as a function of temperature to the structural ordering in these systems.

We also carried out measurements on poly(n-alkyl methacrylate)s with $n = 2$ & 4. Comparison of the SAXS patterns of poly(dibutyl itaconate) and poly(butyl methacrylate) are reported in figure 4. An intense sharp SAXS peak for poly(dibutyl itaconate) indicates the presence of greater structural ordering compared to the very broad peak of poly(butyl methacrylate).

Due to technical problems with the WAXS detector and the temperature controller we lost some beam-time, and we were therefore unable to complete measurements on poly(n-alkyl methacrylate)s with $n = 1$, 3 & 5.
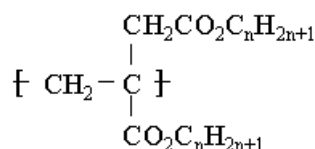

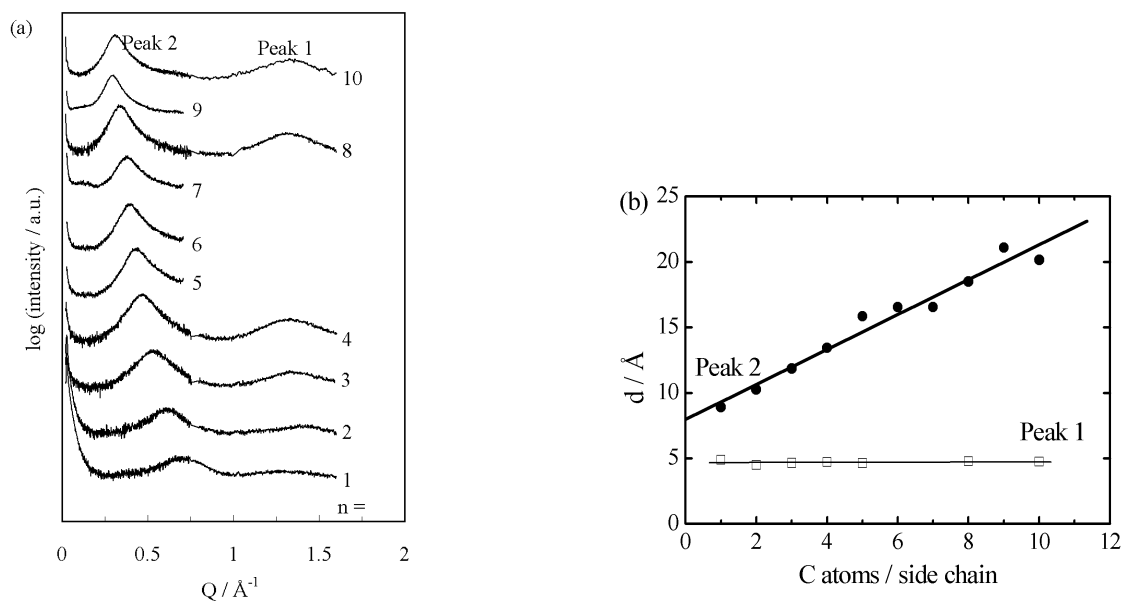**Figure 1.** Structure of Poly(di-n-alkyl itaconate)s

Figure 2. (a) Room Temperature SAXS-WAXS data collected from different itaconates with different length of the side chain, *n*. Intensity is shown on a logarithmic scale, and curves are shifted for clarity. Technical problems with the WAXS detector resulted in the loss of data for *n* = 5, 6, 7 & 9. (b) Bragg distances, Peak 1 (squares) and Peak 2 (circles), obtained from SWAXS data at 298 K as a function of side chain length *n*. The line is the best linear fit to Peak 2 data.
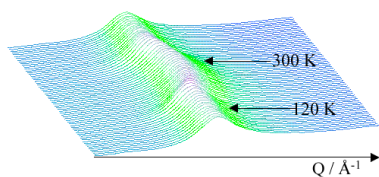
Figure 3. Temperature dependence of the SAXS pattern for poly(didecyl itaconate) in the temperature range 120 K – 300 K, heating followed by cooling.
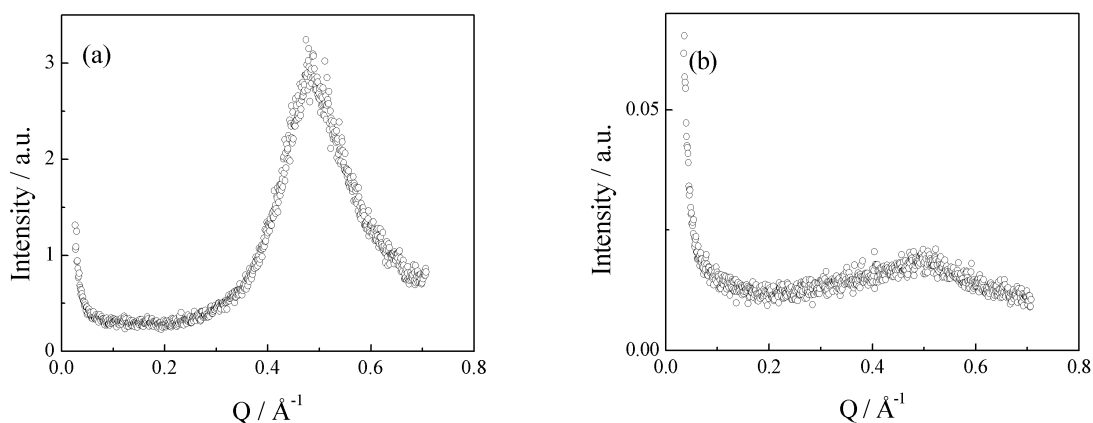
Figure 4. SAXS scattering patterns for (a) poly(dibutyl itaconate) and (b) poly(butyl methcarylate) at 298 K.

[1] Cowie, J.M.G.; Haq, Z.; McEwen I.J. J., Polym. Sci., Polym. Lett. Ed. 1979, **17**, 771.
[2] Cowie, J.M.G.; Haq, Z.; McEwen I.J. *Polymer* 1981, **22**, 327. and ref. therein
[3] Triolo, R.; Triolo, A., Annual Report 1999, Austrian SAXS Beamline at Trieste, p116.
[4] Arrighi, V.; Triolo, A.; McEwen, I.J.; Holmes, P.; Triolo, R.; Amenitsch, H. *Macromolecules* 2000, **14**, 4989.

PHASE TRANSITIONS IN A SCHIFF'S BASE LIQUID CRYSTAL PROBED BY SMALL ANGLE X-RAY SCATTERING

Alok D. Bokare [1], Archita Patnaik[1], Heinz Amenitsch[2], Sigrid Bernstorff[3] and Pavo Dubeck[3]

1.) Department of Chemistry , Indian Institute of Technology, Madras, Chennai 36, India
2.) Institute of Biophysics and X-ray Structure Research, Austrian Academy of Sciences, Schmiedlstraße 6, A-8042 Graz, Austria
3.) Sincrotrone Trieste (Elettra), SS 14, Km 163.5, I- 34012 (TS), Italy

The phase transitions of liquid crystals between the various mesomorphic forms occur at a thermodynamically defined temperature as the liquid crystal undergoes a change in internal order at the point of phase transition. The work reported here makes use of synchrotron x-ray scattering as a tool for studying the phase transition behaviour of a typical thermotropic liquid crystal. Terepthal-bis-4-butyl aniline (TBBA), a Schiff's base, exhibits multiple mesophases including 5 different smectic phases (2 of them obtained only during cooling from the isotropic phase) and a nematic phase in addition to the crystalline and isotropic phases. It also undergoes a crystalline to crystalline phase transition at cryogenic temperature and hence serves as an ideal system to understand the role of various degrees of molecular freedom in liquid crystal phase transformations.

The structure of Terepthal-bis-4-butyl aniline (TBBA) is shown below.

$$H_9C_4 - \bigcirc - N = CH - \bigcirc - CH = N - \bigcirc - C_4H_9$$
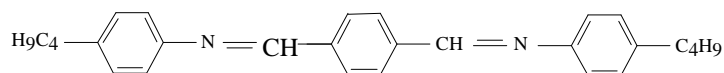
The sequence of phase transitions during heating and cooling cycles respectively is schematically shown (transition temperatures in °C).

Cr $\underline{-42}$ Cr $\underline{113}$ S_B $\underline{144}$ S_C $\underline{173}$ S_A $\underline{198}$ N $\underline{232}$ I

I $\underline{232}$ N $\underline{198}$ S_A $\underline{173}$ S_C $\underline{144}$ S_B $\underline{84}$ VI $\underline{68}$ VII $\underline{52}$ Cr

Preliminary X-ray scattering measurements with an 8 keV beam and within the WAXS 2θ range from 9.4° to 27.6° were performed at the SWAXS beam line with a temperature program covering both heating and cooling cycles. In a separate set of measurements, low temperature runs were acquired for the substrate.

The time (temperature) evolution of the structure of the mesogen during the cooling cycle in Fig.1 shows the occurrence of various phases given in the schematic above. In Fig.2, the variation in the scattered intensity with temperature during cooling implies changes in the positional order ($\tau = \cos(2\pi z /d)$) as a function of temperature. The change of slope at ~ 205 ^{0}C is an indication of the onset of the Nematic - Smectic A transition caused by an increase in the positional order, the characteristic of a Nematic-Smectic transition. Order parameter fluctuations / pre-transition effects before the onset of phase VI at 87 °C in Fig.3 corroborate the sharp deviation in the d-spacing at ~ 130 °C. This observation is in complete agreement with the Positron Annihilation lineshape changes at ~ 125 ± 1 °C in the cooling cycle of TBBA in our laboratory. In liquid crystals, the change in density associated with a phase transition is small and the various mesophases, amongst themselves differ mainly by internal structural order. The change of slope between 140-200 °C in Fig.4 for the low temperature solid-solid phase transition of TBBA possibly is an indicative of a new phase.

References:

[1] D. Dvorjetski, V. Volterra and E. Wiener-Avnear, Phys. Rev. A 12(2) (1975) 681

[2] T. R. Taylor, S. L. Arora and J. L. Fergason, Phys. Rev. Lett. 25(11) (1970) 722
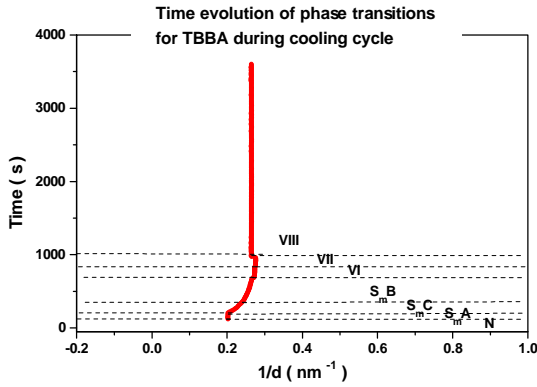
[3] W. L. McMillan, Phys. Rev. A, 6(3) (1972) 936
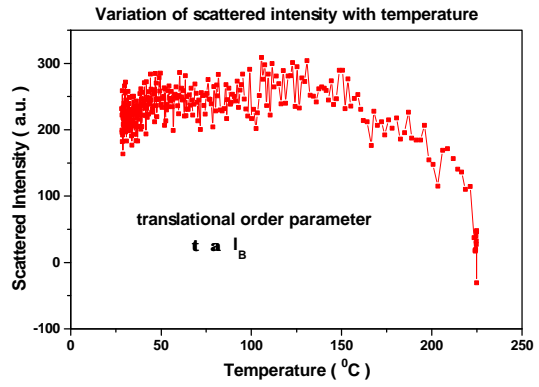
Figure 1. Time evolution of phase transitions of during cooling

Figure 2. Variation of scattered intensity with temperature during cooling
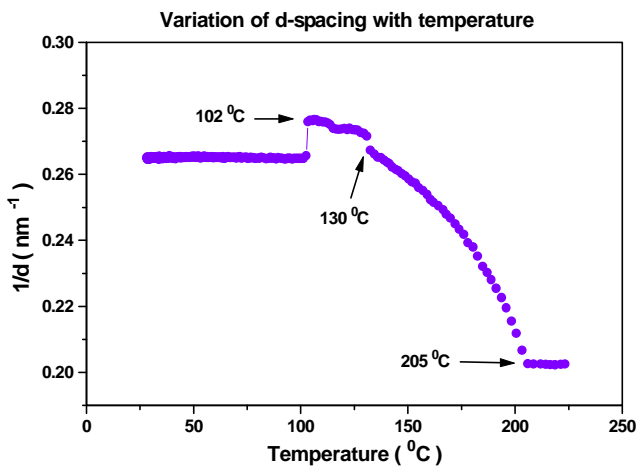
Figure 3. Variation of d-spacing
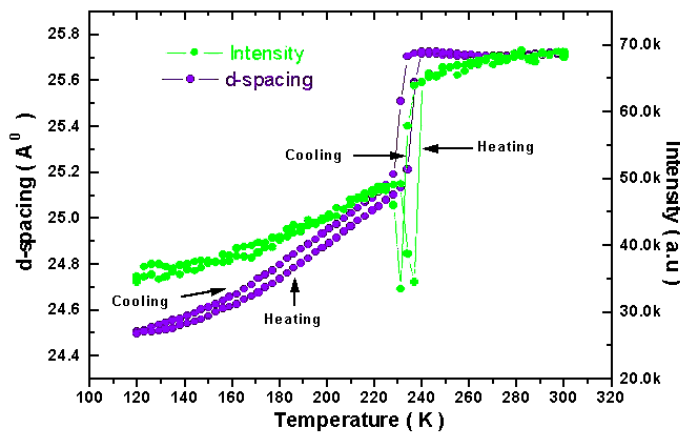
Figure 4. Variation of d-spacing and with temperature scattering intensity for cryogenic temperatures

IN SITU – SAXS INVESTIGATIONS ON ZINC SULFIDE PRECIPITATION IN A LIQUID JET

P. Bussian[1], P. Ågren[1], M. Lindén[2], J. Andersson[2] and H. Amenitsch[3]

1.) Max-Planck-Institute für Kohlenforschung, Kaiser-Wilhelm-Platz 1, D-45470 Mülheim/Ruhr, Germany
2.) Department of Physical Chemistry, Åbo Akademi University, Porthansgatan 3-5, FIN-20500 Turku, Finland
3.) Institute of Biophysics and X-ray Structure Research, Austrian Academy of Sciences, Schmieldstr. 6, A8042, Graz, Austria

Introduction

The understanding of the fundamental processes involved in precipitation reactions from solution is one of the most challenging problems in solid-state chemistry. However, only a few techniques are available for analysis of these reactions. In combination with a tubular reactor setup (represented by a liquid jet), SAXS can give new insights in the early stages of precipitation on a microsecond time scale. We have chosen the precipitation of sparingly soluble sulfides from aqueous solution as a model system.

Experimental setup

The precipitation of ZnS is carried out in a flow jet cell as seen in figure 1. A liquid jet (diameter 80 µm) containing an aqueous $ZnCl_2$ solution (1 molar) is injected into a reactive gaseous atmosphere of H_2S. By diffusion H_2S is transported into the jet and dissolved. Precipitation of ZnS occurs by the reaction of Zn^{2+} cations with S^{2-} anions created by the reaction of H_2S with water:

$$H_2S + H_2O \longrightarrow S^{2-} + 2\,H_3O^+$$

$$S^{2-} + Zn^{2+} \longrightarrow ZnS \downarrow$$
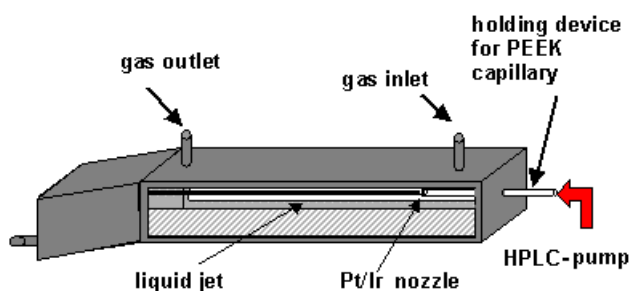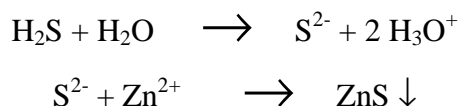
Figure 1: Schematic illustration of a flow jet cell

By measuring at different positions along the jet, the ongoing crystallization reaction can be followed. Every position in the jet corresponds to a certain residence time after mixing the liquid jet and the gas. For a jet with a diameter of 80 µm and a flow rate of 3.5 ml/min, 1 mm in the jet corresponds to a residence time of 86 µs or a velocity of the liquid of 11.6 m/s.
The body of the cell is made of stainless steel and the nozzle, which is connected to a HPLC pump via a PEEK capillary, is made out of a Pt/Ir alloy. Each point was measured for 300 seconds.

Results and discussion

Figure 2 show the results of the Porod data treatment. The resulting Porod constant against the distance from the nozzle or the residence time is shown in figure 3.
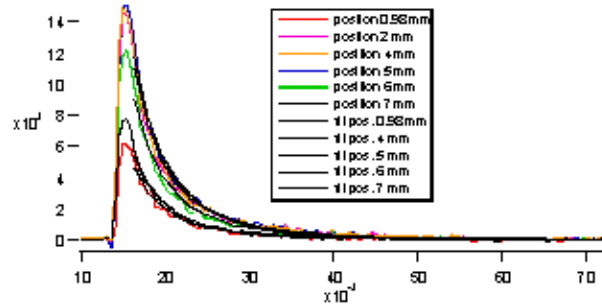

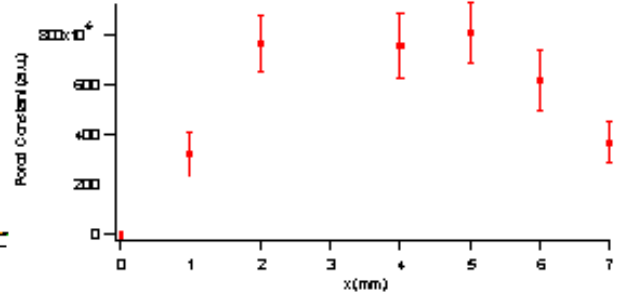**Figure 2:** Results of the Porod data treatment.

Figure 3: The Porod constants versus distance x (1mm ≡ 86 µs residence time) from the nozzle.

Following equation 1 one can state that the increase of the Porod constant in the beginning is mainly dominated by the increase of the difference of the electron density and/or the volume fraction. That means that particles are created in the jet from 1 mm up to 5 mm (corresponding to residence times from 86 to 430 µs). At residence times greater than 430 µs, the Porod constant begins to decrease. This indicates that it is dominated by particle growth or aggregation, assuming a constant volume fraction or a constant difference in electron density, respectively. Guinier treatment of the data show that the particles are definitely larger than 25 nm, even in the early stages.

$$P \propto \frac{p \cdot \Delta\rho^2}{R}$$

Equation 1: With P = porod constant, p = volume fraction, $\Delta\rho$ = difference in electron density, R = particle size.

Outlook

To get a better insight in the very early stages of precipitation (< 86 µs) we plan to use a thinner jet ($\varnothing$= 20 – 50 µm), keeping the flow rate constant to reach shorter residence times. Another approach to measure these stages is to slow down the reaction by diluting the zinc chloride precursor solution. However, both of these methods will result in loss of measured intensity. Therefore the precipitation of manganese sulfide is under investigation, as its solubility product is ten times higher than that of zinc sulfide, indicating slower precipitation kinetics.

IN-SITU TIME-RESOLVED SAXS AND INTERFEROMETRY STUDIES OF MESOSTRUCTURED THIN FILMS FORMATION

D. Grosso[1], G. Soler-Illia[1], B. Alonso[1], P.A. Albouy[2], H. Amenitsch[3], A.R. Balkenende[4], F. Babonneau[1] and C. Sanchez[1].

1.) Chimie de la Matière Condensée, UPMC - CNRS, 4 place Jussieu, 75005 Paris, France.
2.) Lab. de Physique des Solides, Université Paris-Sud, 91405 Orsay, France
3.) Institute of Biophysics and X-ray Structure Research, Austrian Academy of Sciences, Schmiedlstraße 6, 8042 Graz, Austria.
4.) Philips Research Laboratories, Prof. Holstlaan 4, 5656 AA Eindhoven, Netherlands.

Mesoporous silica thin films can be prepared by a sol-gel based dip coating method from a solution containing silicate and surfactant species [1-3]. In such materials the organic phase is organized on a mesoscopic scale, and serves as a template for the inorganic skeleton. During deposition of the wet film on the substrate, the evaporation of the liquid phase takes place and simultaneously induces formation of the surfactant micelles, self-assembly between the micelles and the inorganic phase, and polycondensation of the inorganic phase [2]. The understanding of such a rapid mechanism would be suitable to control the final structure, and also to extend such process to the preparation of films with other chemical compositions. Here, we show that the different steps involved in the formation mechanism of such mesostructured films can be observed using simultaneously in-situ time-resolved SAXS and interferometry analyses, during the minutes that follow the deposition. This technique was used to follow the formation of hexagonal ($P6_3/mmc$), cubic ($Pm3n$), and columnar hexagonal ($p6m$) mesostructured films, with characteristic distances ranging from 35 to 148Å, obtained with cationic or block-copolymer surfactants [4-6].

Experimental: Initial sols were prepared from an ethanolic solution of TEOS (tetraethoxysilane), and CTAB ($C_{16}H_{33}N(CH_3)_3Br$), hydrolyzed under acidic conditions (HCl). The templated films were prepared by dip coating silicon wafers (8μm thick) at rates varying from 0.5 to 5 mm.s^{-1}. A modified dip-coater was built in order to move the container and to keep fixed in position the substrate. The substrates were placed at grazing angle with respect to the incident X-ray beam direction. A linear detector (acquisition time 100 ms) or a CCD camera (acquisition time 1 s) was used to record the time-resolved diffraction patterns. The collection of measurements started when the top edge of the beaker just passed the position of the X-ray beam (time T_0). Simultaneously, a second CCD camera recorded the variation of film thickness by interferometry.

Results: Figure 1a shows the evolution of the X-ray patterns, during the first 60 seconds after deposition, for the CTAB/TEOS = 0.12 system that leads to cubic structures. It was collected using a linear detector placed as to record peaks that correspond to planes parallel to the film surface. The first peak at d = 74 Å that appears less than 1 s after deposition, is due to a small-angle scattering preferentially reflected at the critical angle and attributed to the roughness of the interface. This first intermediate peak disappears suddenly after 26 s and a new peak is now detected that corresponds in d-spacing to the (002) diffraction of a $P6_3/mmc$ 3D hexagonal structure. This peak no longer exists 5 s later and a third diffraction peak attributed to the $Pm3n$ final cubic structure starts to grow after 32 s, suggesting that the $Pm3n$ structure is formed from the $P6_3/mmc$ structure via rapid phase transition. These results combined with the variation of film thickness profile obtained by interferometry lead to Figure 1b. One driving force for the film organization is the evaporation of the liquid phase at the interface that induces gradients of concentration in the film profile and with time. One

first observes a scattering peak due to the air-liquid interface, growing very rapidly, and suggesting that the CMC is instantly reached in this region. The first phase transition, with formation of the intermediate $P6_3/mmc$ phase takes place a few seconds later, when the liquid phase is fully evaporated. At this time, the film can be considered as dry and the formation of the film structure is due to the self-assembly of surfactant molecules with inorganic species in quasi absence of solvent. In the minutes and hours that follow this self-assembly process, the polycondensation of the inorganic network continues, leading to a rigid film.

Conclusion: The in-situ time-resolved SAXS investigations performed at ELETTRA appeared to be highly appropriate to study the mechanism of mesostructured film formation. Similar experiments have also been performed under various experimental conditions (withdrawal rate, dilution, water content, various types of surfactant). The results brought very interesting results ; they not only allowed us to characterise the different film structures, but they showed (i) the formation of intermediate phases, (ii) a period of phase coexistence, (iii) the time scale at which the phase transitions occurred, (iv) the progressive preferential reorientation of the organised domains, and (v) the influence of each experimental condition on the film structure evolution. The formation of highly oriented mesostructured silica films appears clearly as a complex process where the initial concentration in surfactant, the rate of evaporation, the degree of condensation of the silica species and the composition of the liquid phase influence the organisation. It also showed that the formation of such highly organised films requires a rapid liquid phase evaporation only achieved with dip or spin coating.
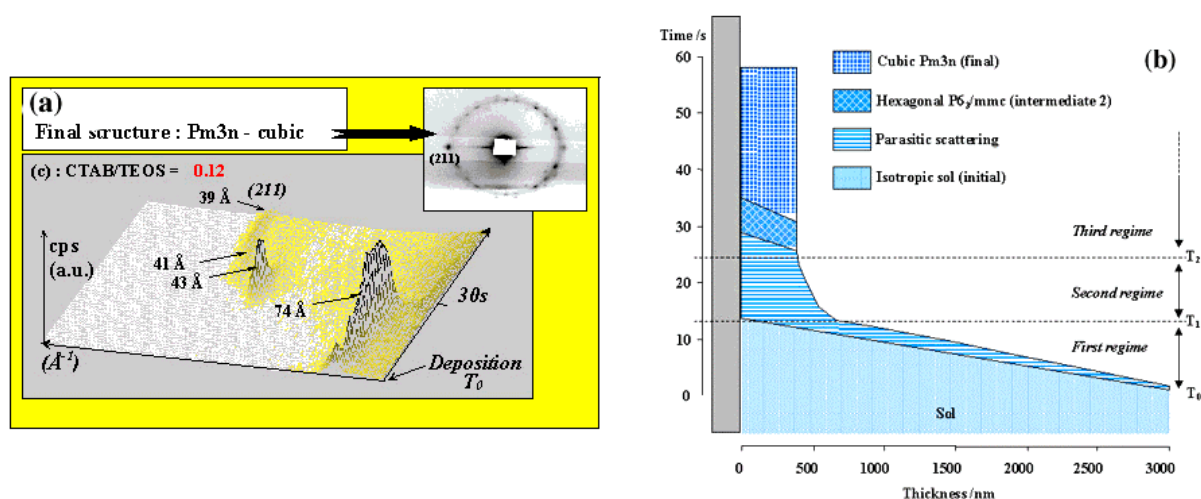

Figure 1. (a) Evolution of the X-ray patterns after deposition and (b) Proposed model for the mesostructured film formation deduced from the SAXS and interferometry data (CTAB/TEOS = 0.12).

References:

[1] Y. Lu, R. Ganguli, C. A. Drewien, M. T. Anderson, C. J. Brinker, W. Gong, Y. Guo, H. Soyez, B. Dunn, M. H. Huang, and J. I. Zink; *Nature*; 389, 364, (1997)

[2] C. J. Brinker, Y. Lu, A. Sellinger, and H. Fan; *Advanced Materials*; 11, 579, (1999)

[3] D. Zhao, P. Yang, N. Melosh, B. F. Chmelka, and G. D. Stucky; *Advanced Materials*; 10, 1380, (1998)

[4] D. Grosso, A. R. Balkenende, P. A. Albouy, M. Lavergne, L. Mazerolles and F. Babonneau; *Journal of Material Chemistry;*10, 2085, (2000)

[5] D. Grosso, A. R. Balkenende, P. A. Albouy, A. Ayral, H. Amenitsch and F. Babonneau, *Chemistry of Materials, (2001), accepted for publication.*

[6] D. Grosso, F. Babonneau, P.A. Albouy, H. Amenitsch, A.R. Balkenende, A. Brunet-Bruneau and J. Rivory, J. Am. Chem. Soc., (2001), submitted.

EFFECT OF ELECTROSTATIC CHARGES ON THE KINETIC OF SOLUBILIZATION AND RECONSTITUTION OF LIPOSOMES INDUCED BY SURFACTANTS: A STUDY USING TIME RESOLVED SAXS

O. López[1], M.Cócera[1], A. de la Maza[1], H. Amenitsch[2] and R. Pons[1]

1.) IIQAB-CSIC, Jordi Girona 18-26 08034 Barcelona, Spain
2.) Institute of Biophysics and X-ray Structure Research, Austrian Academy of Sciences, Schmieldstr. 6, A-8042 Graz, Austria

Surfactants are indispensable reagents in the solubilization and reconstitution of membrane protein. In this sense the study of the interaction of liposomes, lipid-water systems used as simplified model of biological membranes, with surfactants is currently attracting much interest. In previous papers we investigated the solubilization and reconstitution of liposomes induced by surfactants from a structural viewpoint [1-3] that raised a number of questions about the kinetics. Dynamic Light Scattering and Freeze fracture electron microscopy were performed to investigate this kinetic aspect [4,5]. However, the first steps of these two processes resulted too fast to be detected using these techniques. The SAXS instrument at ELETTRA for time resolved using a stopped flow cell allowed us to study in detail the evolution with time of liposome solubilization [6]. Our results appeared to indicate that both the adsorption of surfactant on the liposomes and the release of mixed micelles from the vesicle surface depended on the liposome and surfactant electrostatic charges. The aim of our last measurements at the SAXS of the ELETTRA Synchrotron was to study in depth this effect and to investigate the kinetics of vesicle reconstitution induced by dilution of mixed micelar solutions.

The solubilization and the reconstitution processes were followed by obtaining diffraction spectra every 0.1 sec for the first 50 sec, every 0.5 sec for the following 150 sec, and for the next 5 min every 1 sec, always at room temp. Liposomes and surfactants with different electrostatic charges were used. In the solubilization process we could observe that if surfactant and vesicles have the same type of electrostatic charge the adsorption of surfactant on the liposome is slower and the release of mixed micelles from the liposome surface is faster than when the species are oppositely charged. In fact, for the interaction of sodium dodecyl sulfate, SDS, (anionic surfactant) with negatively charged liposomes, we start to detect the mixed micelles before the complete adsorption of the surfactant on the vesicles. This fact is shown in Fig 1, the diffraction spectra 0.1 sec after mixing surfactant and liposomes shows two peaks: at $Q \approx 0.10\text{Å}^{-1}$ (corresponding to the liposome bilayer) and at $Q \approx 0.13\text{Å}^{-1}$ (corresponding to diameter of the SDS pure micelles). In the spectra 0.3 sec after mixing, two new peaks at $Q \approx 0.07\text{Å}^{-1}$ and $Q \approx 0.12\text{Å}^{-1}$ were detected, we attribute these peaks to the elongated mixed micelles. After 1.2 sec after mixing, the peak corresponding to the pure SDS micelles has disappeared of the spectra, indicating that all the surfactant has been adsorbed. As regards the vesicle reconstitution, our experiments showed that this process is in general faster than the solubilization one. In addition, it was observed that the vesicle reconstitution in systems composed by mixed micelles in which the surfactant and the lipids are oppositely charged are faster than systems without electrostatic charges. Moreover, the reconstitution of vesicles in these last systems are faster than in those in which only one type of charge is present. These facts can be observed in Fig 2, which depicts the spectra of the reconstitution 0.5 sec after dilution of three systems containing SDS and liposomes negatively, neutrally and positively charged.
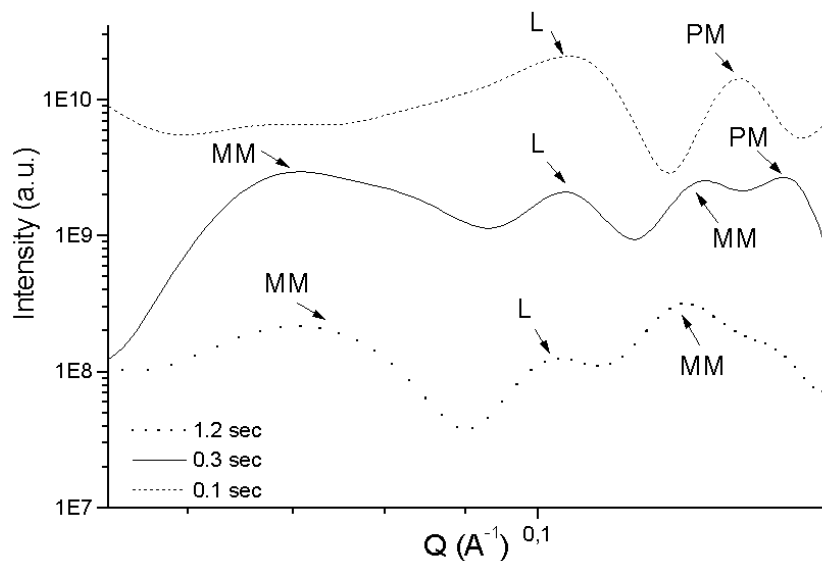
Figure 1. SAXS spectra corresponding to 0.1, 0.3 and 1.2 sec after mixing SDS and negatively charged liposome. The reflections of the different structures are noted as L: liposomes, PM: pure micelles, MM: mixed micelles. The intensities are shifted for better viewing.
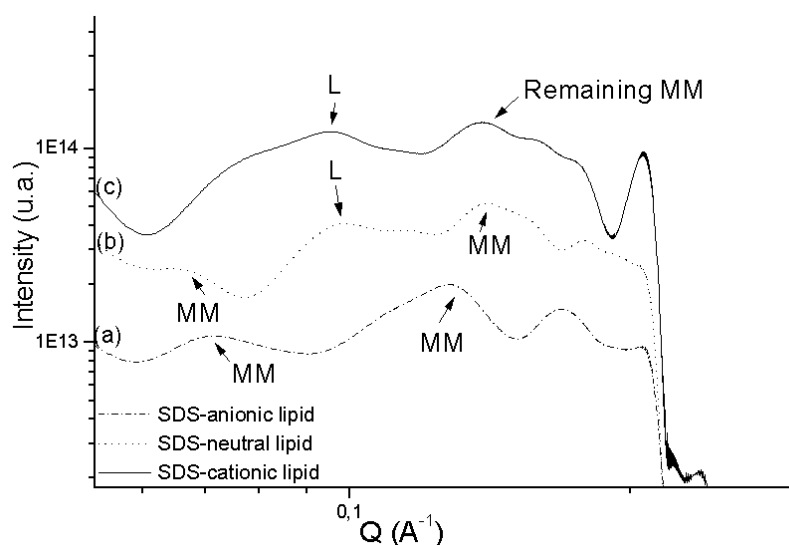

Figure 2. SAXS spectra detected 0.5 sec after dilution of mixed micellar solutions composed by SDS surfactant and negatively (a), neutrally (b) and positively (c) charged liposomes. The reflections of the different structures are noted as L: liposomes, MM: mixed micelles. The intensities are shifted for better viewing.

References:

[1] O. López, A. de la Maza, L. Coderch, C. López-Iglesias, E. Wehrli and JL Parra; Direct formation of mixed micelles in the solubilization of phospholipid liposomes by Triton x-100, FEBS Lett., **426**, 314-318, (1998).

[2] O. López, M. Cócera, E. Wehrli, JL. Parra and A. de la Maza; Solubilization of liposomes by sodium dodecyl sulfate: New mechanism based on the direct formation of mixed micelles, Arch. Biochem. Biophys., **367(2)**, 153-160 (1999)

[3] O. López, M. Cócera, L. Coderch, JL. Parra, L. Barsukov and A. de la Maza; Octyl glucoside-mediated solubilization and reconstitution of liposomes: Structural and kinetic aspects, J. Phys. Chem. B, (2001) *(in press)*.

[4] O. López, M. Cócera, R. Pons, N. Azemar and A. de la Maza; Kinetic studies of liposome solubilization by sodium dodecyl sulfate based on a dynamic light scattering technique Langmuir, **14(16)**, 4671-4674, (1998).

[5] O. López, M. Cócera, R. Pons, N. Azemar, C. López-Iglesias, E. Wehrli, JL. Parra and A. de la Maza; Use of a dynamic light scattering technique to study the kinetics of liposomes solubilization by Triton X-100 Langmuir, **15(13)**, 4678-4681, (1999).

[6] O. López, M. Cócera, A. de la Maza, H. Amenitsch and R. Pons; Kinetics of liposome-surfactant interaction: A study based on small angle x-ray scattering, Annual Report 1999 Austrian SAXS Beamline at ELETTRA, 110-111, (2000).

SAXS/WAXS STUDY OF THE STRUCTURAL AND MORPHOLOGICAL REARRANGEMENTS OF THE MESOPHASES IN QUENCHED iPB-1 AND sPP

S. Piccarolo[1] and V. La Carrubba[1]

DICPM, Università di Palermo, Viale delle Scienze, 90128, Palermo, Italy

The following investigations were made:

1. Morphological rearrangements in semicrystalline polymers solidified under processing conditions, Polymers investigated: PB1, iPP

The structural rearrangement in samples of quenched isotactic polypropylene (iPP) submitted to different annealing treatments has been studied by simultaneous small- and wide-angle X-ray scattering (SAXS/WAXS). It has been demonstrated [1-3] that the SAXS patterns are characterized by two different long period values that can be associated with the relative amount of mesomorphic and α-monoclinic phase, as detected by the WAXS analysis. The hypothesis that individual lamellar stacks characterized by different long period values has been previously put forth. It is demonstrated that the SAXS data can be interpreted as well in terms of statistical sequences of different lamellar thicknesses.

2. Influence of Solidification conditions on Crystallization from the glassy state of PET

Quenched PET is amorphous and therefore can be further crystallized from the glassy state. This is indeed the technique adopted for most of the processing routes for PET. Apparently amorphous PET however contains small amounts of a so called „precrystalline phase", its amount changes with the cooling rate adopted during solidification.

Objective of this study is to investigate in detail the crystallization process which apparently takes place, in the initial stages, with a kinetics recalling a spinodal decomposition. This investigation was performed with the aim of verifying the possibility of a steady isothermal temperature jump to the crystallization and the minimum time available for the experimental conditions to set in. The preliminary data collected are reported in fig. 1 where the crystallinity drawn from the SAXS invariant and from an index obtained from WAXD are compared for different initial cooling rates. They show that temperature and cooling rate significantly affect the initial stages of crystallization of PET.
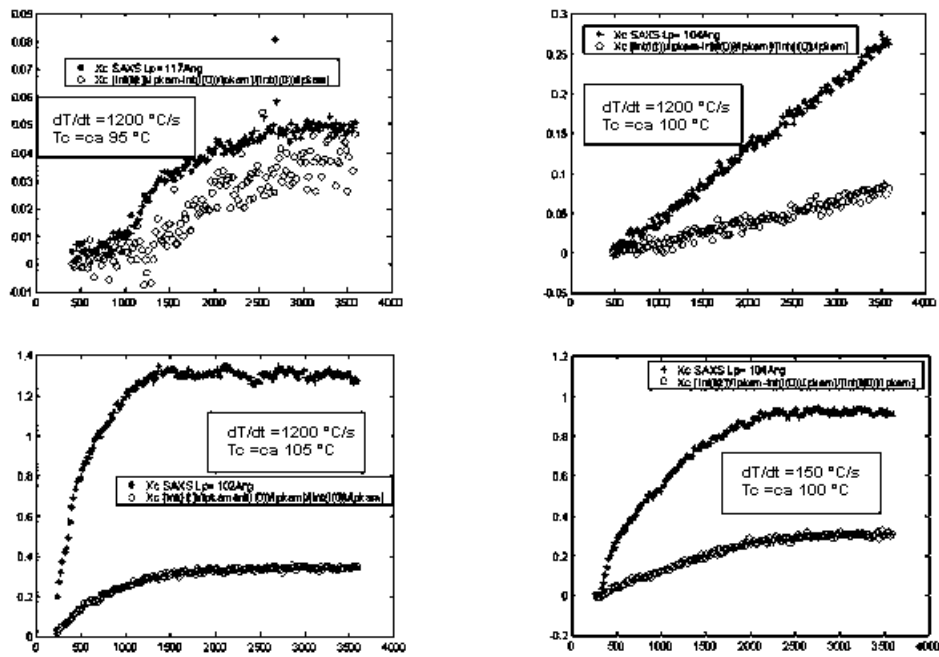
Figure 1. Arbitrary Crystallinity index from SAXS & WAXD (PET)

References:

[1] A. Martorana, S. Piccarolo and D. Sapoundjieva, „SAXS/WAXS study of the annealing process in quenched *Macromol. Chem. &Phys.* **200**, 531 (1999)

[2] D. Sapoundjieva, S. Piccarolo and A. Martorana, "Structural and morphological rearrangements in quenched polyetylene by simultaneous SAXS/WAXD"; Macromol. Chem. & Phys. **201**, 18, 2747-2750 (2000)

[3] S. Piccarolo, D. Sapoundjieva and V. Brucato, "Post processing behaviour of semi-crystaline polymers"; in "Structure development in Processing for property enhancement", Nato Science Series, A.M. Cunha, S. Fakirov Eds, Kluwer Acad, 370, 235 (2000)

EFFECT OF PRESSURE AND COOLING RATE ON CRYSTALLINE POLYMERS: NON ISOTHERMAL CRYSTALLIZATION KINETICS IN QUENCHED iPB-1 AND sPP

S. Piccarolo[1] and V. La Carrubba[1]

DICPM, Università di Palermo, Viale delle Scienze, 90128, Palermo, Italy

Polymer solidification in industrial processes very often involves flow fields, high thermal gradients and high pressures, the development of a model able to describe polymer behaviour turning out to be really complex, due to the large variety of parameters that must be accounted for. The complexity of the investigation concerning polymer solidification under processing conditions is even deeper if the wide latitude of morphologies achievable is considered. Under this perspective, simultaneous WAXS/SAXS experiments using synchrotron light can give a good insight into the global phenomenology occurring during solidification under processing conditions, since it is possible to correlate the final morphology to the physical variables governing the crystallization process, in our case pressure and cooling rate. A modified injection moulding machine equipped with a special injection mould was used, such that samples can be spray cooled at a known cooling rate and under a known pressure under quiescent conditions [1, 2]. A distribution of cooling rates across the sample depth is achieved, since increasing depths (starting from the quenched surface) map decreasing cooling rates. The dependence of long period and phase content on pressure and cooling rate for a PA6 grade by DSM was analyzed by means of simultaneous SAXS/WAXS experiments, performed on 100 μm thin slices cut along a direction parallel to the quenched surface. The raw WAXS and SAXS recorded patterns were preliminary corrected for absorption.

The calculated values of Long Period are reported as a function of sample depth in fig. 1. By examining this figure the following considerations can be drawn: first of all, Long Period regularly increases with depth independently on the applied pressure, ranging from 6-7 nm at the cooled surface (typical value of fully amorphous PA6 samples) up to 8-9 nm in the bulk region of the sample (typical value of highly crystalline PA6 samples). Secondly, the region characterised by a nearly constant Long Period (for large depth values) starts around 1000 μm. As for the low depth region (ranging from 100 to 1000 μm) it is worth noticing that Long Period turns out to be very sensitive to structural changes, showing a monotonous increase with depth. As for the influence of pressure on Long Period values, although data appear to be scattered, it should be underlined that at the lowest explored depth, 100 μm, while there is no evidence of the appearing of a long period for samples solidified at 0.1 and 8 MPa, on the opposite for 24 and 40 MPa the occurrence of a Long Period is largely evident. In other words an increase of „structural regularity" is observed when solidification pressure increases.

WAXS data were subjected to a deconvolution procedure in order to evaluate the volumetric content of alpha, gamma and amorphous phase [3]. The results of deconvolutions on PA6 samples are reported in fig. 2, showing phase distribution as a function of cooling rate for samples crystallized at atmospheric pressure and at 40 MPa. This increase of the alpha phase is mainly compensated by a corresponding decrease of the amorphous phase content, while the variation of gamma phase content is almost negligible. In any case the variation of alpha phase content is very small, and therefore the differenced may be quantified only increasing pressure from 0.1 MPa to 40 MPa.

Crystallization kinetics of PA6 at atmospheric pressure and pressure can be then assessed on the basis of a modified two-phase Kolmogoroff-Avrami-Evans approach [4]. Experimental WAXS deconvolution data and fitting of the phase distribution as a function of cooling rate at atmospheric pressure are reported in fig. 3. The main failure of the fitting is confined to very

high cooling rates. In this region indeed a residual value of about 10% of α phase is obtained by a deconvolution procedure, but the model is not able to predict value of phase larger than zero in this region. As for the effect of pressure on PA6 crystallization kinetics, a change in only one parameter of the model (with respect to the set of parameters found at atmospheric pressure) was able to supply a reasonable prediction of the increase of alpha phase content when pressure increase. The fitting of experimental data at 40 Mpa is reported in fig. 4. The parameter which sensitive to pressure is T_{max}, the temperature at which the maximum crystallization rate falls, which increases on increasing pressure. Furthermore, from this analysis a value of dTm/dP can be indirectly calculated, equal to 0.15°C/MPa, which agrees quite well with literature data on PA6 [5].
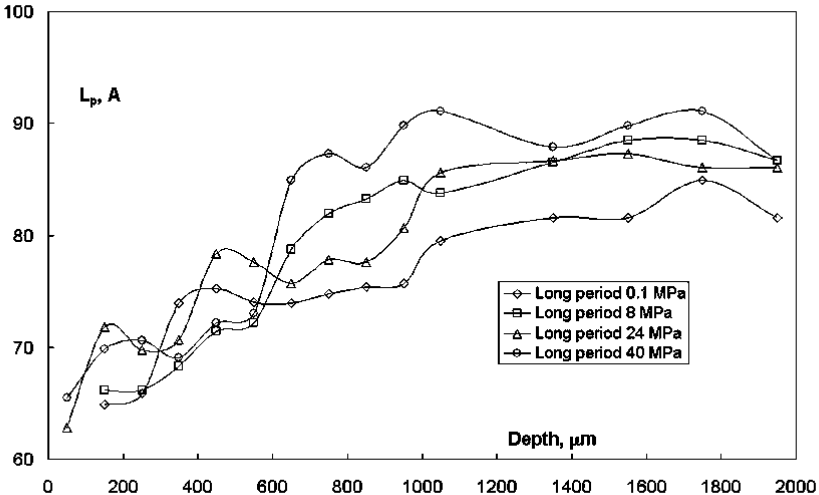
Figure 1. PA6 Long period as a function of depth for different solidification pressures (indicated in the legend)
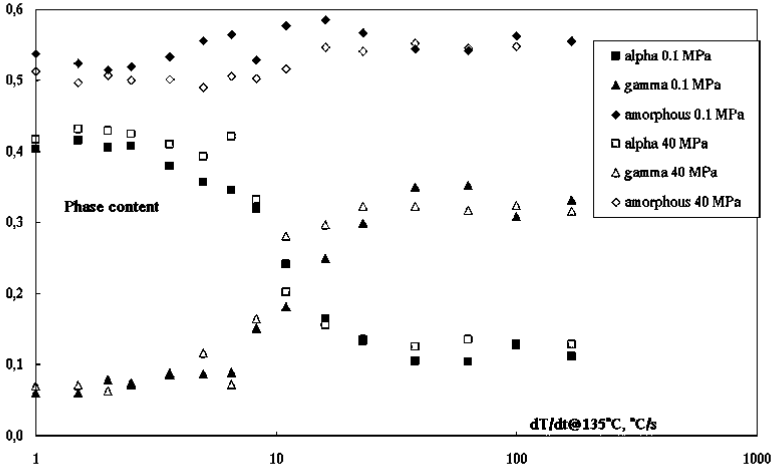
Figure 2. Phase content from WAXS deconvolution (PA6), at two different pressure values (indicated in the legend)
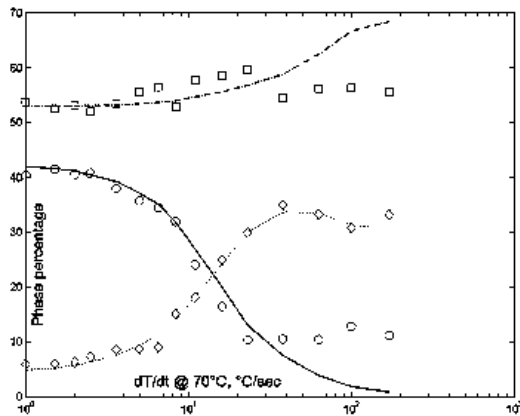
Figure 3. PA6 Phase content versus cooling rate at atmospheric pressure with fitting.
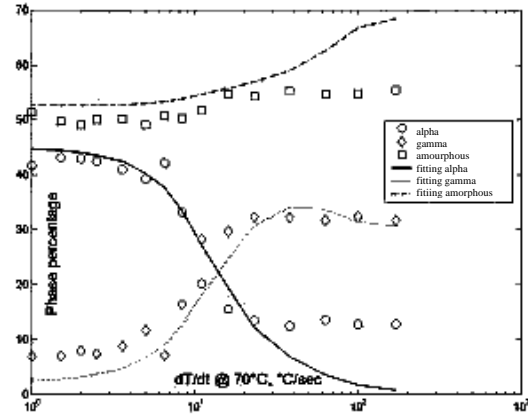
Figure 4 . PA6 Phase content versus cooling rate at 40 MPa with fitting.

References:

[1] La Carrubba V., Brucato V. and Piccarolo S., Isotactic Polypropylene solidification under pressure and high cooling rates. A Master curve approach", *Polym. Eng. And Sci.* **40**, 11 (2000)

[2] Brucato V., Piccarolo S., La Carrubba V., „Polymer solidification under pressure and high cooling rates *International Polymer Processing*, **15**, Issue 1, (2000)

[3] Martorana A., Piccarolo S., Scichilone F., *Macromol Chem. Phys.*, **198**, 597 (1997)

[4] Brucato V., Piccarolo S., Titomanlio G., „Influence of a Nucleating Agent on PA 6 Crystallisation Kinetics", *Int. Jou. of Forming Processes* **1**, 35-52, (1998)

[5] He J., Zoller P., „Crystallization of polypropylene, nylon-66 and poly(ethyleneterephthalate) at pressures to 200 MPa: kinetics and characterization of products"; *J. Polym. Sci.,* Part B: Polym. Phys., P., **32**, No 6, 1049-67 (1994)

DYNAMICS OF OIL-IN-WATER EMULSIONS PREPARED BY MICROEMULSION DILUTION FOLLOWED BY TIME RESOLVED SAXS

R. Pons[1], I. Carrera[1], J. Caelles[1], H. Amenitsch[2]

1.) IIQAB, CSIC, Jordi Girona 18-26, Barcelona 08034, Spain
2.) Institute of Biophysics and X-ray Structure Research, Austrian Academy of Sciences, Schmieldstr. 6, A-8042 Graz, Austria

Emulsions are present in a wide range of products and processes, e.g. pharmaceuticals, papermaking, cosmetics, paints, etc (1). Understanding the processes of emulsification can allow for a better control of their properties. Low energy emulsification methods have attracted increasing interest, not only because of energy savings, but also as a way to control their properties (e.g. particle size and stability). Two promising methods of emulsification have been proposed. a) Phase transition by temperature change (2) and b) phase transition by mixing two different phases (3).

Oil-in-water emulsions have been prepared by dilution of a microemulsion formed in the system sodium dodecyl sulphate/ hexanol/ decane/ water system. At a fixed ratio of surfactant/cosurfactant/oil and increasing water amounts this system goes through different phases. We have followed them by conductivity to obtain information on connectivity. A microemulsion phase with low conductivity is present for a water content of 30%, adding more water the system goes through a two phase region with liquid crystal present (probably lamellar) and again to a microemulsion phase with about a 45% water content and high conductivity. Emulsions formed by diluting further the microemulsions to the same final water content of 80% showed very different droplet size (about 40nm radius for the first micromulsion and about 80nm for the second). We followed the process by time resolved x-ray scattering. In figure 1 we show the spectra taken at several time intervals.
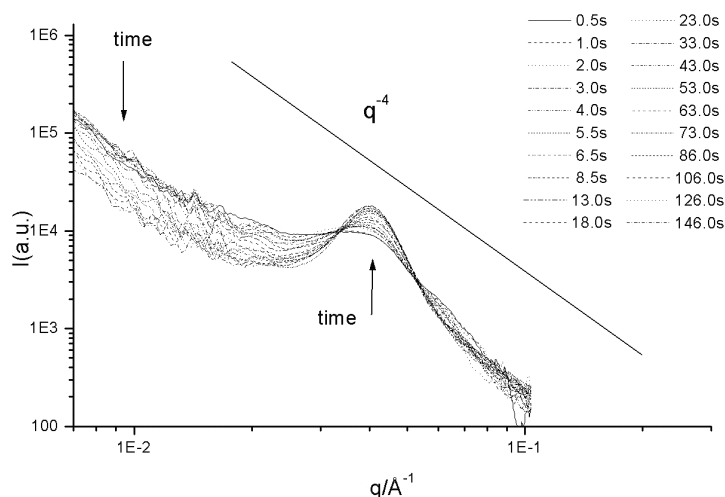

Figure 1. X-ray scattering pattern of emulsion formation from a microemulsion by dilution with water taken at several time intervals.

At the very initial time we could resolve, 0.5s, the microemulsion pattern has already completely disappeared. A tendency at low q that we identify with a Porod behaviour due to the emulsion droplets has already appeared. At the same time, the microemulsion peak converts to an almost non-interacting particles form factor. As the time increases, the intensity of the low q behavior decreases its intensity and at the intermediate q peak of increasing definition appears.
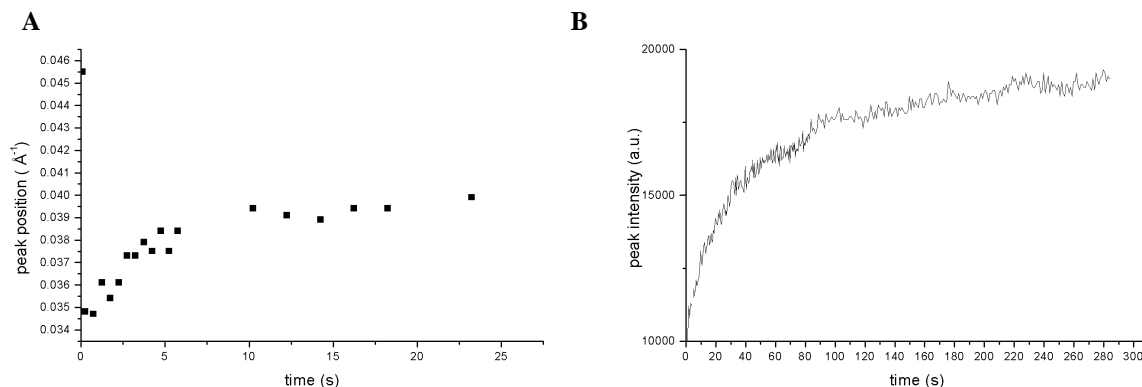
Figure 2. a) Position of the peak at intermediate q and b) Intensity of this peak.

In Fig. 2a we show the evolution for the peak position while in Fig. 2b the intensity of the peak is shown. While the final position is reached after about 10 seconds, the intensity still increases appreciably after 100 seconds. The change of peak position could be due to a change in droplet size or some change in the inter-droplet interaction. The second is likely to have some influence because after some conductivity measurements on the same system we found that the amount of monomeric surfactant in the emulsion continuous phase increases with time.
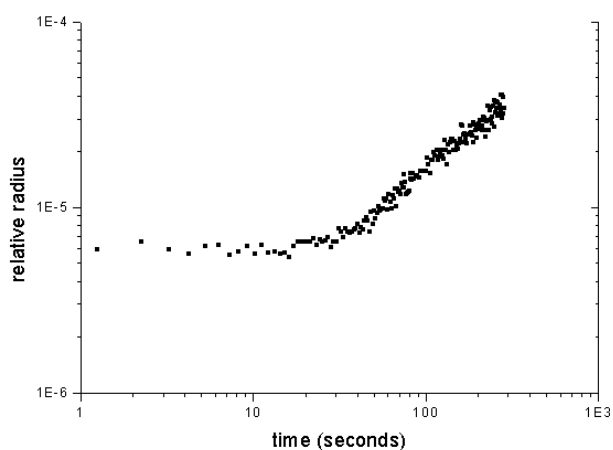
Figure 3. Double log plot of inverse intensity (proportional to the radius) as a function of time.

In figure 3 we show the apparent droplet size for the emulsion taken as the reciprocal of the intensity at $q=0.007\text{Å}^{-1}$. If we consider that this low q behavior is due to the Porod limiting behavior of big droplets (in a similar way as in (4)), the corresponding intensity will be proportional to the specific surface and its inverse to the mean radius. According to independent experiments performed by following the hydrodynamic radius by dynamic light scattering we found an Ostwald-ripening behavior, that is, the cube of the radius increases linearly with time. In this log-log plot this would represent an slope of 1/3. It is evident this is not the case. On the one hand an induction time lasting for about 20 or 30 seconds is apparent and after this the droplets start to grow with a slope close to 1. Further measurements at longer times would be useful to verify whether the 1/3 slope is attained at longer times.

References:

[1] P. Becher (Ed.) "Encyclopedia of Emulsion Technology", Vol 1.Marcel Dekker Inc., N.Y.1983
[2] Shinoda, K., Saito, H. (1969): *J. Colloid Interface Sci*., 30: 258
[3] C.A. Miller, "Spontaneous Emulsification Produced by Diffusion-A Review", *Colloids Surfaces*, 89: 29 (1988)
[4] Egelhaaf, S., Olsson, U., Schurtenberger, P., Morris, J., Wennerström, H. (1999): *Physical Review E*, 60:5681.

CRITICAL MICELLISATION DENSITY (CMD): A SYNCHROTRON SAXS STRUCTURAL STUDY OF THE MONOMER-AGGREGATE TRANSITION OF BLOCK-COPOLYMERS IN NEAR- AND SUPER- CRITICAL FLUIDS

R. Triolo[1], F. Lo Celso[1], A. Triolo[2], F. Triolo[3], M. Steinhart[4], M. Kriechbaum[5] and H. Amenitsch[5]

1.) Department of Physical Chemistry, University of Palermo, 90128 Palermo (Italy)
2.) HMI-BENSC, Glienicker Strasse 100, Berlin, Germany
3.) Mount Sinai School of Medicine, New York, NY (USA)
4.) Institute of Macromolecular Chemistry, Academy of Science of the Czech Republic, Prague, Czech Republic
5.) Institute of Biophysics and X-ray Structure Research, Austrian Academy of Sciences, Graz, Austria

This report deals with the time-resolved small angle X-ray scattering (TR-SAXS) investigation of aggregate formation by fluorocarbon-hydrocarbon block copolymers in supercritical CO_2 (scCO_2) as a function of pressure and temperature. In these systems, by profiling the pressure at constant temperature, a sharp monomer-micelle transition is obtained due to the tuning of the solvating ability of scCO_2. SANS experiments have shown that at high pressure the copolymer is in a monomer state with a random coil structure, while at low pressure core-shell aggregates are formed with the *hydrocarbon* segments forming the core and the *fluorocarbon* segments forming the corona of the aggregate[1].

The experiments reported are part of a Long Term Proposal which was granted to address and answer the following topics:
a) Are the spherical aggregates so far found in scCO_2 the only ones formed in SCF?
b) is the unimer-aggregate transition reversible and reproducible in a wide range of thermodynamic conditions?
c) Does the temperature control the thermodynamics of the unimer-aggregate transition independently from the pressure, or are T and P conjugated through the density of the fluid?
d) Is it reasonable to consider the eventual T/P effect as a secondary fine tuning effect, rather than a primary one?
e) Can the critical micellisation density concept dramatically increase the technological applications of SCF as solvents?

We have studied extensively an amphiphilic polymer with a 10.3 KDalton CO_2-phobic (PVAc) block and a 43.1 KDa fluorinated (PFOA) block. Preliminary batch SANS information and TR-SAXS information on a closely related block copolymer (SAXS Annual Report 1999, p. 114) provided useful guidance for the experiments, and in fact, now we have been able to answer points b),c) and d), at least for coblocks containing PVAc as CO_2-phobic block.

In one set of experiments TR-SAXS data were collected at constant pressure (250 bar and 500 bar) while the temperature was changed between 30 and 65 °C.
In figure 1 it is shown the TR-SAXS pattern obtained at constant pressure (P = 250 bar) changing the temperature between 30°C and 65°C in a series of four alternate heating and cooling ramps. Heating ramps were conducted at a speed of nearly 2 °C/min, while cooling ramps at 1 °C/min. It is clear that the scattering intensity (at $Q = 0.018$ Å^{-1}), going from 30°C to 65°C, shows a dramatic increase due to the formation of aggregates. In fact in this temperature range the CO_2 density changes considerably going from 0.76 g/cm^3 (P=250 bar, T=65°C) to 0.92 g/cm^3 (P=250 bar, T=30°C). The density when the system goes from aggregate to random coil (or vice-versa), which we shall indicate as CMD (Critical

Micellisation Density), in this case is 0.911 g/cm^3 (corresponding to T=35.4°C at 250 bar); also in figure 1 it is depicted, in a schematic way, the dominating species (random coil or aggregate) for two values of temperature. We want to stress that this experiment has shown that the aggregation process is highly reproducible; indeed the cooling ramp, that follows the first heating ramp, brings again the scattering intensity value to the initial one at T=30°C, a very low value typical of a system formed by independent random coil chains. By heating and cooling again the system, with the same speed as the first two ramps, the scattering intensity shows a very similar profile indicating the formation of micelles going towards the temperature of 65°C, and their destruction while cooling the solution at 30°C.
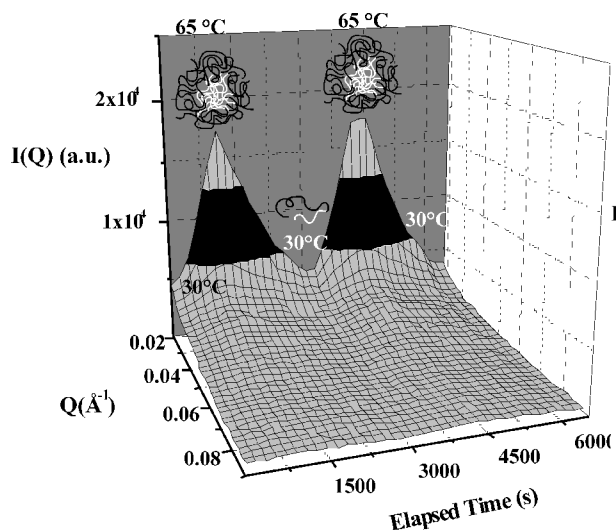
Figure 1. Temperature ramp at 250 bar   **Figure 2.** Pressure ramp at 40°C
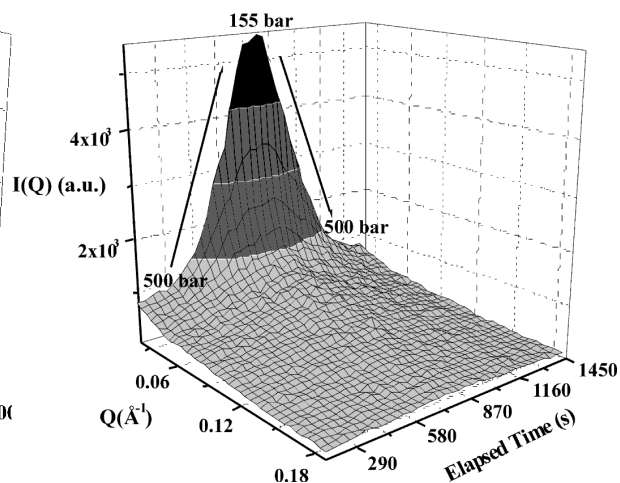
Experiments have been performed also by changing the pressure at constant temperature. In figure 2 it is reported the SAXS pattern obtained at constant temperature (T=40ºC) going from P = 500 bar to P = 150 and backwards to the initial value, with a speed of 0.6 bar/s. The pressure ramp surface shows some similarities with the temperature ramp already seen in figure 1.

At low momentum transfer values, the intensity initially (high pressure) does not show considerable changes in its values until the transition zone is approached. Suddenly it starts increasing as the pressure decreases giving a clear indication that the system is evolving towards the formation of micelles (high intensity values and low pressure) from a collection of random coils (low intensity and higher pressure). The pressure is kept constant at 155 bar and then increased again up to 500 bar; the reversed transition, from micelles to random coil chains, is observed, getting again the low intensity value when the pressure is higher than 400 bar.

Similar P ramps have been obtained in the temperature range 30-65 °C in steps of 5 °C. The results (in term of CMD's) are reported in figure 3, where the bars represent 2% of the CMD values. In figure 4 we have a schematic drawing of the phase diagram of the PVAc-b-PFOA-CO_2 system. Further beam time will be necessary to assess the validity of the CMD concept (points b), c) and d)) for a large variety of block copolymers as well as to explore points a) and e) reported earlier.
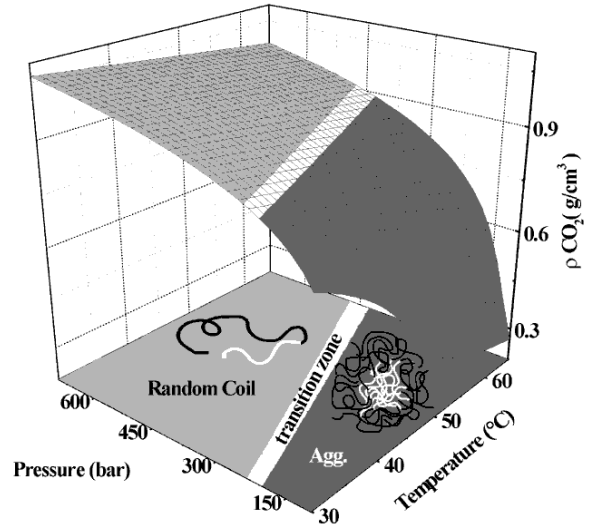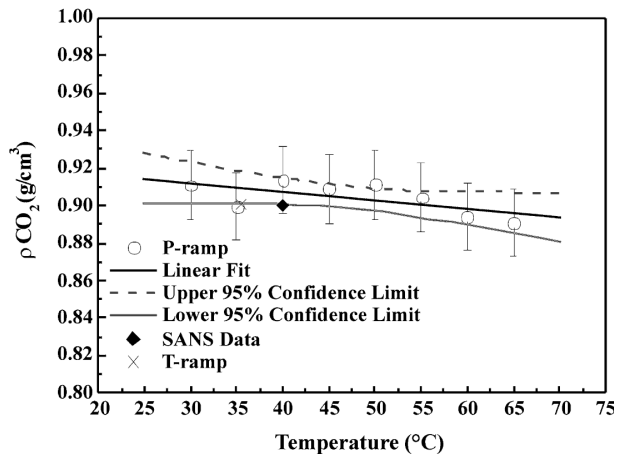
Figure 3. CMD vs. Temperature   **Figure 4.** Phase Diagram of CO_2-PVAc-b-PFOA System

References:

[1] Triolo, F. et al., *J. Appl. Cryst.* **33**, 641- 644 (2000)
[2] Triolo, A. et al., *Phys. Rev. E.* **61**, 4640-4643 (2000)
[3] Triolo, A. et al., *Phys. Rev. E.*, Phys. Rev. E **62**, 5839-5842 (2000)

MORPHOLOGY OF SOLID POLYMER ELECTROLYTES:
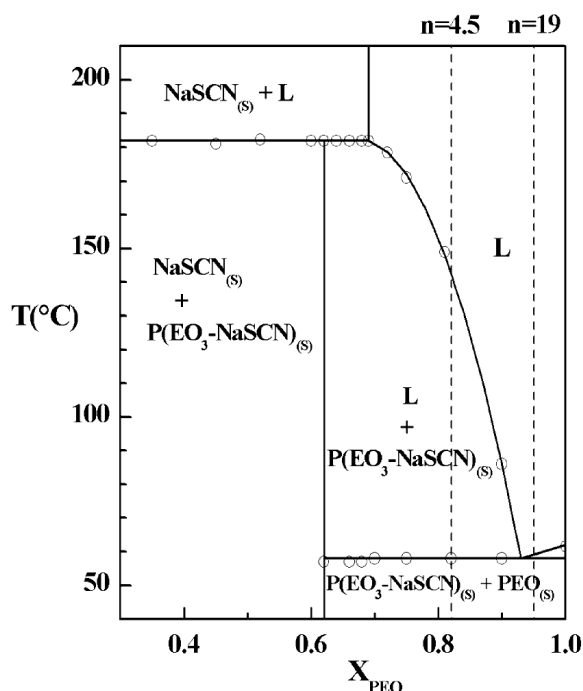## A TIME-RESOLVED WAXS INVESTIGATION

A. Triolo [1], F. Lo Celso [2], C. Di Giovanni [2], H. Amenitsch [3] and R. Triolo [2]

1.) HMI-BENSC, Glienicker Strasse 100, Berlin, Germany
2.) Dipartimento di Chimica-Fisica, Università di Palermo, viale delle Scienze, Parco d'Orleans II, 90128
    Palermo Italy.
3.) Institute of Biophysics and X-ray Structure Research, Austrian Academy of Sciences, Graz, Austria.

Solid state polymer electrolytes have experienced in the last few years a fast growing interest for their wide use in the consumer electronics market as thin-film and long lasting battery supplies [1]. Electrical conductivity of these materials can be controlled by the appropriate dispersion of alkali salts in the polymeric matrix such as PEO (poly (ethylene oxide)) and by the temperature conditions at which they should operate. It has been shown that due to the interaction between the polymer and the salt cation, PEO-salt mixtures are characterized by a complex phase diagram. Accordingly, in the solid state the introduction of ionic components in the pure polymeric matrix beyond a certain concentration, can modify its lamellar morphology (i.e. a morphology where crystalline layers do alternate with amorphous ones in a pseudo-periodical way) since the salt dissolves in both amorphous (APEO) and crystalline (CPEO) phases giving a crystalline complex (CC), with a well defined stoichiometry [2], and therefore a new phase. If an ideal solid polymer electrolytes (SPE) is considered, the conductivity is assured by the cations which are dissolved into the amorphous phase. The ethereal oxygens of the polymer backbone bind electrostatically the cation via complex formation and are able to move by segmental motion of the polymer chain. In this scenario the anions are free to move in the amorphous matrix while the salt that forms the CC cannot contibute to the conduction process. It is known that (PolyEthylene Oxide)$_n$-Sodium Thiocyanate [(PEO)$_n$NaSCN] mixtures [3,4], when NaSCN concentration exceeds a certain value, show a transition from a two phase to a three phase system where a CC phase appears in addition to the CPEO and APEO phases. The CC and CPEO are supposed to be organised as lamellar stacks alternating with the amorphous phase. Investigation on a low molecular weight PEO sample [5], in order to minimise entanglements effects, has confirmed the previous hypothesis and showed a phase diagram (figure 1) identical to the one reported in [3]. Optical Microscopy (OM) measurements on these materials, confirm the occurrence of spherulitic morphologies in the temperature range between the melting of CPEO and the melting of CC, this indicating a lamellar organisation of the CC phase. NMR studies [6] were able to detect the coexistence of the CPEO and CC in a rather large composition range. Moreover indications that the CC phase may develop between the APEO and the CPEO phases were derived. Recently [7] SAXS measurements on (PEO)$_n$NaSCN mixtures showed, in a certain range of composition, clear evidence of a lamellar morphology in the solid state.

Figure 1. Phase diagram for the (PEO)$_n$NaSCN system (from ref. 5). P(EO$_3$-NaSCN) corresponds to the stoichiometry of the crystalline complex.

We report here the results for the WAXS investigation for $(PEO)_n$-NaSCN mixtures for different salt concentration as function of the temperature. If we consider the mixture for n=19, corresponding to a very small molar fraction of NaSCN ($X_{NaSCN} = 0.05$), in this condition there is a quite high percentage of PEO as CPEO (56%) and just a 10% as CC, while the remaining is present as APEO [6]. The WAXS pattern at 30°C shows a sharp peak (Q = 3.02 $\mathring{A}^{-1}$) and a strong double peak (Q = 3.3 $\mathring{A}^{-1}$) that correspond to the pattern from the CPEO phase (figure2). A series on minor peaks is located between those high signals and in the remaining part of the spectrum (from 2.38 to 2.95 $\mathring{A}^{-1}$). The intensity of these minor peaks will increase as the percentage of the CC phase in the mixture increases.
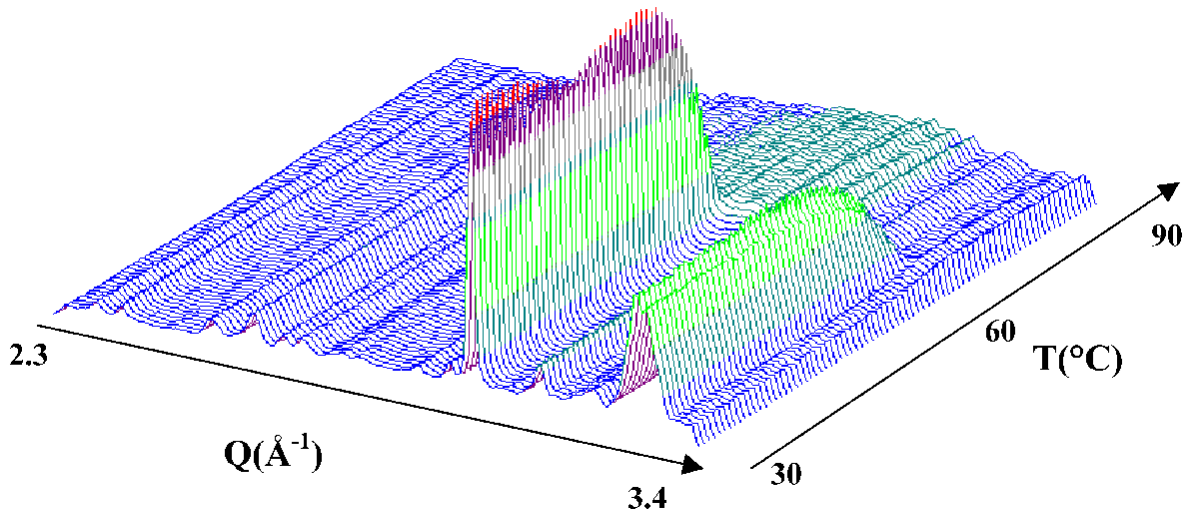

Figure 2. WAXS patterns for $(PEO)_{19}$NaSCN mixtures as function of the temperature.

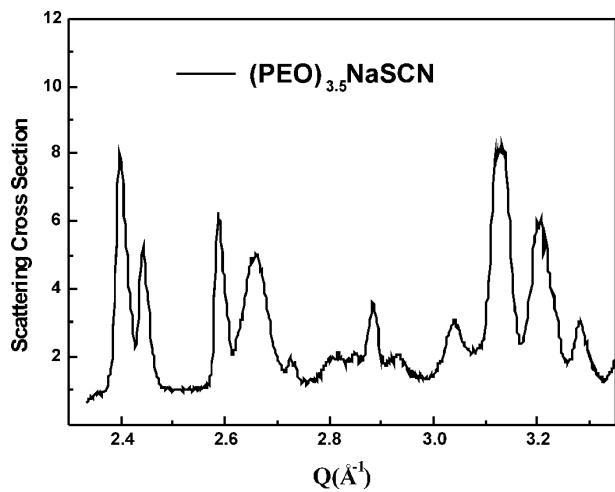**Figure 3.** WAXS pattern for $(PEO)_{3.5}$NaSCN mixtures at T = 30 °C.

This situation is better explained if we consider the diffraction pattern at 30 °C for the mixture where n = 3.5, shown in figure 3 at higher NaSCN molar fraction ($X_{NaSCN} = 0.22$). For this composition the majority of the PEO is in the CC phase (85%) while the CPEO phase is still present (9% of the PEO), basically an opposite situation with respect to the mixture where n = 19. The sharp peak found for the n = 19 mixture (Q = 3.02 $\mathring{A}^{-1}$) has almost disappeared leaving a low intensity broad peak. A similar consideration can be made about the strong double peak (Q = 3.3 $\mathring{A}^{-1}$) found for the n = 19 mixture, which in the spectrum of the n = 3.5 mixture is now a low intensity peak. Some other features of the diffraction pattern have changed going from n = 19 to the n = 3.5 mixture; the intensity of the two peaks found in the region between the sharp and the double peak (n = 19, from 3.02 $\mathring{A}^{-1}$ to 3.21 $\mathring{A}^{-1}$) is considerably increased in the spectrum of the n = 3.5 mixture. The same behaviour has been observed for the four peaks in the lower part of the spectrum (from 2.38 to 2.71 $\mathring{A}^{-1}$) whose intensities became higher going from the n = 19 to the n = 3.5 composition. Those results seem to be in agreement to the evidences found in other experiments that two crystalline phases exist, and by changing the

composition of the mixture, it is possible to detect remarkable effects in the morphology of the WAXS pattern and therefore in the structure of the polymer-salt system. The initial hypothesis that some of the features of WAXS diffraction pattern could be assigned either to the CPEO or the CC phase could be confirmed by looking at the evolution of the diffraction patterns as the temperature increases. In fig. 2 and 4 the WAXS patterns for n = 19 and n = 4.5 mixtures as a function of temperature are reported.
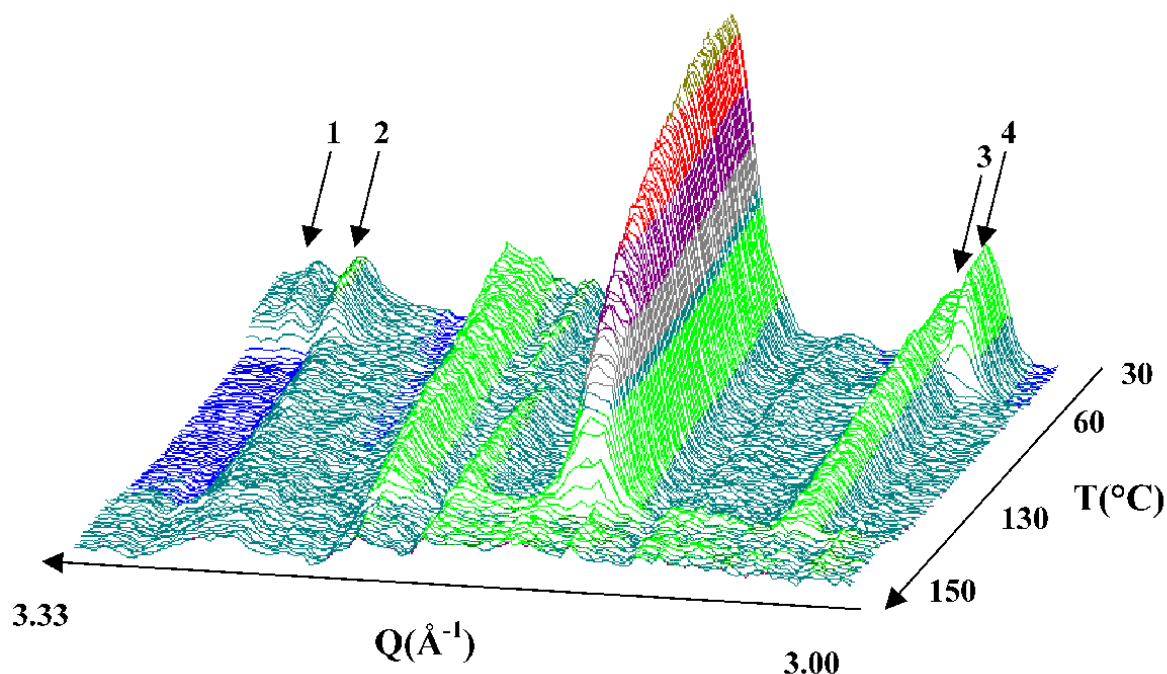
Figure 4. WAXS patterns for $(PEO)_{4.5}NaSCN$ mixtures at function of the temperature.

Looking at the n = 19 mixture, when the phase transition boundary line is reached (T = 58° C) the system goes from a coexisting two crystalline phase (CPEO and CC) to a single liquid phase (see figure 1). In the case of the n = 4.5 mixture a different zone of the phase diagram is observed, in this region as the first phase transition line is crossed (T = 58°C), the system goes from CPEO + CC phases to a CC phase plus a liquid phase, due to the melting of the CPEO phase. The WAXS pattern for this mixture seems to indicate the melting of the CPEO phase; indeed the two peaks observed at the lower temperatures (peak 1 and peak 4), belonging to CPEO phase, disappear at the transition temperature, while the peaks belonging to the CC phase (peak 2 and 3 and the major peaks) remain till the second transition temperature is reached (T = 150°C) and the CC phase melts.

References:

[1] Gray, F. M. *Polymer Electrolytes* Royal Society of Chemistry: Cambridge, 1997
[2] Ratner, M.A., Polymer Electrolytes Reviews I, Elsevier (London), 1987
[3] Lee, Y. L. and Crist, B., J. Appl. Phys., 60, 2683 (1986)
[4] Lee, Y. L. and Wright, P.V., Polymer, 23, 681 (1982)
[5] Robitaille, C., Marques, S., Boils, D. and Prud'homme, J., Macromolecules, 20, 3023 (1987)
[6] Bartolotta, A., Forte, C., Geppi, M., Minniti, D. and Visalli, G., Solid State NMR, 8, 231 (1997)
[7] A. Triolo, G. Visalli and R. Triolo, Solid State Ionics, 133, 99-106 (2000)

IPP BLENDS: CRYSTALLIZATION KINETICS VIA COMBINED SAXS-WAXS TECHNIQUES

A. Triolo [1], F. Lo Celso [2], C. Di Giovanni [2] and R. Triolo [2]

1.) HMI-BENSC, Glienicker Strasse 100, Berlin, Germany
2.) Dipartimento di Chimica-Fisica, Università di Palermo, viale delle Scienze, Parco d'Orleans II, 90128 Palermo Italy.

The main aim of the experiment was to obtain information concerning the structural evolution of isotactic polypropylene (iPP) - oligo ciclo pentadiene (HOCP) during crystallization at different temperatures from the melt state. The mixtures we investigated are of relevance in the field of films preparation for food packaging and a proper knowledge of the kinetic behavior during classical processing conditions (e.g. crystallization from the melt state) would be valuable to improve the overall performances of the materials.

Unfortunately, due to technical problems at the instrument we were not able to collect reliable data in the Wide Angle regime and only SAXS data could be efficiently collected. This represents a big limitation in the amount of information that can be derived on the way the local order develops during the crystallization process.

IPP/HOCP mixtures have been found to show a complex phase behaviour as they have a miscibility gap in the composition range between 70 and 30 %w/w iPP content and between 90 and approx. 150C. In the past we investigated the morphological implications of such a complex phase behaviour and combined SAXS/SANS studies indicated the existence of two different kinds of mesodomains in the phase separated regime, which are characterized by a lamellar-like crystalline iPP phase intercalated by two different kinds of amorphous phase differing in the HOCP content [1, 2]. In order to comprehend and optimize the technical performances of such materials it is then of high relevance to investigate not only the equilibrium morphology of these mixtures (see e.g. ELETTRA Annual Report for year 1999, pgg. 116-118), but also to understand the way that the equilibrium morphology is achieved starting from the fully amorphous melt state. These studies involve fast data collection in order to cover time scales of the order of few minutes.

We explored a variety of iPP-HOCP mixture at different HOCP content aiming to explore the crystallization behavior both outside and inside the miscibility gap.
In the following figures selected data are reported for quenches of iPP/HOCP from the melt to a definite temperature in the semicrystalline regime. We are currently trying to rationalise these data in terms of the current knowledge of the phase diagram.

[1] Triolo et al., Polymer, 39, 1697 (1998)
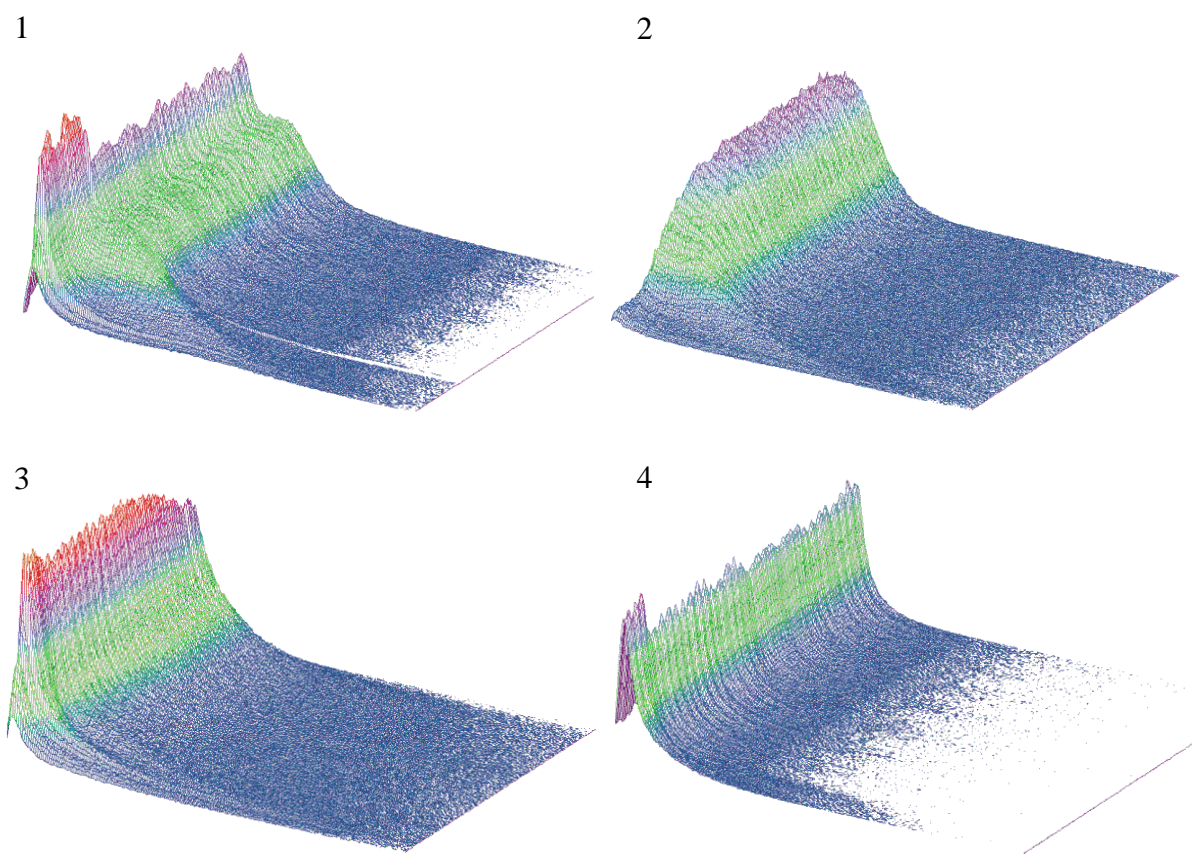[2] Triolo et al., Polymer, 41, 3751 (2000)

1

2

3

4

Figure 1-4. Representative SAXS patterns as obtained from iPP-HOCP mixtures [100/0 (Figure 1), 80/20 (Figure 2), 70/30 (Figure 3), 60/40 (Figure 4)] at 160 C. The complete data sets correspond to 10 minutes accumulation time with a time resolution of 10 seconds.

5. Instrumentation

RECENT ADVANCES WITH THE 2D X-RAY DETECTOR USED FOR SAXS- AND CRYSTALLOGRAPHIC IMAGING

A. Orthen[1], H. Wagner[1], H. Amenitsch[2], S. Bernstorff[3], H.J. Besch[1], R.H. Menk[3], A.H. Walenta[1]

1.) Department of Physics, University of Siegen, Walter-Flex-Str. 3, D-57068 Siegen, Germany
2.) IBR, Steyrergasse 17, Graz, Austria
3.) ELETTRA, Sincrotrone Trieste, S.S.14 km 163.5, Basovizza, 34012 Trieste, Italy

The full exploitation of synchrotron radiation requires highly advanced detector features. Besides good spatial resolutions and surpassing high rate capabilities large active areas are needed. A realisation of a novel two-dimensional gaseous single photon counter with an interpolating pixel readout which satisfies most of the requirements has been carried out for the special use in Small Angle X-Ray Scattering and in X-ray diffraction protein crystallography [1,2,3]. In comparison with the small prototypes used in the past the sensitive area has now been enlarged up to a factor 4 to 56x56 mm^2 almost without loss of spatial resolution [4].

The primary electrons produced by photons which enter the conversion region drift in a homogeneous field towards the amplifying structure. Due to the high electric field between this gas gain structure (MicroCAT [5]) and the readout anode the primary charges are multiplied. This charge avalanche hits the interpolating readout plane (see Fig. 1), designed as a two-dimensional resistive structure, where the sensitive area is subdivided in 7x7 square, 8x8 mm^2 sized interpolation cells. Every cell is read out at its four corners by means of readout nodes in order to reconstruct the event position making use of a suitable algorithm.

Since the gas gain strongly depends on a constant distance between the readout and the MicoCAT structure new challenges have been found in the development of proper spacer elements (see also Fig. 1). The new spacers consisting of glass (height about 200 µm) are printed on the readout nodes by means of a certain silk-screen printing method. Several test measurements studying the image performance of the enlarged detector have been carried out at the SAXS-beamline at ELETTRA [4]. Fig. 2 shows an image of an aperture. The enlarged prototype detector has also shown its efficiency in the sector of biological scattering measurements using e.g. a lipid as sample at the SAXS beamline (Fig. 3). Although the gas gain homogeneity has obviously been improved, further investigations and developments have to be carried out in this field.

References:

[1] H.J. Besch, M. Junk, W. Meißner, A. Sarvestani, R. Stiehler, A.H. Walenta; *An interpolating 2D pixel readout structure for synchrotron X-ray diffraction in protein crystallography*; Nucl. Instr. and Meth. A **392**, 244-248 (1997)

[2] A. Sarvestani, H.J. Besch, M. Junk, W. Meißner, R.H. Menk, N. Pavel, N. Sauer, R. Stiehler, A.H. Walenta; *Gas amplifying hole structures with resistive position encoding: a new concept for a high rate imaging pixel detector*; Nucl. Instr. and Meth. A **419**, 444-451 (1998)

[3] H. Wagner, H.J. Besch, R.H. Menk, A. Orthen, A. Sarvestani, A.H. Walenta, H. Walliser; *On the dynamic two-dimensional charge diffusion of the interpolating readout structure employed in the MicroCAT detector*; accepted for publication in Nucl. Instr. and Meth. A (2001)

[4] A. Orthen; *Entwicklung und Test eines großflächigen MCAT-Detektors mit Stützstruktur*; diploma thesis, University of Siegen (2000)

[5] A. Sarvestani, H.J. Besch, M. Junk, W. Meißner, R.H. Menk, N. Sauer, R. Stiehler, A.H. Walenta; *Study and application of hole structures as gas gain devices for two-dimensional high rate X-ray detectors*; Nucl. Instr. and Meth. A **410**, 238-258 (1998)
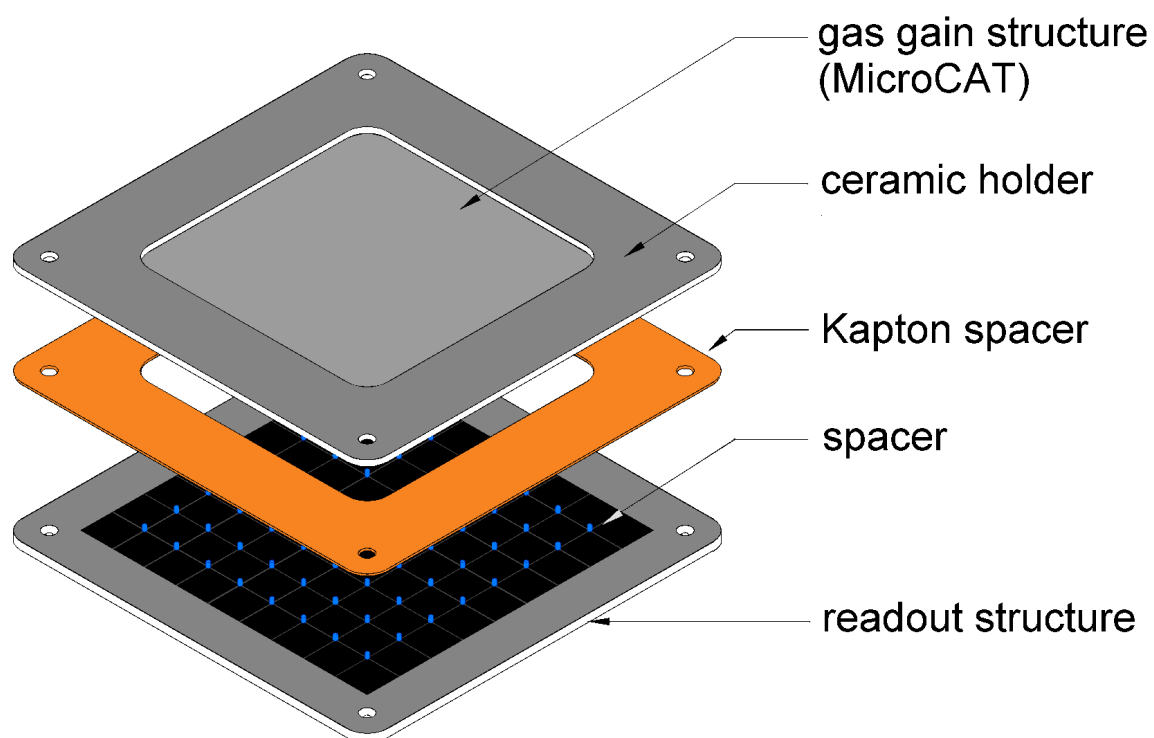
Figure 1. Schematic setup of the MicroCAT detector with its interpolating readout structure.
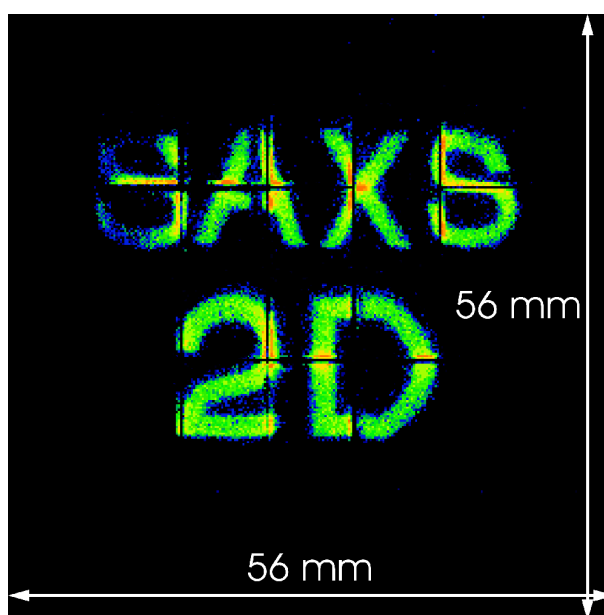

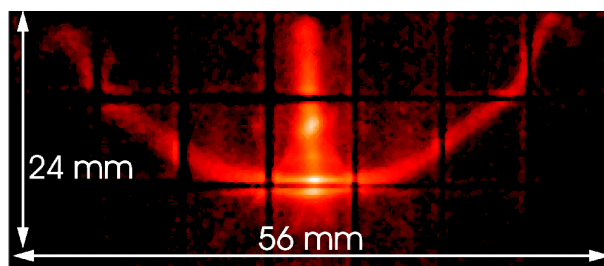**Figure 2.** Aperture measurement.

Figure 3. Diffraction pattern of a lipid.

Publications

Publications in 2000

P Ågren, M. Lindén, J.B. Rosenholm, J. Blanchard, F. Schüth and H. Amenitsch
Kinetics of Co-surfactant – Surfactant – Silicate Phase Behavior. 2. Short-chain Amines.
Langmuir 16, 8809-8813 (2000)

V. Arrighi, A. Triolo, I.J. McEwen,.P. Holmes, R. Triolo, H. Amenitsch
Observation of Local Order in Poly(di-n-alkyl itaconate)s
Macromolecules 14, 4989 (2000)

V.K. Aswal, P.S. Goyal, S. De, S. Bhattacharya, H. Amenitsch and S. Bernstorff
Small-angle x-ray scattering from micellar solutions of gemini surfactants
Chem. Phys. Lett. 329, pp. 336-340 (2000)

Bagni, M.A., Cecchi, G., Colombini, B., Amenitsch, H., Bernstorff, S., Rapp, G., Ashley, C.C. and Griffiths, P.J.
14.5 nm meridional X-ray diffraction intensity changes associated with the myosin head elasticity and the quick recovery phase
Biophysical Journal 78 (1), A227 (2000)

J.Baldrian, M.Horky, M.Steinhart, A.Sikora, P.Vleek, H.Amenitsch, S.Bernstorff
Time-resolved SAXS/WAXS study of polymer blend crystallization
Proceedings SPIE Int. Soc. Opt. Eng. Vol 4240, pp. 51-58 (2000)

J.T. Bonarski, M.Zehetbauer, Z.Swiatek, I.M Fodchuk, I.Kopacz, S.Bernstorff and H.Amenitsch
Structural Disturbances of Near-Surface Areas in Silicon Solar Cell Modified by P^{+} Ion Implantation and Thermal Treatment
Proc. Europ.Conf. on Photovoltaics, Oct.25-27, 1999 (Cracow, Poland),
Opto-Electronics Review 8, No. 4, pp. 323-327 (2000)

G. Cerichelli, C. La Mesa, L. Lucchetti and G. Mancini
Role of Counterions in the Catalytic Activity and Phase Equilibria of Phosphonium Salts in Water.
Langmuir 16 (2000) 166-71

P. Dubcek, O. Milat, B. Pivac, S. Bernstorff, H. Amenitsch, R. Tonini, F. Corni, and G. Ottaviani
GISAXS study of defects in He implanted silicon
Mater. Sci. & Eng. B 71, 292-296 (2000)

M. Forstner
SAXS, SANS, and X-ray Crystallography as complementary methods in the study of biological form and function
J. Appl. Cryst. 33 (2000) 519-523

G. Garab, K. Lohner, P. Laggner, T. Farkas
Self-regulation of the lipid content of membranes by non-bilayer lipids. A hypothesis.
Trends in Plant Sci. 5 (11), 492-497 (2000)

S. Gomez, R. Toffanin, S. Bernstorff, M. Romanello, H. Amenitsch, M. Rappolt, R. Rizzo
and F. Vittur
*Collagen Fibrils are differently organized in weight-bearing and not-bearing regions of Pig
Articular Cartilage*
Journal of Exp. Zoology 287, pp. 346-352 (2000)

H.Grigoriew, A.Wolinska-Grabczyk, A.G.Chmielewski, H.Amenitsch and S.Bernstorff
*SAXS study of the influence of ethanol on the microstructure of polyurethane-based
membrane*
Journal of Membrane Science 170 (2000) 275-279

A. Gupta, N. Bhagat, G. Principi, A. Maddalena, N. Malhotra, B.A. Dasannaccharya, P.S.
Goel, H. Amenitsch and S. Bernstorff
*Nanocrystallization of amorphous alloys: comparision between furnace and current
annealing*
Intermetallics 8, 287-291 (2000)

Ch.Kühne, D.Gardiol, C.Guarnaccia, H.Amenitsch, and L.Banks,
*Differential regulation of human papillomavirus E6 by protein kinase A: conditional
degradation of human discs large protein by oncogenic E6*
Oncogene 17, 5884-5891 (2000)

M. Linari, G. Piazzesi, L. Lucii, H. Amenitsch, S. Bernstorff, V. Lombardi
*A time resolved X-ray diffraction study of the structural aspects of after-stretch potentiation
in single frog muscle fibres*
Pflügers Arch. 439, abstract R276/84, 2000

M. Linari, L. Lucii, M. Reconditi, M.E. Vannicelli Casoni, H. Amenitsch, S. Bernstorff, G.
Piazzesi and V. Lombardi
*A combined mechanical and X-ray diffraction study of stretch potentiation in single frog
muscle fibres*
J. Physiol. 526, pp. 589-596 (2000)

M. Lindén, P. Agren, S. Karlsson, P. Bussian, H. Amenitsch
Solubilization of oil in silicate-surfactant mesostructures
Langmuir 16 (2000) 5831-5836

P. Mariani, F. Carsughi, F. Spinozzi, S. Romanzetti, G. Meier, R. Casadio, C.M. Bergamini
*Ligand-induced conformational changes in tissue Transglutaminase: Monte Carlo analysis of
small angle scattering data*
Biophysical Journal , 78, 3240-3251 (2000)

R.H. Menk, A.Sarvestani, H. Amenitsch, S.Bernstorff, H.J. Besch, A. Orthen, N. Pavel, M.
Rappolt, N. Sauer and A.H.Walenta
Novel detector systems for time resolved SAXS experiments
J. Appl. Cryst. 33 (2000) 778-781

R.H. Menk, A.Sarvestani, H.J. Besch, A.H.Walenta, H. Amenitsch and S.Bernstorff
Gas Gain Operations with Single Photon Resolution Using an Integrating Ionization Chamber in Small Angle X-Ray Scattering Experiments
Nucl.Instr.&Meth. A440 (2000) 181-190

G. Pabst, M Rappolt, H. Amenitsch, S. Bernstorff and P. Laggner
X-ray kinematography of temperature-jump relaxation probes the elastic properties of fluid bilayers
Langmuir 16, 8994-9001 (2000)

Pabst, G., Rappolt, M., Amenitsch, H. & Laggner, P.
Structural information from multilamellar liposomes at full hydration: full q-range fitting with high-quality X-ray data
Phys. Rev. E 62, 4000-4009 (2000)

Pabst, G., Rappolt, M., Amenitsch, H. & Laggner, P.
Structural information from X-ray experiments on unoriented phospholipid bilayers at full hydration by means of an inverse Fourier method
Biophys. J. 78 (1), A21 (2000)

O. Paris, I. Zizak, H. Lichtenegger, P. Roschger, K. Klaushofer and P. Fratzl
Analysis of the hierarchical structure of biological tissues by scanning X-ray scattering using a micro-beam
Cellular and Molecular Biology 46, 993-1004 (2000)

R.Prassl, R. Schwarzenbacher, M.Kriechbaum, H. Amenitsch, M. J. Chapman, and P.Laggner
Low Resolution X-ray Crystallography on Human Low Density Lipoprotein
Biophys. J. 78(1), 484 (2000)

G. Principi, A. Maddalena, A. Gupta, N. Bhagat, N. Malhotra, B.A. Dasannacharya, H. Amenitsch and S. Bernstorff
Furnace and current annealing of the amorphous $Fe_{72}Cu_1Nb_{4.5}Si_{13.5}B_9$ alloy
J. Appl. Phys. 87 (2000) 7109 - 7111

M. Rappolt, G. Pabst, G. Rapp, M. Kriechbaum, H. Amenitsch, C. Krenn, S. Bernstorff and P. Laggner
New evidence for gel-liquid crystalline phase co-existence in the ripple phase of phosphatidylcholines
Eur. Biophys. J. 29, 125 - 133 (2000)

R. Resel, U. Theissl, C. Gadermaier, E. Zojer, M. Kriechbaum, H. Amenitsch, D. Gin, R. Smith and G. Leising
The H_2 – phase of the lyotropic liquid crystal sodium 3,4,5 – tris (omega-acryloyloxyundecyloxy)benzoate
Liquid Crystals 27/3, 407-411 (2000)

M. Roessle, E. Manakova, I. Lauer, T. Nawroth, J. Holzinger, T. Narayanan, S. Bernstorff, H. Amenitsch and H. Heumann
Time-resolved small angle scattering: kinetic and structural data from proteins in solution
J. Appl. Cryst.33, 548-551 (2000)

I. Simidjiev, S. Stoylova, H. Amenitsch, T. Javorfi, L. Mustardy, P. Laggner, A. Holzenburg, and G. Garab
Self-assembly of large, ordered lamellae from non-bilayer lipids and integral membrane proteins in vitro
Proc. Natl Acad. Sci USA, Vol. 97, Issue 4, 1473-1476 (2000)

E.Schafler, M.Zehetbauer, P.Hanak, T.Ungar, T.Hebesberger, R.Pippan, B.Mingler, H.P.Karnthaler, H.Amenitsch and S.Bernstorff
Fragmentation in Large Strain Cold Rolled Aluminium as observed by Synchrotron X-Ray Bragg Peak Profile Analysis (SXPA), Electron Back Scatter Diffraction (EBSD) and Transmission Electron Microscopy (TEM)
Proc. NATO Adv.Res.Workshop "Investigations and Applications of Severe Plastic Deformation", (Aug. 2-6, 1999, Moscow, Russia); ed. T.C.Lowe and R.Z.Valien, Kluwer Acad. Publ., The Netherlands, p.163-171 (2000)

E.Schafler, M.Zehetbauer, T.Ungar, S.Bernstorff, H.Amenitsch,
Key Eng. Mater. 177-180, 159 (2000)

D. Sen, S. Mazumder, R. Tewari, P.K. De, H. Amenitsch and S. Bernstorff
Investigation on precipitation in Zircaloy-2 fuel cladding tube
J. of Alloys and Compounds 308, 250-258 (2000)

A.Turkovic
Grazing-incidence SAXS/WAXD on nanosized TiO_2 films obtained by ALE
Materials Science & Engineering B75, pp. 85-91 (2000)

A.Turkovic
Nanostructured materials
Book of Abstracts MATH/CHEM/COMP 2000, Inter-University Centre, Dubrovnik, Croatia 19-24 june 2000, Dubrovnik, p. 93 (ISBN 953-6690-08-X)

M.E. Vannicelli Casoni, L. Lucii, M. Linari, H. Amenitsch, S. Bernstorff, G. Piazzesi, V. Lombardi
Mechanical and structural evidences of an increased fraction of attached heads as responsible for after-stretch potentiation in frog single muscle fibers
Biophys. J. 78, abstract 231/1362-Pos (2000)

M.Zehetbauer
Strengthening Processes of Metals at Severe Plastic Deformation: Analyses with Electron and Synchrotron Diffraction
Proc. NATO Adv.Research Workshop "Investigations & Applications of Severe Plastic Deformation", August 2-6 (Moscow, Russia 1999), ed. T.C.Lowe and R.Z.Valiev, Kluwer Acad. Publ., The Netherlands, p.81-91 (2000)

M.Zehetbauer, T.Ungar, E.Schafler, S.Bernstorff, H.Amenitsch
Microscale Spatial Distribution of Dislocations and Long Range Internal Stresses in Cold Worked bcc Fe
Key Eng.Mater. 177-180, 159-164 (2000)

A. Zidansek, S. Kralj, R. Repnik, G. Lahajnar, M. Rappolt, H. Amenitsch and S. Bernstorff
Smectic ordering of octylcyanobiphenyl confined to control porous glasses
Journal of Physics-Condensed Matter 12, A431-A436 (2000)

I. Zizak, K. Misof, P. Roschger, G. Rapp, H. Amenitsch, S. Bernstorff,
D.J.S. Hulmes and P. Fratzl
Synchrotron x-ray scattering studies of the elastic properties of type I collagen
Proceedings of the Sixth International Conference on the "Chemistry and Biology of Mineralized Tissues", (Vittel, France, November 1-6th, 1998), Eds. M. Goldberg, A. Boskey, C. Robinson, American Academy of Orthopaedic Surgeons, 423 Abstract 63 (2000)

I. Zizak, O. Paris, P. Roschger, S. Bernstorff, H. Amenitsch, K. Klaushofer, P. Fratzl
Investigation of bone and cartilage by synchrotron scanning SAXS and -WAXD with micrometer spatial resolution
J. Appl. Cryst. 33, pp. 820-823 (2000)

Publications in January - May 2001

Cecchi, G., M.A. Bagni, B. Colombini, H. Amenitsch, S. Bernstorff, C.C. Ashley and P.J. Griffiths
Temperature effects on the equilibrium tilt of the myosin heads during sinusoidal length oscillations
Biophysical Journal, 80 (1), A26 (2001)

H.Grigoriew, S.Bernstorff, A.Wolinska-Grabczyk, J.Domagala, A.G.Chmielewski;
Depth-influenced structure through permeating polymer membrane using SAXS synchrotron method
Journal of Membrane Science 186, 1-8 (2001)

H. Grigoriew, A.G. Chmielewski, H. Amenitsch
Structural temperature transformation of the cellulose-water system using time-resolved SAXS
Polymer 42, pp. 103-108 (2001)

A. Turkovic, Z. Crnjak-Orel and P. Dubcek
Grazing-incidence small-angle X-ray scattering on nanosized vanadium oxide and V/Ce oxide films
Materials Science & Engineering B79/1, 11-15 (2001)

Publications, in print

Bagni, M.A., G. Cecchi, B. Colombini, P.J. Griffiths, C.C. Ashley, H. Amenitsch and S. Bernstorff
Effects of temperature on the intensity changes of the meridional 14.5nm X-ray reflection from activated skeletal muscle during sinusoidal oscillations
Journal of Physiology

Bagni, M.A., G. Cecchi, B. Colombini, H. Amenitsch, S. Bernstorff, C.C. Ashley, G. Rapp and P.J. Griffiths
Frequency dependent distortion of meridional intensity changes during sinusoidal length oscillations of activated skeletal muscle
Biophysical Journal

P. Dubcek, B. Pivac, O. Milat, S. Bernstorff and I. Zulim
X-Ray Reflectivity and Gisaxs Study of Derelaxation in Kr implanted Si
Proccedings of the Spring 2001 Meeting of the Materials Research Society

R. Gianni, F. Delben, G. Liut, S. Bernstorff, H. Amenitsch, R. Rizzo
Synthesis and conformational properties of cyanoethylscleroglucan
Carbohydrate Polymers

D. Grosso, P.A. Albouy, H. Amenitsch, A.R. Balkenende and F. Babonneau
Time-resolved in-situ X-ray diffraction study of the formation of 3D-hexagonal mesoporous silica films
Mater. Res. Soc. Symp. Proc. Vol 628

D. Grosso, A. R. Balkenende, P.A. Albouy, A. Ayral, H. Amenitsch, F. Babonneau
Formation mechamism of 2D-hexagonal mesoporous silica thin films prepared from block copolymers
Chem. Mater.

T.Hebesberger, E.Schafler, M.Zehetbauer, R.Pippan, T.Ungar, S.Bernstorff
Electron Back Scatter Diffraction (EBSD) and Synchrotron X-Ray Profile Analysis (SXPA) as Tools for Microstructural Characterisation of Large Strain Work Hardened Metals
Z.Metallkde.

E.F. Marques, H. Edlund, A. Khan and C. L Mesa
Liquid Crystals and Phase Equilibria in Binary Bile Salt-Water Systems.
Langmuir, 2000, 16

Mazumder et al.
Title: not communicated
Journal of Alloy & compounds

M. Pisani, S. Bernstorff, C. Ferrero and P. Mariani
Pressure induced cubic-to-cubic phase transition on the monoolein hydrated system
J. Phys. Chem. B, (Apr. 2001)

N. Prasanth Kumar, S. Major, S. Vitta, S. S. Talwar, P. Dubcek, H. Amenitsch, S. Bernstorff, V. Ganesan, A. Gupta and B. A. Dasannacharya
Molecular packing in Cadmium and Zinc Arachidate LB multilayers
Journal of Colloids and Interfaces

N. Prasanth Kumar, S. Major, S. Vitta, S. S. Talwar, P. Dubcek, H. Amenitsch, S. Bernstorff, V. Ganesan, A. Gupta and B. A. Dasannacharya
Molecular packing in CdS containing conducting polymer composite LB multilayers
Journal of Colloids and Interfaces

N. Prasanth Kumar, Bhavin Shukla, S. Major, S. Vitta, S. S. Talwar, P. Dubcek, H. Amenitsch and S. Bernstorff
Structure of ZnS-Arachidic Acid Composite LB multilayers
Journal of Colloids and Interfaces

M. Rappolt, G. Pabst, H. Amenitsch and P.Laggner
Salt induced phase separation in the liquid crystalline phase of phosphatidylcholines
Colloids and Surfaces A

A. Sarvestani, N. Sauer, C. Strietzel, H.J. Besch, A. Orthen, N. Pavel, A.H. Walenta and R.H. Menk
Microsecond Time-resolved 2D X-ray Imaging
Nucl.Instum.&Methods

E.Schafler, M.Zehetbauer, I.Kopacz, T.Ungar, S.Bernstorff
Investigations of the Microstructural Evolution of Cold Worked Metals by means of Synchrotron Radiation – A Comparative Survey
J.Eng.Mater.Technol.ASME

H. Wagner, H.J. Besch, R.H. Menk, A. Orthen, A. Sarvestani, A.H. Walenta and H. Walliser
On the dynamic two-dimensional charge diffusion of the interpolating readout structure employed in the MicroCAT detector
Nucl.Instum.&Methods

Publications, submitted

J.Baldrian, M.Horky, M.Steinhart, P.Laggner, P.Vleek, H.Amenitsch, S.Bernstorff
Time-resolved SAXS/WAXS study of phase behaviour and crystallization in polymer blends
Polymer

P. Dubcek, N. Radic, O. Milat and S. Bernstorff
Grazing Incidence Small Angle X-Ray Scattering Investigation of Tungsten-Carbon Alloys Produced by Reactive Magnetron Sputtering
Proceedings of Spring Meeting of the European Materials Science Conference, Strasbourg, France, June 5-8, 2001 (Elsevier/North Holland)

F. Lo Celso, A. Triolo, M. Steinhart, M. Kriechbaum, H. Amenitsch and R. Triolo
TR SAXS Investigation on Aggregation Phenomena in Supercritical CO_2
Phys. Rev. E

D. Grosso, F. Babonneau, P.A. Albouy, H. Amenitsch, A.R. Balkenende, A. Brunet-Bruneau and J. Rivory
An in-situ study of mesostructured CTAB-silica film firmation during dip-coating, using time-resolved SAXS and interferometry measurements
J. Amer. Chem. Soc.

127

R. Puxkandl, I. Zizak, O. Paris, J. Keckes, W. Tesch, S. Bernstorff, P. Purslow and P. Fratzl
Viscoelastic properties of collagen - synchrotron radiation investigations and structural model
Philos Trans R Soc Lond B – Special Issue: Elastomeric Proteins

E.Schafler, M.Zehetbauer, I.Kopacz, B.Ortner, S.Bernstorff, H.Amenitsch, T.Ungar
Local Dislocation Densities and Internal Stresses by High Lateral Resolution Peak Profile Analysis in Plastically Deformed Polycrystalline Nickel
Scripta Mater.

E.Schafler, M.Zehetbauer, I.Kopacz, I. Altpeter, B.Ortner, H.Amenitsch, S.Bernstorff, T.Ungar
Messungen der Verteilung von Versetzungsdichten und inneren Spannungen in plastisch verformtem Ni mittels hochauflösender Synchrotron-Linienprofil-Analyse und magnetischer Mikroskopie
Scripta Mater.

A. Triolo, F. Lo Celso, C. Di Giovanni, H. Amenitsch and R. Triolo
Morphology of Solid Polymer Electrolytes: a TR WAXS Investigation
Physica A

F. Triolo, A. Triolo, F. Lo Celso, D.I. Donato and R. Triolo
Dilute and Semi dilute Solutions of Block Copolymers in water, Near-critical and Super-Critical CO_2: a Small Angle Scattering Study of the Monomer-Aggregate Transition.
Physica A

International Conferences and Workshops in 2000

H.Amenitsch, S.Bernstorff, K.Lohner, G.Pabst, R.Prassl, M.Rappolt, and P.Laggner
Structure of Phospholipids and Lipoproteins Probed with Fast Jump-Relaxation Techniques
Workshop on "Fast Structural Changes", Grenoble, France, 8.2.00-9.2.00, (Invited Talk)

H.Amenitsch, H.J. Besch, S.Bernstorff, R.H. Menk, A.Orthen, H.Wagner, A.H. Walenta
Gaseous detectors for SAXS experiments
International Conference on "Synchrotron Radiation Instrumentation" (SRI 2000), Berlin, Germany, August 21-25, 2000 (Poster)

H. Amenitsch, M. Kriechbaum, M.Rappolt, G.Papst, P. Laggner, S. Bernstorff, P.Dubcek
Fast Structural Studies at the Austrian Small Angle X-ray Scattering Beamline (ELETTRA)
10 years Hercules, Grenoble, France, 6.4.00-9.4.00, (Poster)

H. Amenitsch, M. Kriechbaum, M. Rappolt, M. Steinhart, S. Bernstorff and P. Laggner
Surface Diffraction on Highly Aligned Phospholipids at the SAXS Beamline
8th International Users' Meeting, ELETTRA, Trieste, Italy, 4. - 5.12.2000 (Poster)

H.Amenitsch, M.Rappolt, P.Laggner,
Novel X-ray sample cell suitable for surface diffraction on aligned multilayers under variable solvent conditions
14th Conference of the European Colloid and Interface Society, Patras, Greece, Sept. 17-22, 2000, (Talk)

H.Amenitsch, M.Rappolt, S.Bernstorff, P.Laggner
Tutorial: Time resolved experiments at the SAXS beamline
School on Synchrotron Radiation 6-8.12.00, Trieste, Italy, 27.11.00-28.11.00, (Tutorial)

V. Arrighi, A. Triolo, I.J. McEwen, P. Holmes
Local Ordering in Poly(di-n-alkyl itaconate)s
RSC Annual Conference – Macrogroup young researchers' meeting, UMIST, Manchester,

V. Arrighi, A. Triolo, I.J. McEwen, P. Holmes
Local Motion in Poly(di-n-alkyl itaconate)s
QENS 2000 Conference, Royal Botanic Garden, Edinburgh, UK. 31 August – 1 September 2000 (poster)

F. Babonneau
Surfactant-templated silicates : access to materials with ordered porosity
5th French-Swedish meeting of solid state chemistry, Abo (Finland), 4-8 October 2000 (invited talk)

F. Babonneau
Various characterization techniques applied to self-assembled silica thin films
Department of Chemical Engineering, University of California, Santa Barbara (USA), 11 August 2000.

F. Babonneau
Various characterization techniques applied to self-assembled silica thin films
Advanced Materials Laboratory, University of New Mexico/Sandia National Laboratories, Albuquerque (USA), 23 August 2000

Bagni, M.A., G. Cecchi., B. Colombini, H. Amenitsch, S. Bernstorff, G. Rapp, C.C. Ashley, and P.J. Griffiths
14.5 nm meridional X-ray diffraction intensity changes associated with the myosin head elasticity and the quick recovery phase
44th Biophysical Society Meeting, New Orleans, Louisiana, USA, 12-16 February, 2000 (poster)
Biophysical Journal, 78 (1), A227 (2000)

J.Baldrian, M.Horky, M.Steinhart, P.Laggner, H.Amenitsch, S.Bernstorff
Crystallization of Poly(ethylene oxide) Blends using Time-Resolved SAXS/WAXS
2nd Meeting of the COST P1 working Group 6: Polymer Crystallization, Vught, (poster)

J.Baldrian, M.Horky, M.Steinhart, P.Laggner, P.Vleek, A.Sikora, H.Amenitsch, S. Bernstorff
Real-time SAXS and SAXS/WAXS studies of ordering phenomena in PEO/PMMA blends during crystallization
3rd Czech-Korean Joint Symposium on Macromolecular Chemistry, Pohang 2000
Abstracts, pp. 13-14 (lecture)

J. Baldrian, M.Horky, M.Steinhart, A. Sikora, H.Amenitsch, S. Bernstorff and P.Laggner
Real-time microstructure development of PEO/PEO blends
8th International Users' Meeting, ELETTRA, Trieste, Italy, 4. - 5.12.2000, Abstracts, p. 28 (Poster)

J.Baldrian, M.Steinhart, M.Horky, P.Laggner, H.Amenitsch, S.Bernstorff
Real-Time Crystallinity and Crystalline Density Evolution of PEO in PEO/PMMA Blends
Int.Workshop "Scattering Studies of Mesoscopic Scale Structure and Dynamics in Soft Matter, Messina, Abstracts 1, (poster)

S. Bernstorff, H. Amenitsch, P.Dubcek, P. Laggner, M. Rappolt
Recent experiments at the SAXS-beamline
Joint Indo-Italian Workshop on "Collaboration with Synchrotron Trieste", Trieste, Italy, November 30th- December 1st, 2000 (talk)

J. Caelles, I. Carrera, H. Amenitsch, R. Pons
Emulsificación por cambio de temperatura seguida mediante dispersión de rayos-x en función del tiempo
4ª reunión GECI, Barcelona, 3-5 July 2000 (proceedings are in press) (talk)

Flavio Carsughi, Paolo Mariani, Francesco Spinozzi, Stefania Cinelli, Giuseppe Onori, Rosangela Itri
Study of the Structural Properties and Solvent Role in Soluble Proteins by Small Angle X-Ray Scattering
INFMeeting, Genua, Italy, June 12-16, 2000

P. Dubcek, B. Pivac, O. Milat, S. Bernstorff
Grazing incidence Small-Angle X-Ray Scattering Study of the rapid thermal chemical vapour deposited silicon
8th International Users' Meeting, ELETTRA, Trieste, Italy, 4. - 5.12.2000 (Poster)

M. Forstner
SAXS, SANS, and X-ray Crystallography as complementary methods in the study of biological form and function
4th Annual Conference of the Swedish Structural Biology Network, Tällberg, Sweden, 2000 (talk)

P.J. Griffiths, H. Amenitsch, M.A. Bagni, S. Bernstorff, G. Cecchi, R. Colombini and C.C. Ashley,
14.5 nm Meridional Reflection Intensity Changes in Frog Muscle Fibres During Sinusoidal Lenght Oscillations at Various Temperatures
8th International Users' Meeting, ELETTRA, Trieste, Italy, 4. - 5.12.2000 (Poster)

H.Grigoriew, S.Bernstorff, A.Wolinska-Grabczyk, A.G.Chmielewski
Depth-influenced Synchrotron SAXS measurements of the system: membrane- solvent
Euromembrane-2000, Hills of Jerusalem, Israel, September 24-27, 2000 (poster)

D. Grosso, F. Babonneau, P.-A. Albouy, A.R. Balkenende
Structural Characterization of Surfactant-templated mesoporous silica thin films
102nd Annual Meeting of The American Ceramic Society, Saint Louis (USA), 1-3 May 2000
(invited talk)

D. Grosso, F. Babonneau, P.A. Albouy, H. Amenitsch, M. Lavergne, L. Mazerolles, R.
Balkenende, Brunet-Bruneau and J. Rivory
Structural Formation of Mesoporous Templated Silica Films
International Symposium on Mesoporous Molecular Sieves, Québec City, (Canada), 27
August-1 September 2000 (poster)

D. Grosso, F. Babonneau, P.-A. Albouy, R. Balkenende, H. Amenitsch
Mesoporous silica thin films with various structures: in-situ time-resolved XRD experiments
ACS National Meeting, San Diego (USA), 1-5 April 2001 (talk)

Frank Häußler and J. Tritthart
SANS und SAXS zur Untersuchung der Zementsteinmikrostruktur – SAXS/WAXS-Studien zur
Hydratationsfrühphase am Synchrotron Triest,
Seminarvortrag, TVFA der TU Graz, Austria, 20.06.2000

F. Häußler
Der Zusammenhang zwischen gemessenen Neutronenstreukurven und den
Zementsteineigenschaften Permeabilität und Dauerhaftigkeit
Beitrag im Sachstandsbericht gegenüber der Deutschen Forschungsgemeinschaft (DFG),
DFG-Geschäftszeichen: HA2759/3-1, Germany, 2000

Solubilization of Polar Benzene Derivatives in Silicate-Surfactant Systems
10th Symposium of the Finnish Surface and Colloid Society, Turku, Finland, 7-8 September,
2000 (talk)

M. Lindén, P. Ågren, S. Karlsson, H. Amenitsch, J. Blanchard
Solubilization behavior of composite mesophases at low degrees of condensation as studied
by in situ-SAXS
2nd International symposium on "mesoporous molecular sieves", Quebec City, Canada,
August 27 - September 3, 2000 (poster)

Fabrizio Lo Celso
Unimer-Aggregate Transition in Block Copolymers Dissolved in Supercritical CO_2. A P-jump
Relaxation Study by Synchrotron TR SAXS
Scattering Studies of Mesoscopic Scale Structure and Dynamics in Soft Matter, Messina,
Italy, November 22-25, 2000 (talk)

Fabrizio Lo Celso and Roberto Triolo
Morphology of Solid Polymer Electrolytes
Scattering Studies of Mesoscopic Scale Structure and Dynamics in Soft Matter, Messina, Italy, November 22-25, 2000 (poster)

A. Longo, A. Martorana, S. Piccarolo and H. Amenitsch
Lamellar thickness statistics in quenched Polypropylene
VIII Convegno SILS; Palermo, Italy; June; 29; 2000

Paolo Mariani, Flavio Carsughi, Francesco Spinozzi, Sandro Romanzetti, Gerd Meier, Rita Casadio, Carlo M. Bergamini
Ligand-induced conformational changes in tissue transglutaminase: Monte Carlo Analysis of Small Angle Scattering Data
XV Congresso della Società Italiana di Biofisica Pura ed Applicata, Parma, Italy, October 23-25, 2000

R. Menk
Novel Micro hole structures as gas gain devices for high rate x-ray detectors
Fast changes workshop, ESRF, France, Feb 2000 (talk)

R. Menk
How far can we go with gaseous detectors ?
FEL instrumentation Workshop, Hamburg, Germany, 23 + 24 June 2000 (talk)

R.H.Menk, H.Amenitsch, H. J. Besch, S.Bernstorff, A. Sarvestani, A.Orthen, H.Wagner, A.H. Walenta
Gaseous high Speed Imaging Micro-CAT Detectors in the Energy Range from 5-20 keV
Frontier Detectors for frontier physics, 8th Pisa meeting on advance detectors, Pisa, Italy, May, 2000 (poster)

LaMesa et al.
Title not communicated
National Congress of the Italian Chemical Society, Rimini, June 2000 (talk)

Georg Pabst
Characterization of Structural Intermediates in Phospholipid Phase Transitions
Seminar at Neutron Program for Materials Research National Research Council of Canada, Chalk River Laboratories, Station 18, Chalk River, Ontario, K0J 1J0, Canada, 15. 12. 2000 (talk)

G. Pabst, M. Rappolt, H. Amenitsch, S. Bernstorff and P. Laggner,
Structure analysis of unoriented phospholipid bilayers at full hydration by means of an inverse Fourier Method
8th International Users' Meeting, ELETTRA, Trieste, Italy, 4. - 5.12.2000 (Poster)

G. Pabst, M. Rappolt, H. Amenitsch & P. Laggner
Unoriented phospholipid bilayers at full hydration by means of an inverse Fourier method
50th Annual Meeting of the Österreichische Physikalische Gesellschaft, University of Graz, Austria, 25.-29.09.2000 (Talk)

G. Pabst, M. Rappolt, H. Amenitsch & P. Laggner
Unoriented phospholipid bilayers at full hydration by means of an inverse Fourier method
Conference: "Budapest Colloids 2000: Adsorption and Nanostructures – from Theory to Application", Budapest, Hungary, 24.-28.09.2000 (Talk)

G. Pabst, M. Rappolt, H. Amenitsch & P. Laggner
Structural information from X-ray experiments on unoriented phospholipid bilayers at full hydration by means of an inverse Fourier method
44th Annual Meeting of the Biophysical Society, New Orleans, LA, U.S.A, 12.-16.02.2000 (Talk)

S. Piccarolo
Structure development in amorphous PET upon fast cooling from the melt
EUPOC; Crystallization of Polymers; Gargnano; May, 28, 2000

Michela Pisani, Sigrid Bernstorff, Claudio Ferrero, Paolo Mariani
Pressure induced cubic to cubic phase transition in monoolein hydrated system
XV Congresso della Società Italiana di Biofisica Pura ed Applicata, Parma, Italy, October 23-25, 2000

Michela Pisani, Sigrid Bernstorff, Claudio Ferrero, Paolo Mariani
Pressure induced transitions in monoolein hydrated system
Third European Biophysics Congress, Munich,Germany, September 9-13, 2000

N. Prasanth Kumar, Bhavin Shukla, S. Major, S. Vitta, S. S. Talwar, P. Dubcek, H. Amenitsch and S. Bernstorff
Structure of ZnS- Arachidic Acid Composite LB Multilayers
9th International Conference on 'Organized Molecular Films', 28.8.- 1.9.2000, Potsdam, Germany

N. Prasanth Kumar, S. Major, S. Vitta, S. S. Talwar, P. Dubcek, H. Amenitsch, S. Bernstorff, V. Ganesan, A. Gupta and B. A. Dasannacharya
Molecular Packing in Cadmium and Zinc Arachidate LB Multilayers
9th International Conference on 'Organized Molecular Films', 28.8.- 1.9.2000, Potsdam, Germany

N. Prasanth Kumar, S. N. Narang, S. Major, S. Vitta, S. S. Talwar, P. Dubcek, H. Amenitsch and S. Bernstorff
Structure of CdS-Arachidic Acid Composite LB Multilayers
9th International Conference on 'Organized Molecular Films', 28.8.- 1.9.2000, Potsdam, Germany

R.Prassl, R. Schwarzenbacher, M. Kriechbaum, H. Amenitsch, M.J.Chapman, P. Laggner
Low resolution X-ray crystallography on Human Low Density Lipoprotein
8th International Users' Meeting, ELETTRA, Trieste, Italy, 4. - 5.12.2000 (Poster)

M. Rappolt, H. Amenitsch, S. Bororocci & G. Mancini
Organization of geometrical isomers in polymolecular aggregates.
COST-D11 Workshop on Supramolecular Chemistry, Vienna, Austria, 26.-29.10.2000 (Poster)

M. Rappolt, G. Pabst, G. Rapp, M. Kriechbaum, H. Amenitsch, C. Krenn, S. Bernstorff and P. Laggner
New evidence for gel-liquid crystalline phase co-existance in the ripple phase of Phosphatidylcholines
8th International Users' Meeting, ELETTRA, Trieste, Italy, 4. - 5.12.2000 (talk+poster)

M. Roessle, E. Manakova, I. Lauer, T. Nawroth, P. Panine, T. Narayanan, S. Bernstorff, H. Amenitsch and H. Heumann
Low contrast, short times and a lot of photons - Time resolved small angle scattering of proteins in solution;
Workshop on "Fast Structural Changes", ESRF, Grenoble, France 8.- 9.02.2000 (talk)

P. Roschger
The collagen mineral composite at the bone-cartilage interface of joints
Materials Week, International Congress on "Advanced Materials, their processes and applications", (oral presentation) Munich, Sept. 25-28 (2000)

P. Roschger, I. Zizak, O. Paris, G. Grabner, S. Bernstorff, H. Amenitsch, K. Klaushofer and P. Fratzl
Micro- and nanostructure of the bone-cartilage interface in joints
International Conference on "Progress in Bone and Mineral Research 2000", Vienna, Nov 30-Dec 3, 2000; Bone 27: 18, Abstract 21 (2000), (oral presentation)

Rustichelli F., Valkova L, Pisani M., Carsughi F., Maccioni E., Bernstorff S.
The structural investigation of tbu substituted azaporphyrins Langmuir-Blodgett films
INFM meeting, Genova, Italy, June, 2000

Rustichelli F.,Valkova L.,Pisani M.,Carsughi F.,Maccioni E.,Bernstorff S.
Temperature dependent structural rearrangements of azaporhyrines LB films
INFM meeting, Genova, Italy, June, 2000

E. Schafler, M. Zehetbauer, P. Hanak, T. Ungar, T. Hebesberger,
R. Pippan, S. Bernstorff and H. Amenitsch
In-Situ Synchrotron Bragg Peak Profile Analysis of Microstructural Parameters During Discontinuos Plastic Deformation of fcc Metals.
8th International Users' Meeting, ELETTRA, Trieste, Italy, 4. - 5.12.2000 (Poster)

F. Sussich, H. Amenitsch, S. Bernstorff and A. Cesàro
Small and wide angle x-ray scattering on trehalose polymorphs.
8th International Users' Meeting, ELETTRA, Trieste, Italy, 4. - 5.12.2000 (Poster)

F. Sussich, H. Amenitsch and A. Cesàro
Small and wide angle x-ray scattering on trehalose polymorphs
Conference on "Scattering studies of mesoscopic scale structure and dynamics in soft matter", Messina, Italy, 22-25 11.2000

A. Triolo, F. Triolo, F. Lo Celso, R. Triolo, M. Steinhart, M. Kriechbaum and H. Amenitsch
Watching Polymer Aggregates Forming in scCO$_2$: A Synchrotron study
8th International Users' Meeting, ELETTRA, Trieste, Italy, 4. - 5.12.2000 (Poster)

Roberto Triolo
From unimers to aggregates and back: exploring the critical micellisation concept
SILS 2000, Palermo 29 /6-1/7/2000 (talk)

Roberto Triolo
Tailored surfactants for polymerisation processes in SCF
Euro Summer School on CO2 Based Supercritica Fluids Applications: Chemistry and Materials, Palermo 29/9-5/10/2000 (talk)

Roberto Triolo
From unimers to aggregates and back: exploring the critical micellisation concept
SIF 2000 Palermo 6-11/10/2000 (talk)

Roberto Triolo
Dilute and Semi dilute Solutions of Block Copolymers in water, Near-critical and Super-Critical CO_2: a Small Angle Scattering Study of the Monomer-Aggregate Transition
Scattering Studies of Mesoscopic Scale Structure and Dynamics in Soft Matter, Messina, Italy, November 22-25, 2000 (talk)

A.Turkovic
Nanostrukturirani materijali
Invited lecture, given for Section for Education of Croatian Chemical Society, In Academy for Education, 16 october 2000, Savska cesta 77, Zagreb, Croatia.

A.Turkovic , Z.Crnjak-Orel, P.Dubcek
Grazing-incidence small-angle X-ray scattering on nanosized vanadium oxide and V/Ce oxide films
8th International Users' Meeting, ELETTRA, Trieste, Italy, 4. - 5.12.2000 (Poster)

M.Vidal, M. Kriechbaum, M. Steinhart, H. Amenitsch, S. Bernstorff and P. Laggner
Influence of Cholesterol on the Barotropic Phase Transition of the Phospholipid POPC Studied by Small-Angle X-Ray Scattering
8th International Users' Meeting, ELETTRA, Trieste, Italy, 4. - 5.12.2000 (Poster)

V. Vidya, S. Major, S. Vitta, S. S. Talwar, A. Gupta, P. Dubcek, H. Amenitsch and S. Bernstorff
Monolayer Behavior and Structure of POT-CdA LB Multilayers
9th International Conference on 'Organized Molecular Films', 28.8.- 1.9.2000, Potsdam, Germany

I. Winter, G. Pabst , R.N.A.H. Lewis, R.N. McElhaney, M. Rappolt & K. Lohner
What an additional ethyl group can cause: studies on the bilayer structure of 1,2-diacyl-P-O-ethyl phosphatidylcholines, potential cationic DNA transfection lipids
Annual Meeting of the Austrian Biochemical Society, Innsbruck, Austria, 25.-27.09.2000 (Talk)

M.Zehetbauer
Merkmale extremer plastischer Verformung zur Realisierung von Nanostrukturen in Metallen
Kolloquium am Max Planck Institut für Eisenforschung, Düsseldorf, Deutschland (April 2000)

M.Zehetbauer
Fundamentals of Severe Plastic Deformation
Workshop "Severe Plastic Deformation and Nanostructured Advanced Materials"
Conference Center "Am Spiegeln", Vienna, Austria (June 2000)

M.Zehetbauer
Principles of Severe Plastic Deformation Providing Nanostructures in Materials"
Moscow State Steel and Alloys Institute, Moscow, Russia (October 2000)

M.Zehetbauer
Principles of Severe Plastic Deformation Providing Nanostructures in Materials"
Institute for Physics of Advanced Materials, Ufa Aviation State University, Russia (October 2000)

M.Zehetbauer
Investigations of Microstructural Evolution During Plastic Deformation of Metals by   X-Ray Line Profile Analysis Using Synchrotron Radiation
Paul Scherrer Institute, Villigen, Switzerland (October 2000)

M.Zehetbauer
Conditions of Plastic Deformation for Achieving Nanostructures in Metals
Institute of Physics of Materials, Czech Academy of Sciences, Brno (November 2000)

M.Zehetbauer, T.Ungar, E.Schafler, S.Bernstorff, H.Amenitsch
Microscale Spatial Distribution of Dislocations and Long Range Internal Stresses in Cold Worked bcc Fe
Proc.5th Asia Pacific Symposium on Advances in Engineering Plasticity & Applications (AEPA 2000), July 12-16, Hong-Kong (2000)

Non-refereed Publications in 2000

G. Pabst, M. Rappolt, H. Amenitsch, S. Bernstorff and P. Laggner
More Structural Information from Smectic Phases Full Q-Range Fitting with High Quality X-Ray Data
ELETTRA Highlights 1999/2000

R.Schwarzenbacher, H.Amenitsch, F.Nigon, M.J.Chapman, S.Bernstorff, P.Laggner and R. Prassl
Low Resolution Crystallography on Human Plasma Low Density Lipoprotein (LDL)
ELETTRA Highlights 1999/2000

Doctoral Theses

Vincenzo La Carrubba
Polymer Solidification Under Pressure and High Cooling Rate
Tesi di dottorato XIII ciclo in "tecnologie Chimiche e dei nuovi Materiali", Tutor: Prof. S. Piccarolo, Submitted to the University of Palermo 15/12/2000

Georg Pabst
Characterization of Structural Intermediates in Phospholipid Phase Transitions
Technische Universitaet Graz, April 2000

Robert Schwarzenbacher
*The Crystal Structure of **b**2-Glycoprotein-I.*
Technische Universitaet Graz, May 2000

Ivo Zizak
Time- and position-resolved synchrotron X-ray scattering for structure research on biological connective tissue
University of Leoben, Austria, March 2000

Doctoral Theses in 2001

Manfred Roessle
Time resolved small angle scattering of proteins: The structural intermediates of the chaperonin GroEL and GroES upon ATPase cycle
Technische Universität München 2001

Diplom Theses (Tesi di Laurea)

Danilo Calandri
Analisi delle proprietà strutturali della Gliossalasi II umana mediante scattering dei raggi X e dei neutroni
Università di Ancona, Italy, (Relatore: P. Mariani), 2000

Caterina Di Giovanni
Caratterizzazione strutturale di miscele polimeriche semicristalline
Tesi di Laurea A.A. 1999-2000

Marco Nevijel
Sintesi e caratterizzazione di nuovi derivati di polisaccaridi da microorganismi
Università di Trieste, Italy, (Relatore: R. Rizzo), December 2000

Andre Orthen
Entwicklung und Test eines großflächigen MCAT-Detektors mit Stützstruktur
University of Siegen, Germany, December 2000

R. Puxkandl
Beziehung zwischen Struktur und Mechanischen Eigenschaften von Kollagen
University of Leoben, Austria, November 2000

Hendrik Wagner
Einfluß der dissipativen Fläche der Widerstandsschicht auf zweidimensionale Ortsmessung im MicroCAT-Detektor
University of Siegen, Germany, August 2000

Author Index